Thermo Electron Corporation, 85 First Avenue, Waltham, Massachusetts 02154

Report No. TE4049-30-68

FINAL REPORT
THERMAL ENERGY STORAGE/CONVERTER PROTOTYPE DESIGN, FABRICATION AND TESTING

January 1968

Contract No. 950976/NAS7-100

by

B. Gunther
S. Merra
P. Pantazelos

Prepared for

Jet Propulsion Laboratory
Pasadena, California

This work was performed for the Jet Propulsion Laboratory, California Institute of Technology, sponsored by the National Aeronautics and Space Administration under Contract NAS7-100.

TABLE OF CONTENTS (Continued)

TABLE OF CONTENTS

VOLUME 1

SUMMARY

Program Goals

The purpose of the program described here was to attempt to join a container of thermal energy storage (TES) material to an existing thermionic converter and thus demonstrate the feasibility of using the stored energy to power the converter when external solar power was not available. Such a combined TES-thermionic system showed promise of being a lighter and more reliable means of providing electric power from solar energy in orbiting applications, where the sun was periodically shaded, than the use of batteries during the dark portion of the cycle.

Before the initiation of this program, considerable work had been done[1,2,3] on finding means of containing suitable TES materials. This work indicated that the binary mixture of 3 BeO-2 MgO had a melting point compatible with thermionic emission (2145°K), had a high specific heat of fusion (370 cal/g), and was chemically compatible with rhenium at the oxide's melting point. The program described here was therefore based upon the use of this oxide in a rhenium container.

Concurrent with this program another[4] was initiated in which supporting research was conducted to measure the properties of this and other oxides and to carry out further studies on the containment of the oxide. Much of the data generated was used in the design of the TES feasibility model.

The work on the TES feasibility model was not intended to encompass the generation of property data or the investigation of various means of containment. Its purpose was to assemble a device using then current technology and to demonstrate in a working model the operation of a converter with thermally stored energy.

Method of Attack

In view of the limited scope of the program, the Series VIII SET converter, modified to include a monolithic rhenium emitter and emitter sleeve, was chosen as the conversion device. Its performance was well established, as were the construction techniques. The complete TES model included a converter, a container of oxide welded to the emitter of the converter, and multiple-layer radiation shields enclosing the part of the container that did not abut on the emitter. An electron-bombardment heater was included between the shields and the container to provide the heat to melt the oxide. Figure 1 is a cutaway drawing of the converter and container. The shields and the heater are not included. Figure 2 shows the container-converter combination. In Figure 3 the complete TES model is shown mounted for test. The electron-bombardment heater leads can be seen extending downward from the top of the setup and entering the thermal shielding. The shielding is in place around the container, and the converter is below the shielding.

A computer study was made of the interaction of such parameters as the quantity of oxide, the shielding effectiveness, and the converter's performance. The parameters chosen for use were the following:

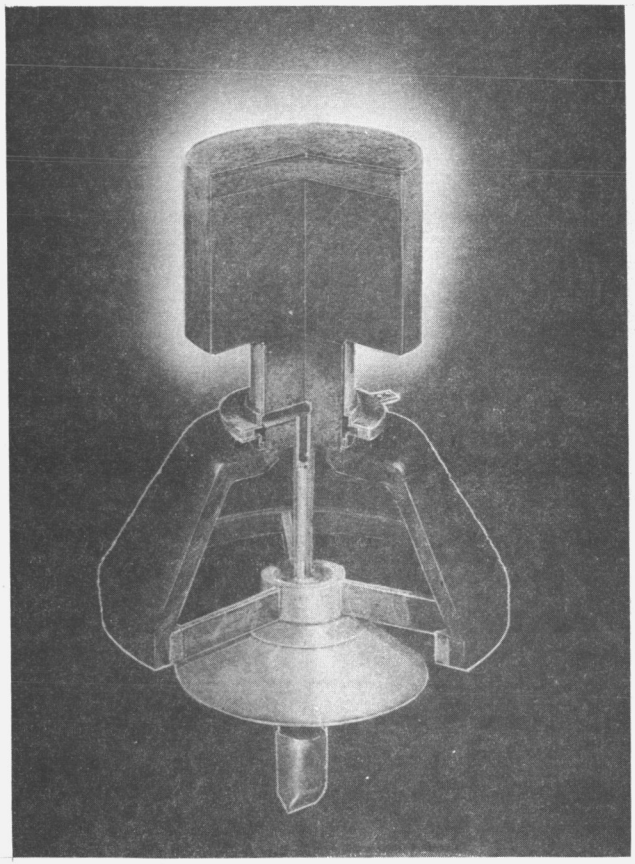

Figure 1. Cutaway Drawing of Converter and Container.

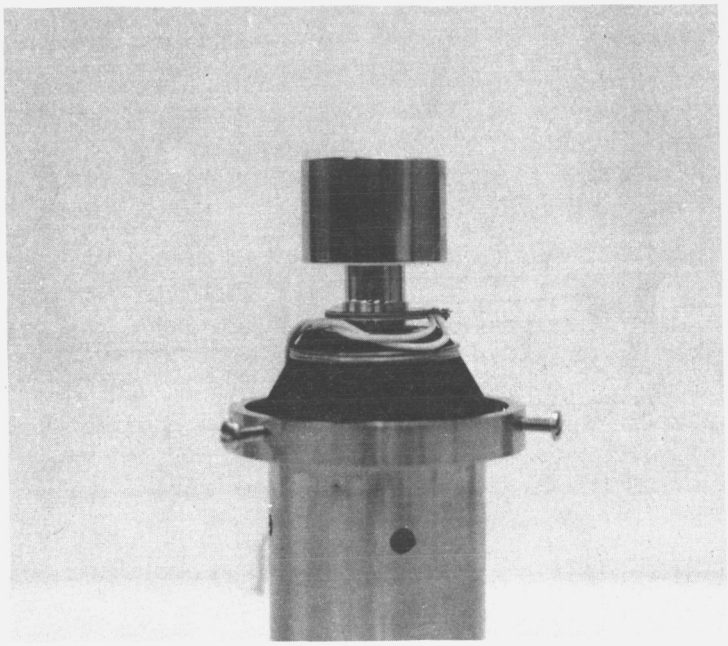

Figure 2. Container-Converter Combination.

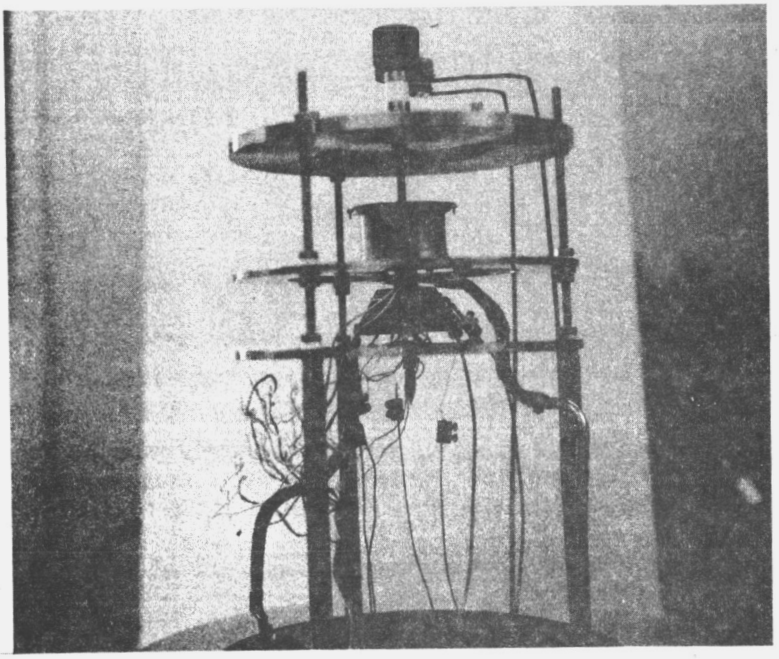

Figure 3. Complete TES Model Mounted for Test.

Container Height	3 cm
Container Diameter	4 cm
Container Volume	37.8 cm^3
Percent of Container Filled with Oxide	70%

The expected performance of the model was as follows:

Calculated Operating Time on TES	9.5 min
Calculated Specific Power	11.6 W-hr/lb

The container for the oxide was made of rhenium and was designed so that its bottom surface also acted as the emitter of the converter. The assembly procedure consisted of assembling and testing the entire converter and then adding the cylindrical sides, the oxide, and the flat lid. All joints in the container were made by electron-beam welding. The performance of the converter at 1900, 2000, and 2150° K emitter temperature is shown in Figure 4.

The oxide was prepared by mechanically mixing BeO and MgO in the proper proportions in a blender, melting the mixture and forming slugs of the 3 BeO-2 MgO, machining the slugs to the proper size, and inserting them into the container. Figure 5 shows a typical disc of the oxide.

A small test container was fabricated, loaded with oxide, welded shut and tested. Its height was 0.87 inch, and its diameter 1 inch, and it was filled to 58.5% of capacity. The capsule was heated above the melting point of the oxide sixteen times without oxide leakage and without any change in the appearance of the container's surface. Based on this test, a full-size container was fabricated for the TES model.

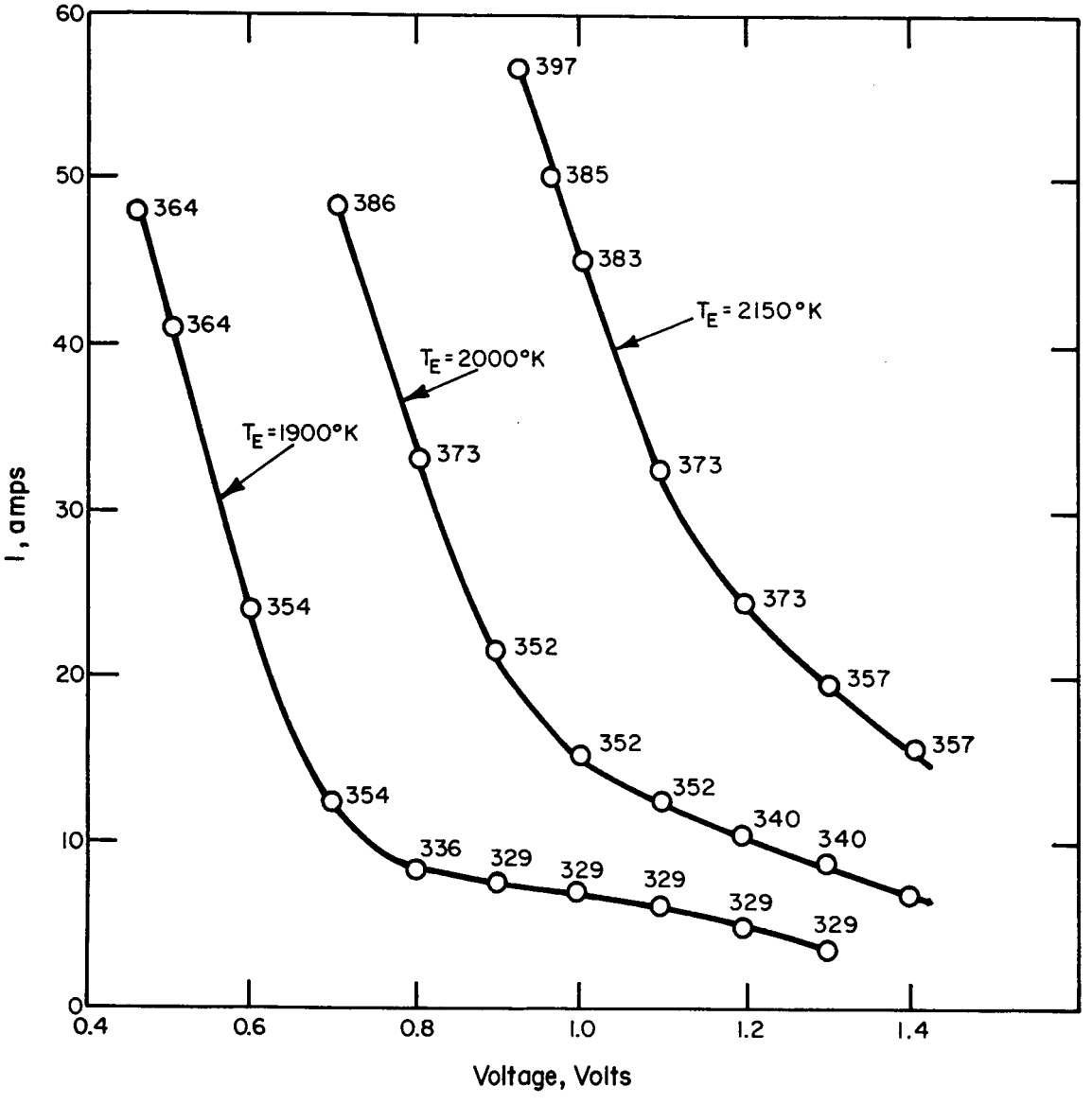

Figure 4. Converter Performance.

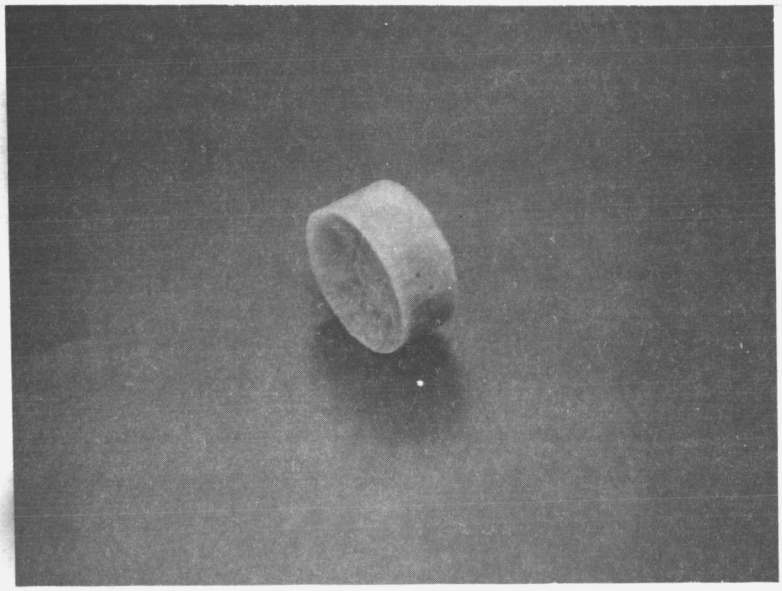

Figure 5. Typical Disc of 3 BeO - 2 MgO.

The TES model was tested by slowly heating and melting the oxide. When the oxide had melted, an increase was noted in the pressure in the vacuum system. The heating was terminated and the model was cooled. During the cooling a record was made of the converter's output, and this is shown in Figure 6. Examination of the model showed an oxide leak in the weld joining the lid of the container to the side wall. This is shown in Figure 7.

The performance of the model during cool-down showed that the converter output followed that predicted by the earlier computer calculations.

Following this test, another full-size container was constructed in an effort to achieve a leak-tight unit, but this container also leaked when the oxide was melted. In addition, it exhibited severe distortion, as if a large pressure had been exerted against the inner walls, causing them to bulge outward. Figure 8 shows the container after test. Since the oxide used in this container had been purified by melting, and the container had been thoroughly evacuated before the lid was welded, the source of the pressure was difficult to determine. This container leaked at the weld of the emitter piece to the cylinder after the second heating.

Conclusions and Recommendations for Further Action

The results of this program showed that a container of thermal energy storage material can be integrated with a thermionic converter using available fabrication technology. Furthermore, the exposed surface of the container can be adequately shielded with multi-layer radiation shields to concentrate the bulk of the heat into the thermionic

emitter. Finally, the method of calculating the output of the model during cool-down was proved valid.

However, before a long-lived model can be constructed, the problem of containing the oxide must be solved. Now that definitive property data describing the 3 BeO - 2 MgO oxide is available, containment tests can be performed to establish the phenomena taking place within the sealed capsule. Further experimentation is also necessary to establish a reliable means of preventing contamination of the final weld by the oxide. When this information is available a second TES model with the dark-cycle operating capability of an actual mission can be built.

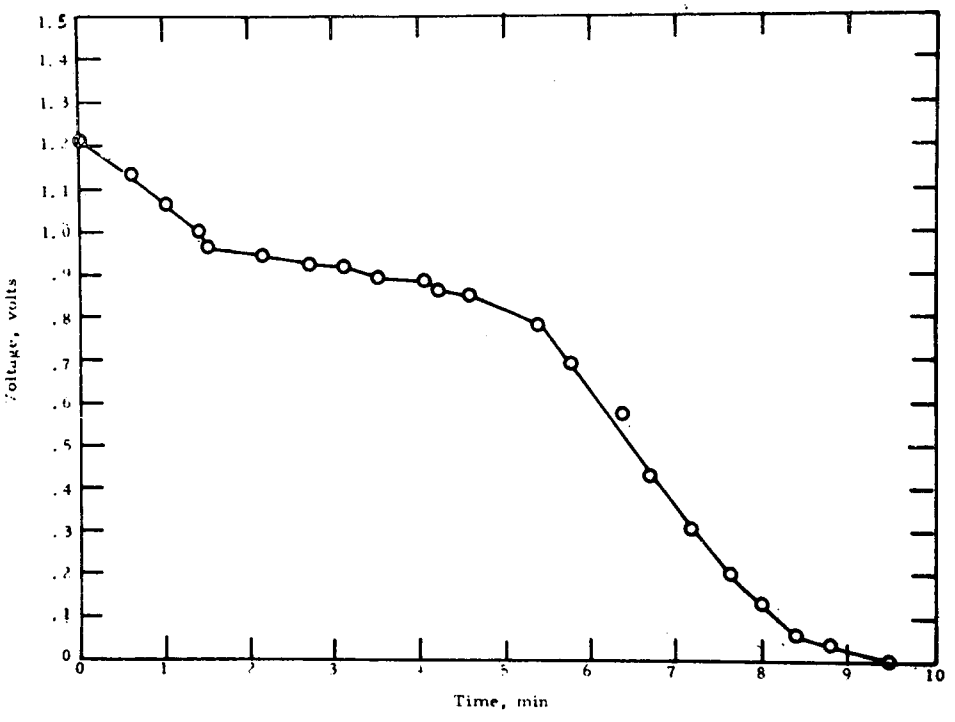

Figure 6. Converter Output During Cooling of Oxide.

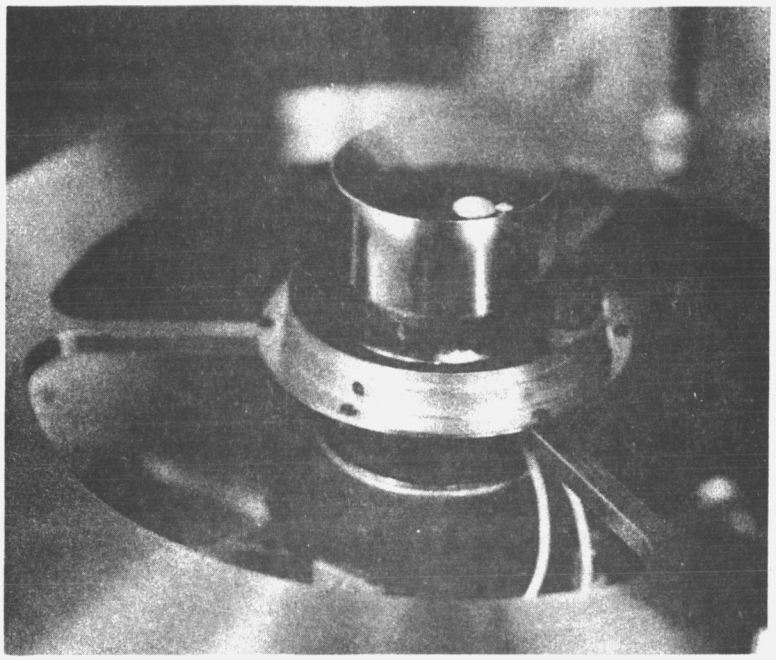

Figure 7. Oxide Container, Showing Leak in Weld Joining Lid to Side Wall.

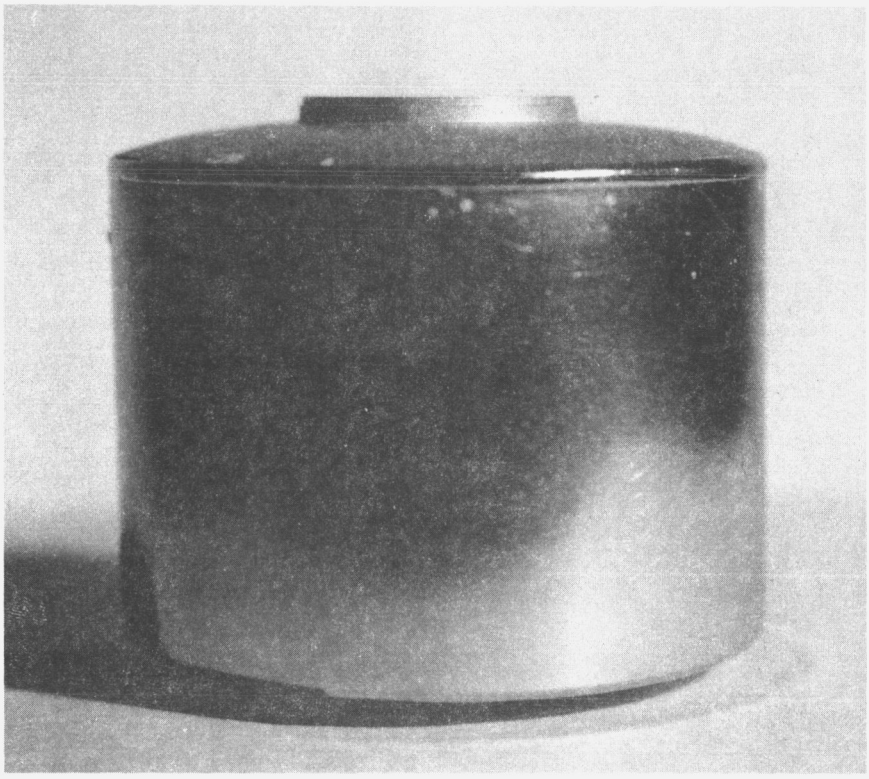

Figure 8. Oxide Container, Showing Bulging of Bottom and Top Surfaces.

various converter components. Both electron-beam and inert-gas welds had proven satisfactory. However, the proximity of the molten oxide to the welds led to concern about its interaction with the weld. Consequently the program plan stressed component testing and examinations in this area.

Although most anticipated orbital applications required energy storage for periods of 20 minutes or more, the goal for this feasibility device was established as 10 minutes. Operation for 10 minutes would prove feasibility while also minimizing the amount of very costly rhenium that would be consumed. A computer study early in the program established 9.5 minutes as the expected operating time following termination of power input, and the feasibility model produced power for exactly that length of time.

VOLUME II

1. INTRODUCTION

The program described here was initiated at the Thermo Electron Engineering Corporation by the Jet Propulsion Laboratory in the spring of 1965. Its purpose was to join a thermionic energy converter to a container of thermal energy storage material using existing technology, and to show the feasibility of the integrated device and point out the problem areas.

Earlier work had shown that the oxide mixture 3 BeO - 2 MgO had a high heat of fusion and a melting point compatible with high-temperature thermionic converters. For orbiting space power applications, where solar power was available for part of each orbit, solar-powered generators were generally provided with battery storage. By the use of thermal energy storage a lighter overall system appeared possible, and also the conversion devices would be subjected to far less thermal cycling.

At the outset of this work solar thermionic converters and generators had reached the stage of development where long-lived and light-weight devices were available. Furthermore, these had successfully withstood the shock and vibration environment of a launch vehicle. The most advanced converter at that time was the Series VIII type developed under the SET (Solar Energy Thermionic) program. This converter was chosen for use in the construction of the thermal energy storage feasibility model.

The principal problem anticipated at the outset was that of welding the rhenium thermal storage container. Sound and vacuum-tight welding of rhenium had been accomplished many times for

An electron-bombardment gun was designed for heating the container to melt the oxide and was placed within the shielding.

2.2 Influence of Variables on the Specific Power and the Operating Time

The equation describing the heat flow, Q, through the Series VIII converter is:

$$Q = 10 + 39\left(\frac{T_E}{1000} - 1\right) + 4.6\left(\frac{T_E}{1000}\right)^4 + 2.66\, I_o, \text{ watts}$$

where:

the first term is the cesium conduction,

the second term is the loss from the spacer,

the third term is the sum of interelectrode radiation and radiation loss from the sides of the emitter, and

the last term is the electron cooling.

This expression was formulated from the data obtained on several Series VIII converters. Figure 2.3 illustrates the total heat input measured for several diodes as a function of the output current, while Figure 2.4 shows the heat required by the converter with the cesium conduction term deleted. From the latter figure, the heat required to obtain an emitter temperature of 2000°K at zero amperes was obtained by extrapolating the curve to zero amperes. This value was 185 watts and consisted of emitter radiation and conduction through the emitter spacer.

From the geometry of the Series VIII emitter structure and from the total heat required to achieve the rated emitter temperature, the radiation loss from the upper portion of the emitter was estimated

2. DESIGN

2.1 Design Approach

The approach to the design of the thermal energy storage feasibility model was to use as many proven components and techniques as possible. For this reason the Series VIII SET converter was chosen, and it was modified only to the extent necessary to couple it to a container of thermal energy storage material. The program called for the use of 3 BeO-2MgO oxide as the storage material and, because earlier work[1, 2, 3] had shown this oxide to be compatible with rhenium, the container was designed of this metal. Similarly, the method of fabricating the container was based on the same earlier work and consisted of purchasing 20-mil rhenium sheet, rolling the sheet into a cylinder, seam welding the cylinder by electron-beam welding, and attaching bottom and top plates by electron-beam welding. To avoid the formation of brittle intermetallics, the emitter support sleeve of the Series VIII converter was changed from tantalum to rhenium, and the rhenium container was then electron-beam welded to the sleeve. Figure 2.1 shows the Series VIII converter in simplified cross section. Figure 2.2 shows the container attached to the converter.

As can be seen in Figure 2.2, the heat from the container had to be concentrated into an emitter that constituted a small fraction of the container's surface area. The remainder of the surface required thermal shielding to minimize radiation losses and maximize operating time after the driving power was terminated. Multiple-layer shielding that had been used successfully in other thermionic programs was also used here.

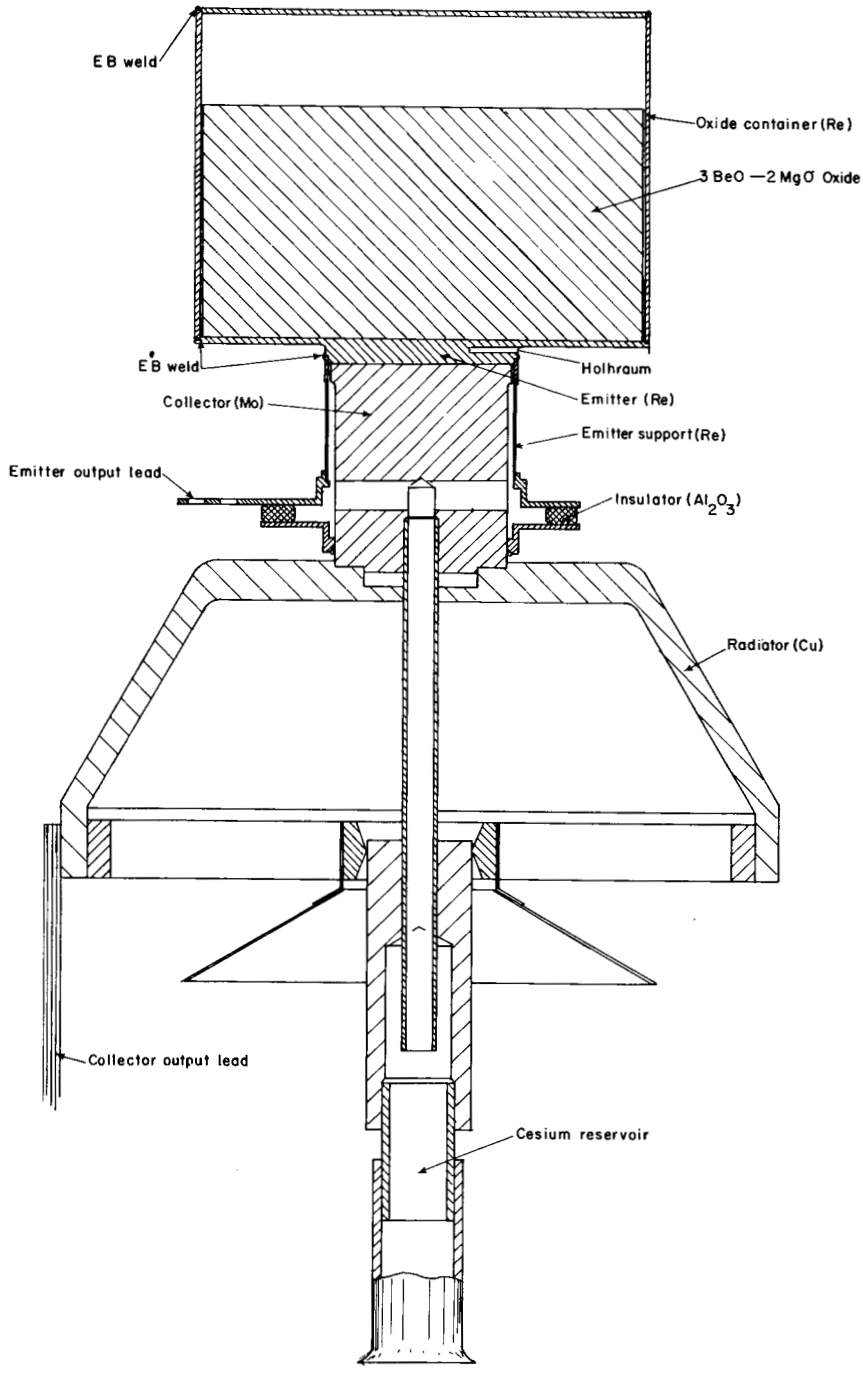

Figure 2. 2. Cross Section of TES Container-Converter Module.

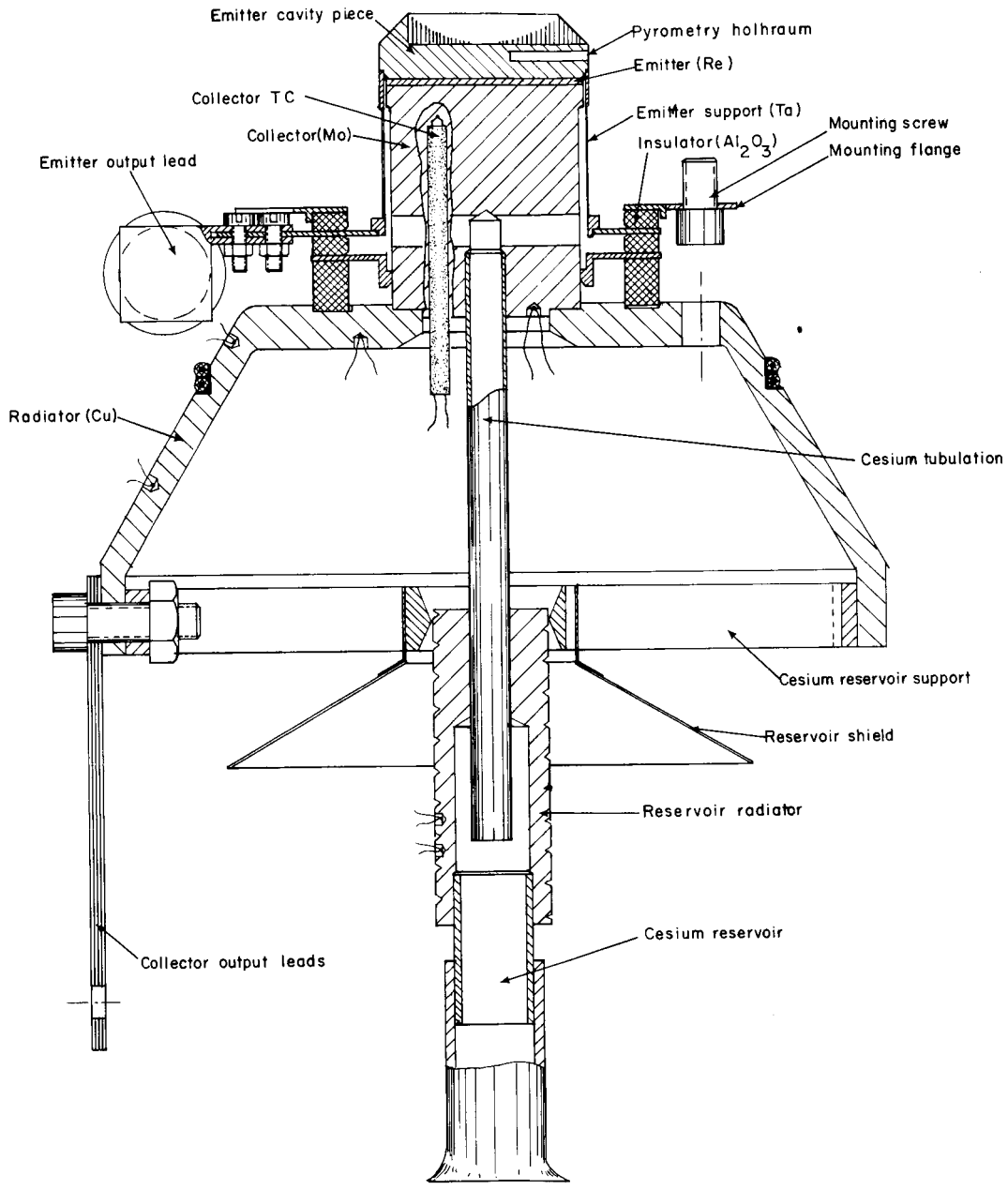

Figure 2.1. Cross Section of Series VIII Thermionic Converter.

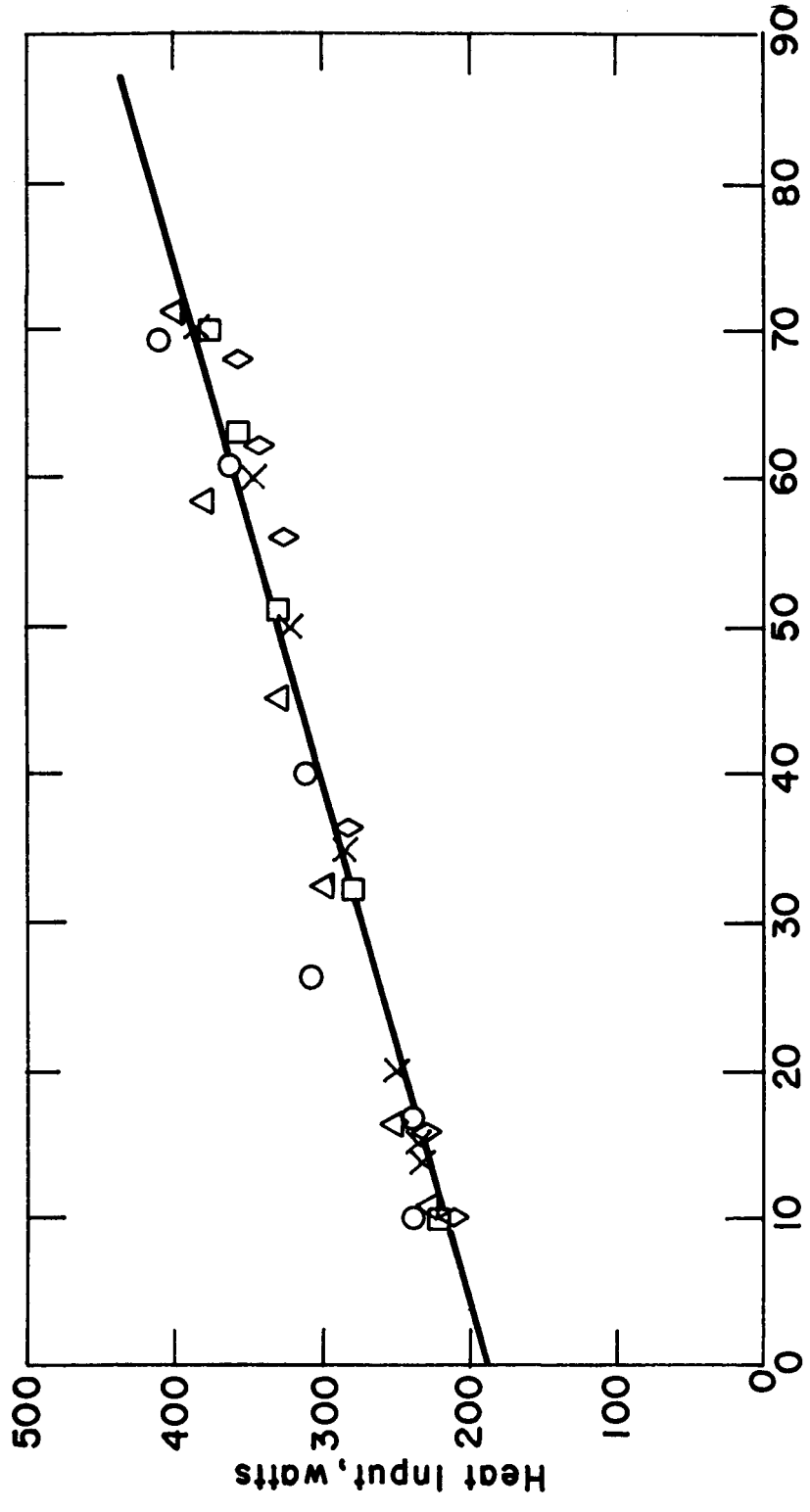

Figure 2.3. Total Heat Input versus Output Current for Series VIII Converter.

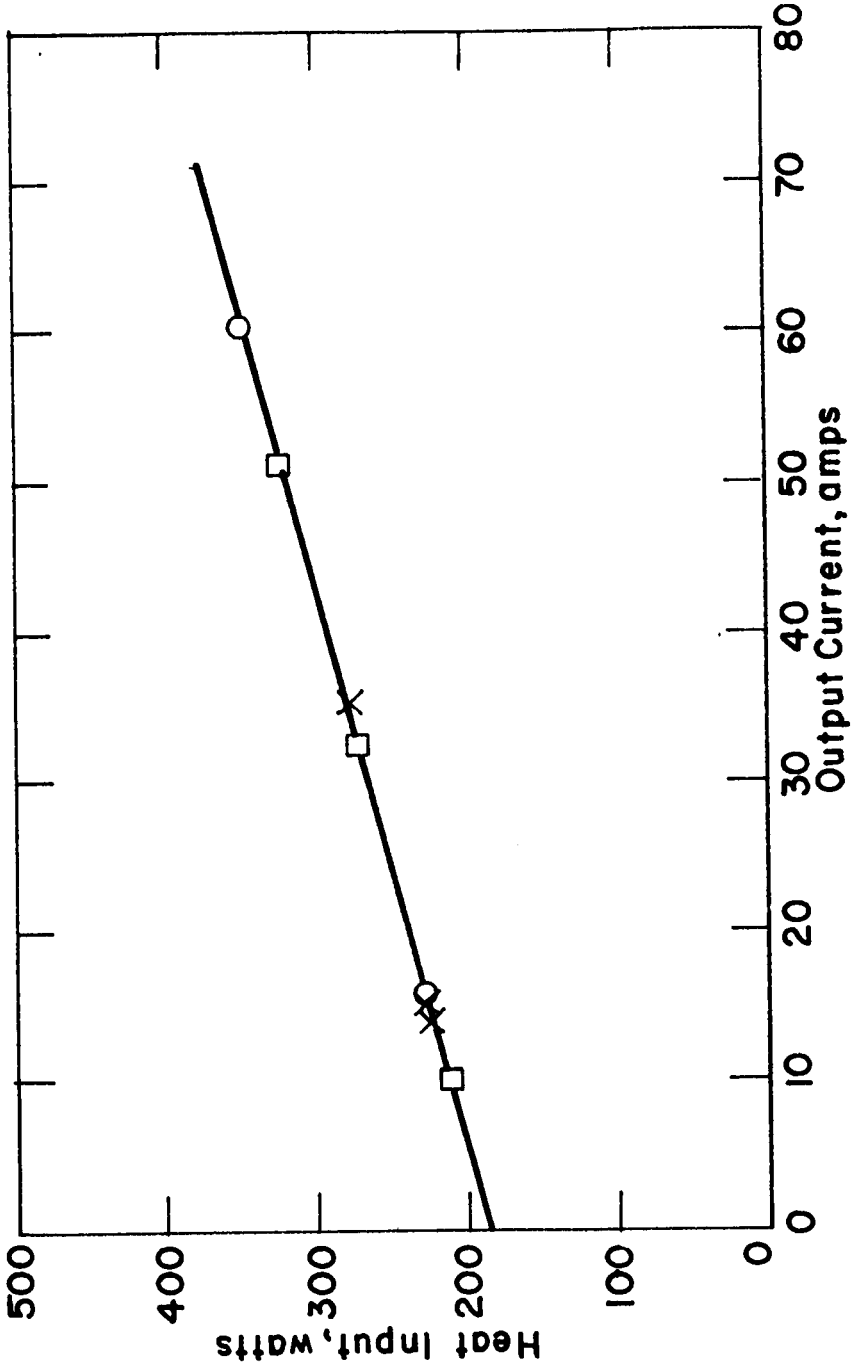

Figure 2.4. Total Heat Input minus Cesium Conduction versus Output Current for Series VIII Converters.

as 2.84 $(T_E/1000)^4$. The interelectrode radiation term was estimated as 1.76 $(T_E/1000)^4$, giving a total of 4.6 $(T_E/1000)^4$. The spacer term coefficient, therefore, was taken to be 39 in order to give a total heat flow of 185 watts at 2000°K.

By calculating the slope of the curve, namely, 2.66 watts/ampere, an estimate of the electron cooling was obtained.

Figure 2.5 is a plot of the output of the VIII-P-3 converter at pyrometer hole temperatures of 1500°C, 1600°C, 1700°C, and 1800°C. The cesium reservoir temperature (°C) at the various points is also shown. This data showed that as the emitter cooled, a constant-voltage mode of operation resulted in a 50 to 80°C variation of optimum cesium reservoir temperature at any constant output voltage. For constant-current operation, the optimum cesium temperature varied between 5 and 25°C. This smaller range was expected to be easier to maintain during the cooling cycle. Table 2.1 shows both modes of operation versus emitter temperature. For the same starting points, the constant-current mode gave much larger average power outputs.

The model used for computation of the TES model's operating time assumed all the oxide to be initially liquid. Heat flowing into the emitter caused solidification in the axial direction from the emitter towards the top of the container. Heat losses through the shield surrounding the container produced solidification in a radial direction from the sides towards the center.

The heat to the emitter was computed from

$$Q_E = S_A + S_B (T_E/1000-1) + S_C (T_E/1000)^4 + S_D I \text{ watts}$$

where

S_A = cesium condition
S_B = spacer loss constant
S_C = radiation loss constant
S_D = Electron cooling constant
T_E = emitter surface temperature, °K
I = output current, amperes

The emitter surface temperature was assumed to be equal to the melting point of the oxide minus the temperature drops through the already solidified oxide and the emitter proper.

$$T_E = T_m - Q_E\left(\frac{X}{K\bar{A}} + R_e\right)$$

where

T_M = oxide melting point = 2145°K
X = axial thickness of solid oxide, cm
K = oxide thermal conductivity, W/cm °K
$\bar{A}$ = average area for heat transfer, cm^2
R_e = emitter thermal resistance, °K/W

The volume of oxide freezing in the axial direction during a time interval Δt due to the heat flowing to the emitter was

$$\Delta V_x = \frac{Q_E\ \Delta t}{H} ,$$

where H was the oxide heat of fusion (watt sec/cc).

Heat losses through the shield were

$$Q_y = j q,\ A_s$$

TABLE 2.1

POWER OUTPUT VERSUS EMITTER TEMPERATURE FOR CONSTANT-VOLTAGE AND CONSTANT-CURRENT OPERATION

Emitter Temperature (°K)	Constant Output Voltage			Constant Output Current		
	Voltage (Volts)	Current (Amperes)	Power (Watts)	Voltage (Volts)	Current (Amperes)	Power (Watts)
2100	0.9	55	49.5	0.9	55	49.5
2000	0.9	31	27.9	0.71	55	39.0
1900	0.9	10	9.0	0.56	55	30.8
1800	0.9	6	5.4	0.39	55	21.4
2100	1.0	43	43	1.0	43.5	43.5
2000	1.0	17.5	17.5	0.8	43.5	34.8
1900	1.0	8.0	8.0	0.62	43.5	27.0
1800	1.0	5.0	5.0	0.43	43.5	18.7
2100	1.2	23	27.6	1.2	23	27.6
2000	1.2	12.5	15.0	0.97	23	22.3
1900	1.2	6.0	7.2	0.73	23	16.8
1800	1.2	3.0	3.6	0.505	23	11.6

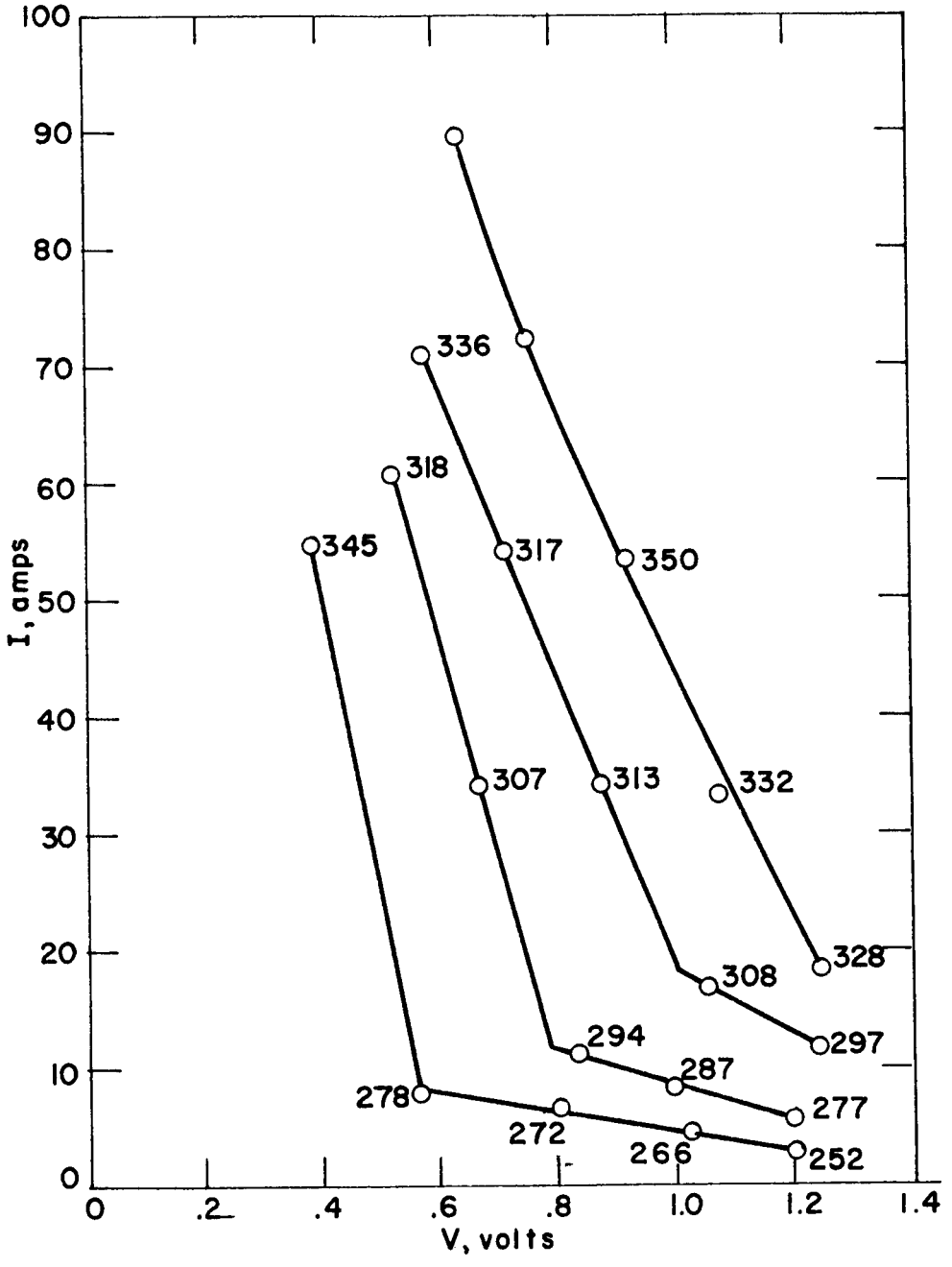

Figure 2.5. Performance of Converter VIII-P-3 at 1500°C, 1600°C, 1700°C and 1800°C Emitter Temperatures.

A computer was used to calculate the expected output of the TES model versus time. The numerical values used in the computer program were:

$\bar{A}$ = 5 cm^2

H = 6600 watt sec/cc

K = 0.08 W/cm °K

q_s = 110 W/cm^2

R_e = 0.252°K/W

S_A = 10.0

S_B = 39

S_C = 4.6

S_D = 2.66

T_m = 2145°K

T_y = 2100°K

Δt = 30 sec

I = 23, 43.5, 55 amperes

j = 0.005, 0.01, 0.02, 0.05, 0.10

α = 0.6, 0.7, 0.8, 0.9 (fraction of the container filled with oxide)

D = 2, 3, 4 cm

L = 1.5, 2, 2.5, 3, 3.5 cm

The diode's interelectrode spacing, because of the use of a rhenium rather than tantalum emitter support sleeve, was calculated to be 3 mils instead of 2.2 mils. To allow for the larger spacing and the resulting lower performance, the curves shown in Figure 2.5 were shifted by 50 mV to the left. Figure 2.6 shows the resulting emitter temperature versus voltage for three currents of 23, 4.35, and 55 amperes. This

where

$A_s = (2\pi D^2/4 + \pi DL)\ cm^2$, surface area of container

j = shielding loss, fraction

q_s = black-body radiation at container temperature T_y, °K

The volume of oxide freezing in the radial direction was

$$AV_y = \frac{Q_y \Delta t}{H}\ cm^3$$

The oxide volumes ΔV_x and ΔV_y were converted to a disc and a cylinder of suitable dimensions and fitted to the walls of the container for the first step, and against the already solidified oxide thereafter. The procedure was repeated at successive time intervals until no liquid oxide remained.

Each computer run produced the following information:

T = cumulative operating time, sec

T_E = emitter surface temperature, °K

I = output current, amperes

x = distance from emitter to liquid oxide, cm

y = distance from container wall to liquid oxide, cm

Q_E = heat flowing into emitter, watts

Using the diode performance obtained experimentally during previous programs, curves were constructed (Figure 2.6) showing the TES model's output voltage versus emitter temperature, at several constant output currents. By computing the emitter temperature, the appropriate output voltage and power were found from these curves for each time interval.

data was used in the computer program to arrive at the model's output. The data shown in Figure 2.5 was measured at emitter temperatures of 1500°C(1773°K), 1600°C(1873°K), 1700°C(1973°K), and 1800°C (2073°K), and was considered adequately valid for operation at 1800°K, 1900°K, 2000°K, and 2100°K. Thus the data in Figure 2.6 was slightly conservative.

The results of the computer runs are tabulated in Tables 2.2 through 2.6. Information received from JPL suggested that the oxide's expansion might be as great as 30%. Consequently, only the results for $\alpha = 0.7$ were considered because this amount of oxide would approximately fill the container when liquid. The results are summarized in Figure 2.7. From these results, a container 4 cm in diameter and 3 cm long was selected for the model. Under constant-current operation, the specific power was calculated to be 11.56 $\frac{W\text{-}hr}{lb}$ and the time to solidification of the order of 9.5 minutes if a shielding effectiveness of 2% of black-body radiation was achieved. The average power output during the cooling cycle was estimated to be 12.95 watts.

2.3 Final Design

2.3.1 Capsule Design

As explained in Section 2.2, the capsule size was chosen to be 4 cm in diameter and 3 cm long. Previous experience at GEMSD[1, 2, 3] had shown successful containment of the 3 BeO - 2 MgO oxide in containers made with 20-mil sheet rhenium, electron-beam welded at the joints. A similar procedure was chosen here.

A rolling fixture was designed for the purpose of rolling the flat 20-mil rhenium sheet into cylindrical form. Then the cylinder was to be held in the welding fixture shown in Figure 2.8 and passed under an electron beam to weld the seam.

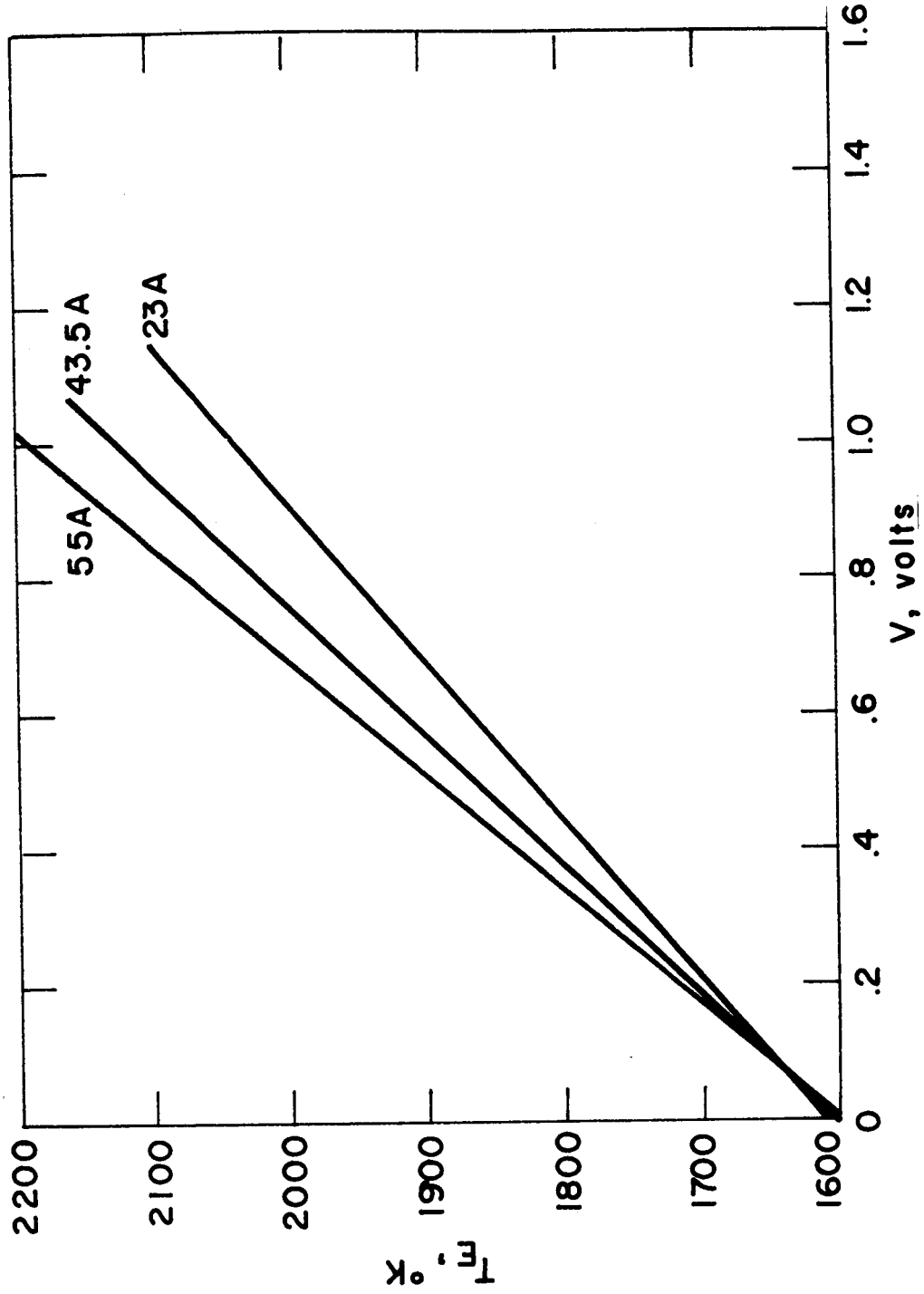

Figure 2.6. Emitter Temperature versus Voltage for Three Output Currents (Converter Spacing = 3 mils).

TABLE 2.3

CONSTANT-CURRENT MODE OF OPERATION

(I_o = 43.5 amperes)

D (cm)	L (cm)	J*	α**	P (W-hr/lb)	t (min)
2	2.5	0.05	0.8	13.78	1.5
3	2.5	0.05	0.8	11.34	3.0
4	2.5	0.05	0.8	9.89	5.0
3	1.5	0.05	0.8	17.61	2.5
3	3.5	0.05	0.8	8.22	3.5
3	2.5	0.05	0.6	14.09	2.5
3	2.5	0.05	0.7	14.45	3.0
3	2.5	0.05	0.9	10.16	3.0
3	2.5	0.10	0.8	10.2	2.5
3	2.5	0.01	0.8	12.6	4.0
2	1.5	0.05	0.6	26.3	1.0
2	1.5	0.05	0.9	20.1	1.5
4	3.5	0.05	0.6	8.55	4.5
4	3.5	0.05	0.9	6.29	5.5
4	1.5	0.05	0.8	14.67	3.5

* Shielding loss - fraction of black-body radiation at 2100°K.

** Fraction of container filled with oxide.

TABLE 2.2

CONSTANT-CURRENT MODE OF OPERATION

(I_o = 23 amperes)

D (cm)	L (cm)	J*	**	P (W-hr/lb)	t (min)
2	2.5	0.05	0.8	13.2	2.5
3	2.5	0.05	0.8	10.67	4.0
4	2.5	0.05	0.8	9.13	6.0
3	1.5	0.05	0.8	13.94	2.5
3	3.5	0.05	0.8	8.09	5.0
3	2.5	0.05	0.6	12.34	3.0
3	2.5	0.05	0.7	13.02	3.5
3	2.5	0.05	0.9	9.92	4.5
3	2.5	0.10	0.8	8.2	2.5
3	2.5	0.01	0.8	13.66	7.0
2	1.5	0.05	0.6	19.08	1.0
2	1.5	0.05	0.9	16.3	1.5
4	3.5	0.05	0.6	8.23	5.5
4	3.5	0.05	0.9	6.47	8.0
4	1.5	0.05	0.8	12.23	4.0

* Shielding loss - fraction of black-body radiation at 2100°K.

** Fraction of container filled with oxide.

TABLE 2.5

CONSTANT-CURRENT MODE OF OPERATION

(I_o = 23 amperes, α = 0.7)

D (cm)	L (cm)	J*	P (W-hr/lb)	t (min)
2	1.5	0.02	21.2	1.5
2	2.0	0.02	18.3	2.0
2	1.5	0.005	24.69	2.0
2	2.0	0.005	20.16	2.5
3	2.5	0.005	16.04	7.5
4	1.5	0.005	21.76	7.5
4	1.5	0.01	21.86	6.5
4	1.5	0.02	15.86	5.0
3	1.5	0.02	19.68	3.5
3	2.0	0.02	16.61	4.5
3	2.5	0.02	14.16	5.5
3	3.0	0.02	12.08	6.0
4	2.0	0.02	14.89	7.0
4	2.5	0.02	12.71	8.5
4	3.0	0.02	11.56	9.5

* Shielding loss - fraction of black-body radiation at 2100°K.

TABLE 2.4

CONSTANT-CURRENT MODE OF OPERATION

(I_o = 55 amperes)

D (cm)	L (cm)	J*	α**	P (W-hr/lb)	t (min)
2	2.5	0.05	0.8	12.7	1.5
3	2.5	0.05	0.8	10.38	2.5
4	2.5	0.05	0.8	9.04	4.0
3	1.5	0.05	0.8	16.15	2.0
3	3.5	0.05	0.8	7.44	2.5
3	2.5	0.05	0.6	13.33	2.5
3	2.5	0.05	0.7	13.24	2.5
3	2.5	0.05	0.9	9.22	2.5
3	2.5	0.10	0.8	15.5	2.0
3	2.5	0.01	0.8	10.6	3.0
2	1.5	0.05	0.6	21.1	0.5
2	1.5	0.05	0.9	17.95	1.0
4	3.5	0.05	0.6	8.48	4.0
4	3.5	0.05	0.9	5.98	4.5
4	1.5	0.05	0.8	14.27	3.5

* Shielding loss - fraction of black-body radiation at 2100°K.

** Fraction of container filled with oxide.

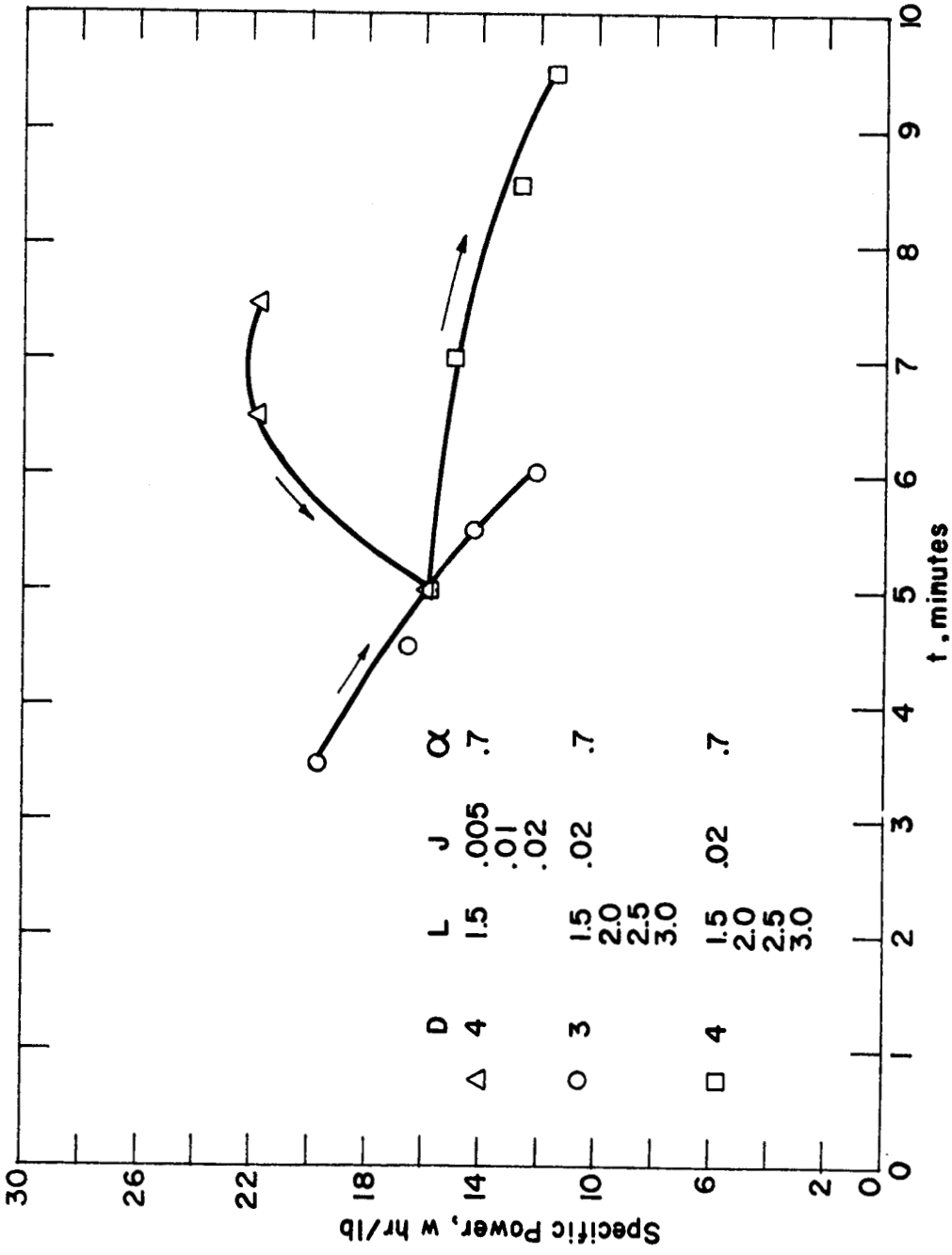

Figure 2.7. Specific Power versus Time.

TABLE 2.6

CONSTANT-CURRENT MODE OF OPERATION

(I_o = 43.5, α = 0.7)

D (cm)	L (cm)	J*	P (W-hr/lb)	t (min)
2	1.5	0.02	22.6	1.0
2	2.0	0.02	19.8	1.5
2	1.5	0.005	26.57	1.5
2	2.0	0.005	20.17	2.0
3	2.5	0.005	14.49	4.0
4	1.5	0.005	22.42	6.0
4	1.5	0.01	21.24	5.5
4	1.5	0.02	19.44	4.5
3	1.5	0.02	23.38	2.5
3	2.0	0.02	16.98	3.5
3	2.5	0.02	17.79	3.5
3	3.0	0.02	11.52	3.5
4	2.0	0.02	15.47	5.5
4	2.5	0.02	12.61	6.0
4	3.0	0.02	10.73	6.0

* Shielding loss - fraction of black-body radiation at 2100°K.

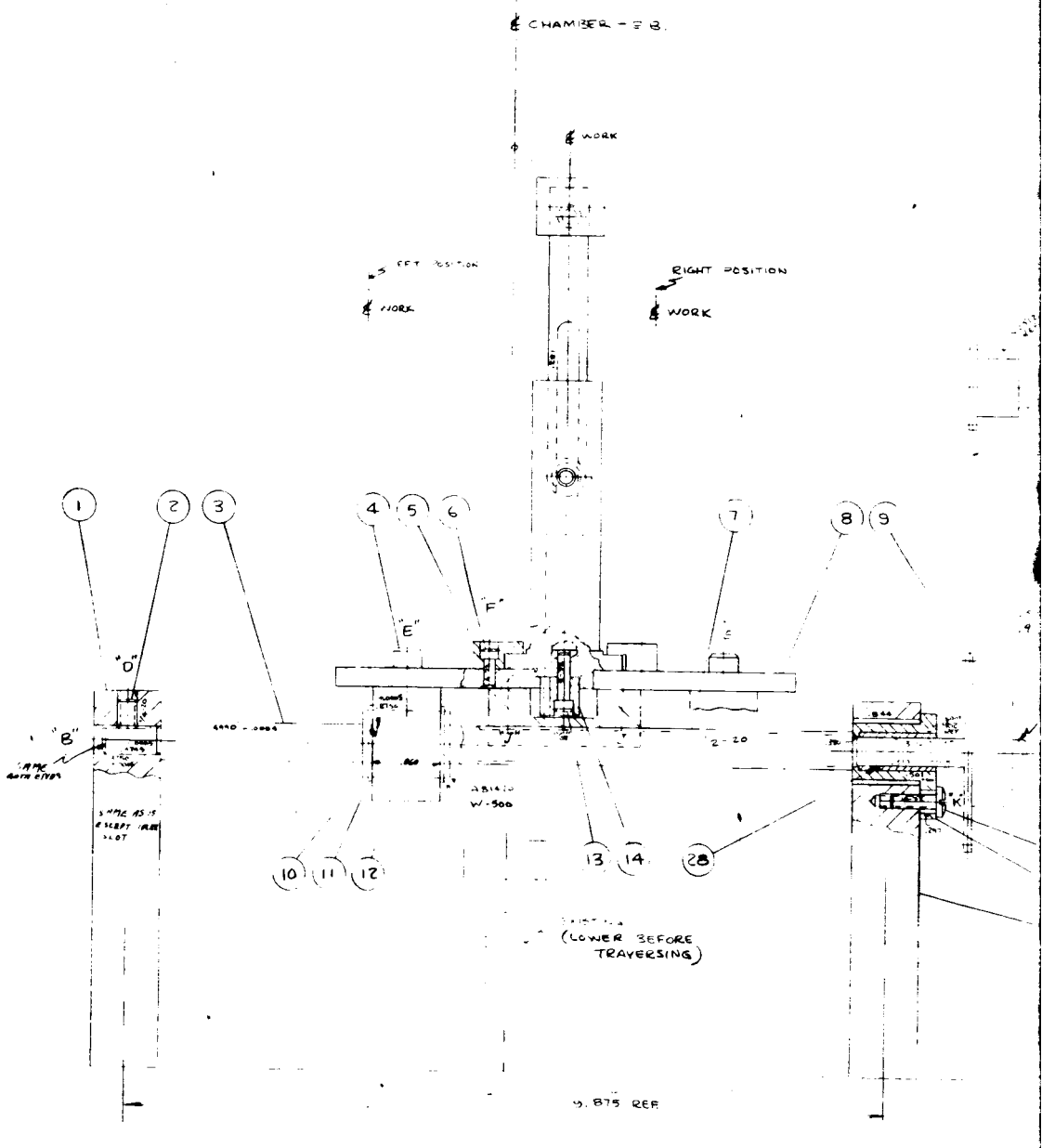

FOLDOUT FRAME

FOLDOUT FRAME

REV	DESCRIPTION	DATE	BY	APPR
A	ADDED PN 32	3-30-65		

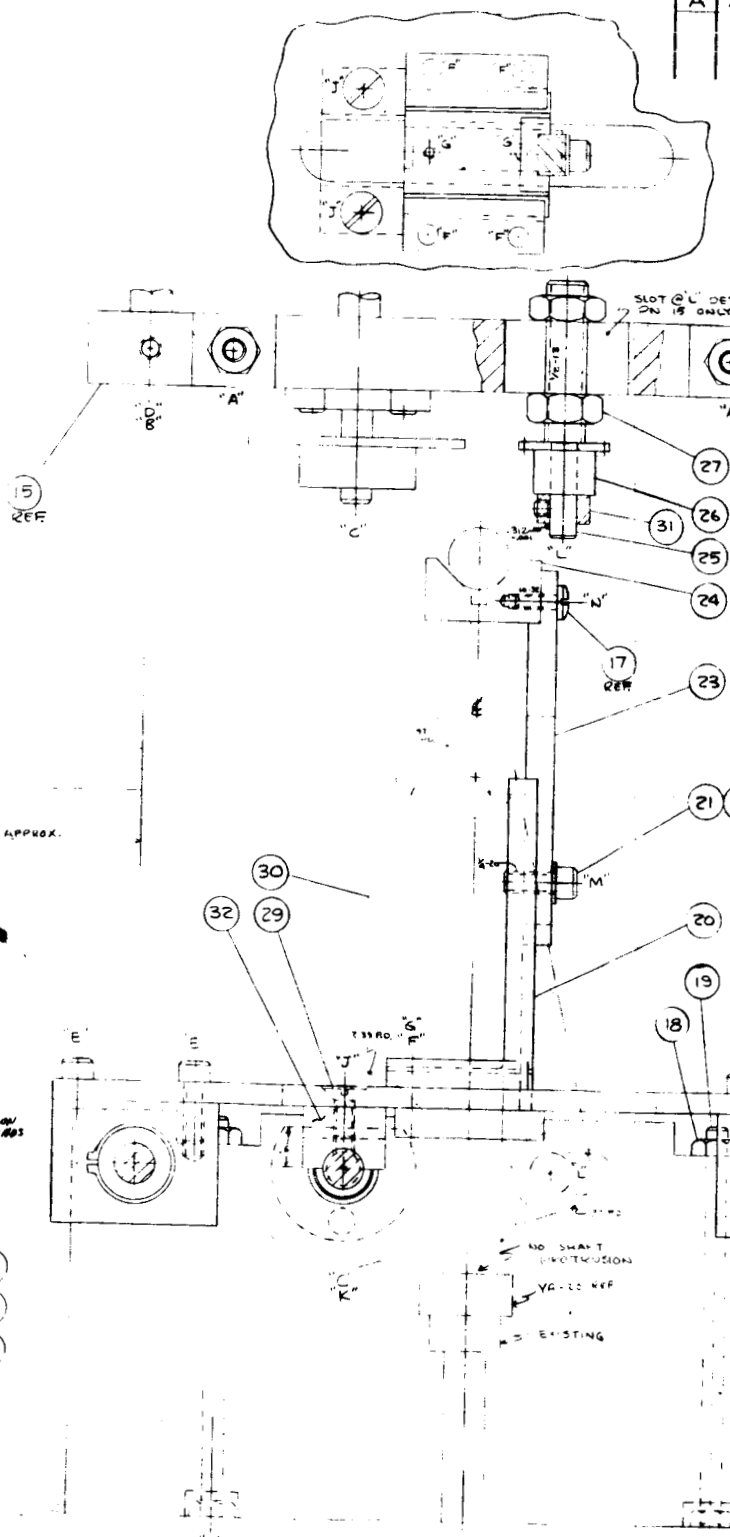

1001	B	1		PN. 16 & 28 PR & BORE
PART	SIZE	REQ	REV.	NOTES
				LAYOUT & SUB-ASSEM

PART	SIZE	REV	REQ	MAT'L	NOTES
32	A	A	1	304 S.S.	
31	ND		1	STEEL	COLLAR - BOST. GEAR # SC31
30	ND		1	STEEL	CHAIN - BOST. GEAR # 25 x 16 APPROX
29	ND		2	ST. ST.	FHMS 1/4-20 x 5/8
28	ND		2	BRONZE	"BEAR-N-BRONZ" BOST. GEAR # MSB-8
27	ND			ST. ST.	HEX. JAM NUT - 1/2-13"
26	ND		1	STEEL	SPROCKET BOST. GEAR # K2512
25	A		1	304 S.S.	
24	A		1	304 S.S.	
23	B		1	304 S.S.	
22	ND		1	ST. ST.	PLAIN WASHER
21	ND		1	ST. ST.	SHCS 1/4-20 x 5/8
20	C		1	304 S.S.	
19	ND		4	ST. ST.	1/4-20 x 4.75 LG.
18	ND		4	ST. ST.	HEX. NUT
17	ND		7	ST. ST.	BHMS # 10-32 x 1/2
16	B		2	304 S.S.	
15	C		1	6061 ALUM.	
14	A		1	STEEL	RACK BOST GEAR # LZ020
13	ND		2	ST. ST.	SHCS # 6-32 x 5/8
12	A		3	304 S.S.	
11	ND		6	ST. ST.	RET. RING THOMSON # W-500-SS
10	ND		3	ST. ST.	BALL BUSH. THOMSON # A-8142-SS
9	ND		1	STEEL	SPROCKET BOST. GEAR # KZ590
8	C		1	304 S.S.	
7	B		1	304 S.S.	
6	ND		4	ST. ST.	SHCS # 6-32 x 3/8
5	A		2	304 S.S.	
4	ND		6	ST. ST.	SHCS 1/4-20 x 3/4
3	B		2	304 S.S.	
2	ND		4	ST. ST.	SET SCR. 1/4-20 x 3/8 FLAT POINT
1	C		1	6061 ALUM.	

UNLESS OTHERWISE SPECIFIED

DECIMAL: X ± .03, .XX ± .01, .XXX ± .005
FILLET RADIUS: .010 MAXIMUM
THREADS: CLASS 2
⌀ DIA. CONC. WITHIN T.I.R.
ALL OTHER DIA. CONC. WITHIN .005 T.I.R.
SURFACES TO BE PERP. WITHIN .005 T.I.R.
SURFACES TO BE PAR. WITHIN .005 T.I.R.
HOLE ANGULAR TOL. 0-2.0 RAD. ± 0° 5'
2.0-4.0 RAD. ± 0° 3'
ALL OTHER ANGULAR TOL. TO BE ± 0° 30'
REMOVE ALL BURRS AND EDGES

SCALE: FULL | FINISH

NEXT ASSY | SIMILAR TO

THERMO ELECTRON

DRAWN	CHECKED	ENGINEER
W/F 3-16-65		

TITLE: TRAVERSING MECH. FOR E.B. WELDER

SIZE	DRAWING NUMBER	REV.
D	534-1000	A

Figure 2.8

FOLDOUT FRAME 2-22

The bottom of the container was designed to be made from 100-mil rhenium plate. First this was to be machined into a circular slug with an electric-discharge machine (EDM) and then the emitter was to be formed with additional EDM cuts. The details are shown in Figure 2.9.

The capsule assembly sequence consisted of first assembling and testing the converter with electron bombardment and then adding the cylindrical part of the capsule, adding the oxide, and finally welding the lid to close the capsule.

To provide the oxide, the program plan was to purchase purified beryllia and magnesia powder, check the purity, conduct additional purification if necessary, mix the powders, and finally melt the mixture in vacuum to form solid oxide slugs which could be inserted into the capsule.

2.3.2 Converter

Of the various thermionic converters available at the outset of this program, the Series VIII SET converter was the most advanced and the most reliable. In addition, its performance was well documented over a wide range of operating conditions. This converter is shown in Figure 2.10 (Dwg. 479-1000, Rev. L).

The emitter of this converter was constructed of rhenium sheet 20 mils thick, isostatically pressure-bonded to a tantalum substrate that formed a portion of the cavity of a solar-powered generator. The cavity piece and the rhenium emitter are shown in Figure 2.10 as part 1001, which is electron-beam welded to a thin tantalum emitter support sleeve shown as part 20. This sleeve is about 3 mils thick and functions both as the emitter support and as one current lead.

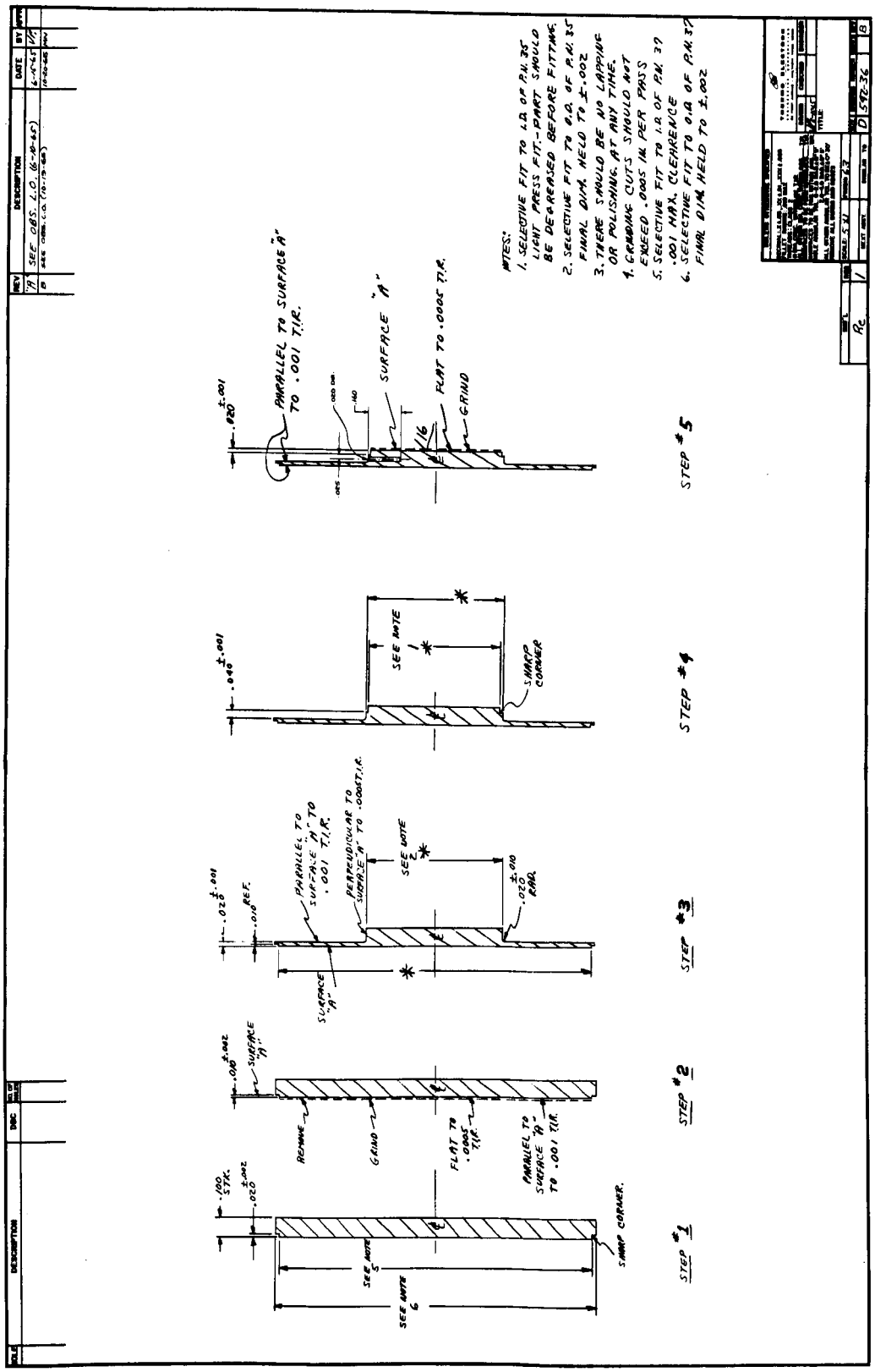

Figure 2.9. Emitter and Oxide Container Bottom.

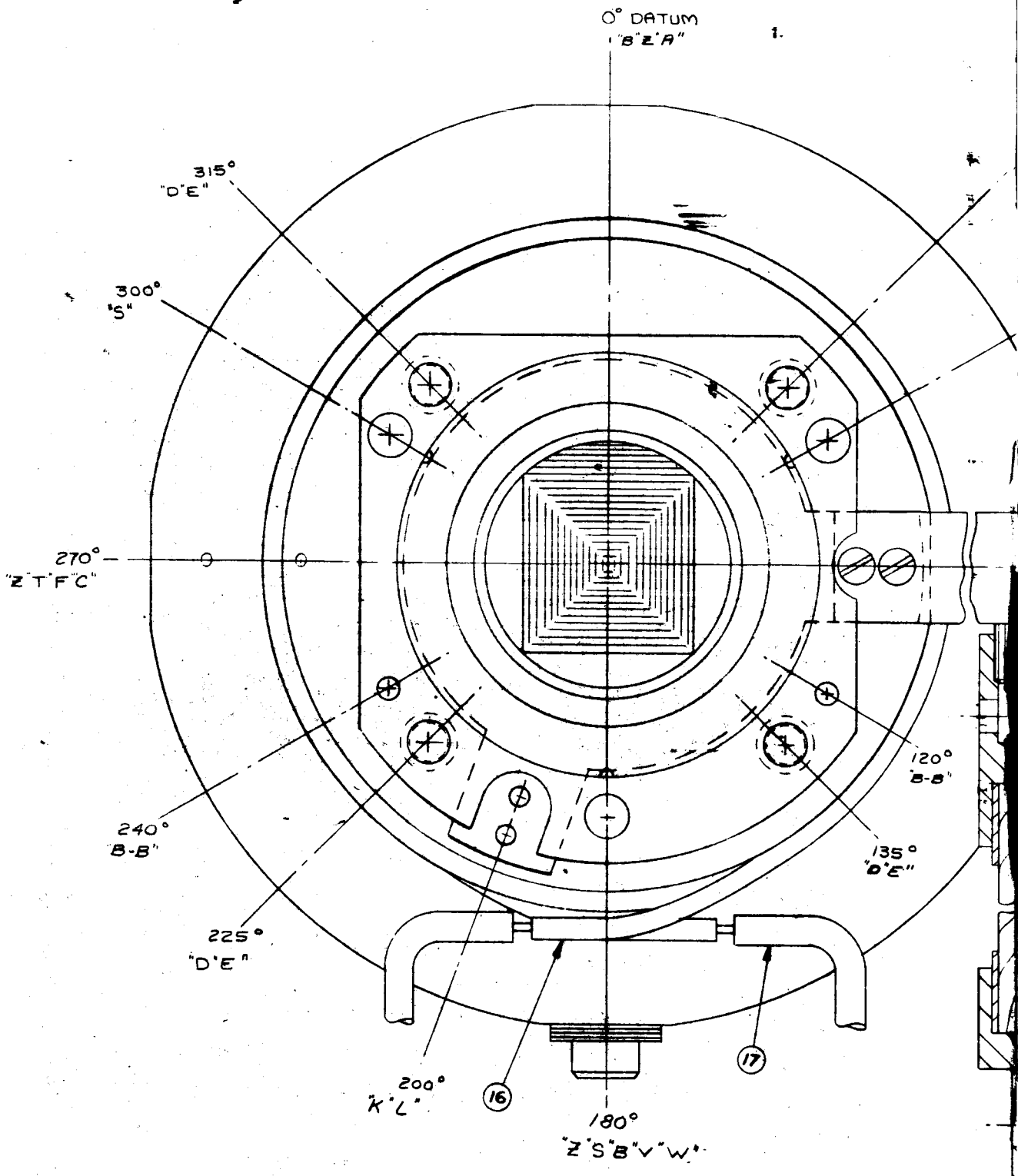
0° DATUM
"B" "Z" "A"
315°
"D" "E"
300°
"S"
270°
"Z" "T" "F" "C"
240°
B-B
225°
"D" "E"
200°
"K" "L"
16
180°
"Z" "S" "B" "V" "W"
17
120°
B-B
135°
"D" "E"

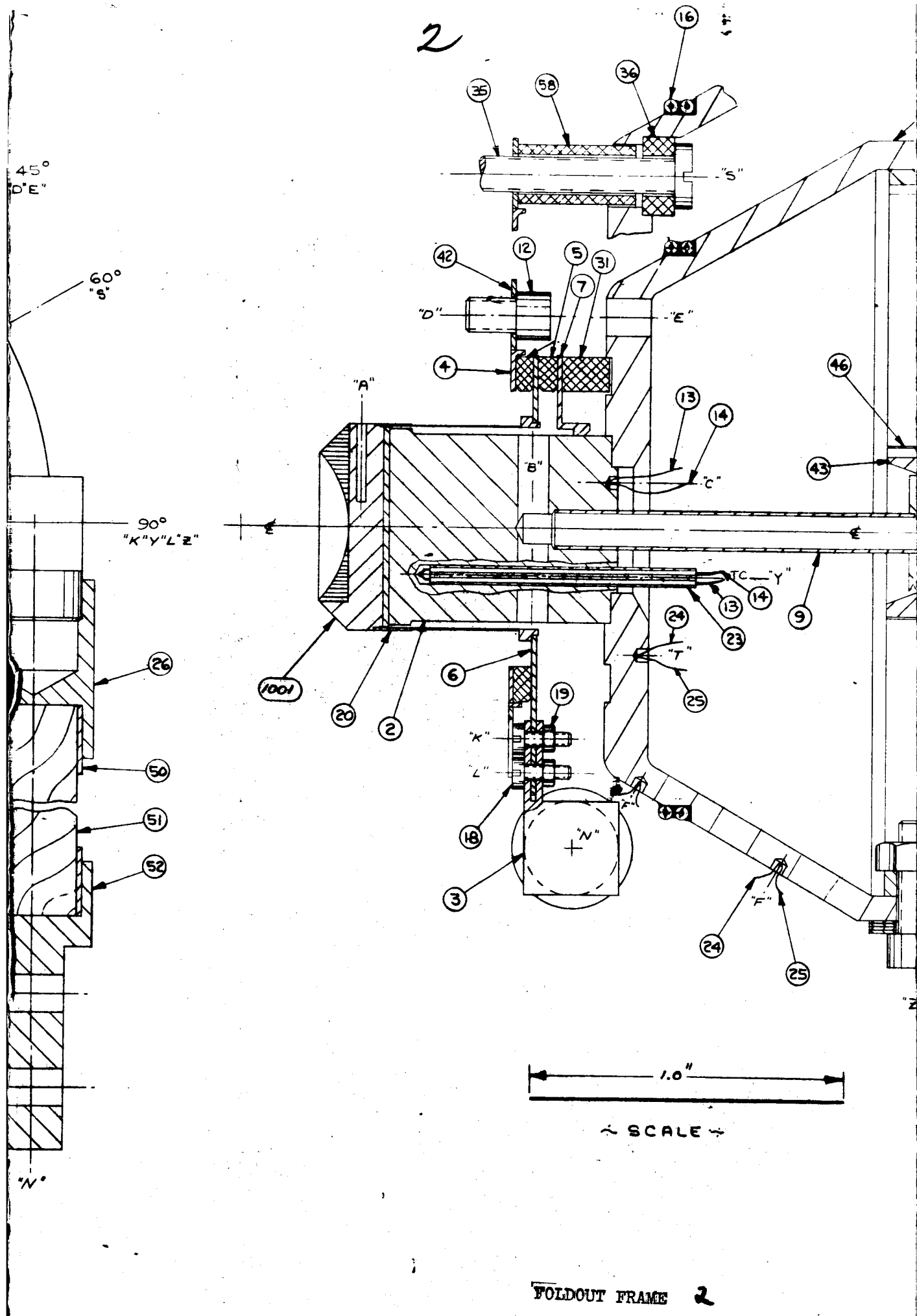

FOLDOUT FRAME 2

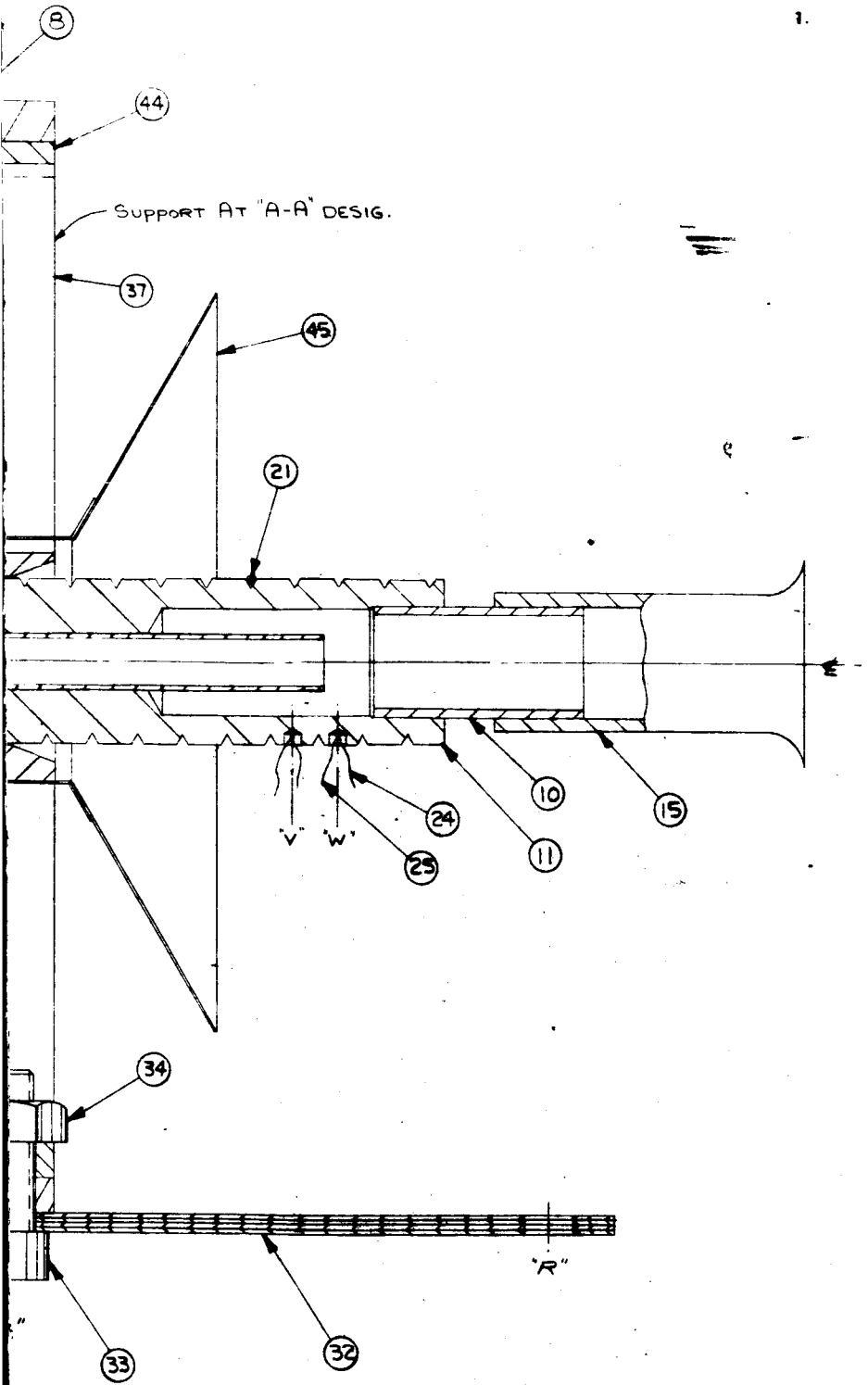
8
44
SUPPORT AT "A-A" DESIG.
37
45
21
"V"
"W"
24
23
10
11
15
34
"R"
33
32

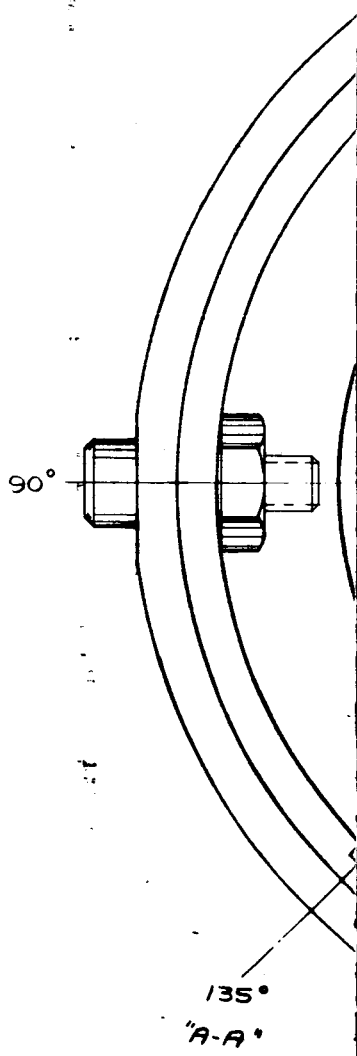
90°
135°
"A-A"

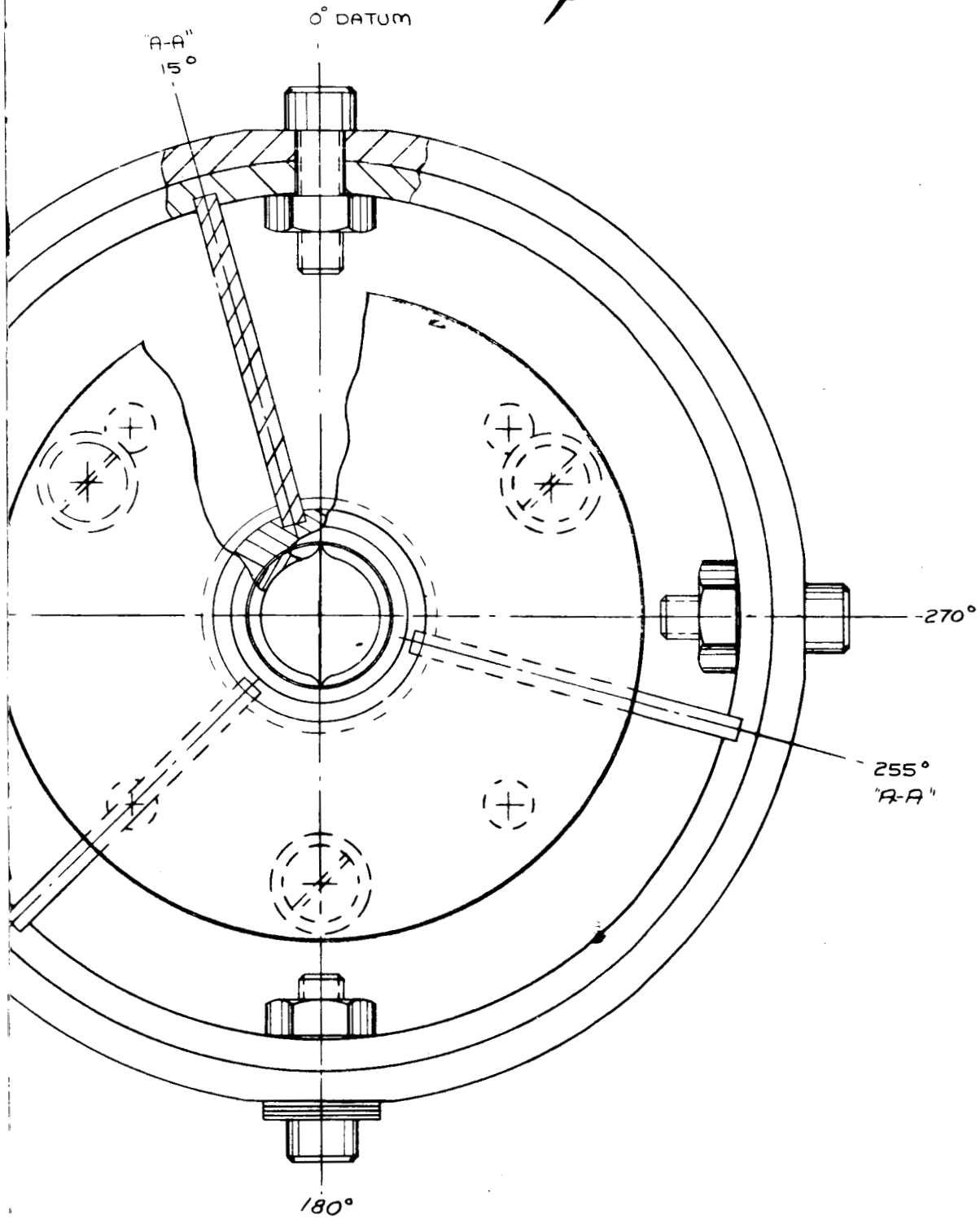

FOLDOUT FRAME 4

ITEM	SIZE	REV	REQ	MAT'L	NOTES
					FIN. 47,48,49 PRESS. BOND.
58	A		3	Al_2O_3	
57					
56					
55					
54					
53					
52	B		1	Cu	
51	B		1	Cu	
50	B		2	Ni	
49	A		1	Ta	
48	A		1	Ta	
47	A		1	Re	
46	C		1	Ni	
45	B		1	Ni	
44	D		1	S.S.	
43	B		1	S.S.	
42	C	D	1	Nb	
41	OBS.				
40	OBS.				
39	OBS.				
38	OBS.				
37	B		3	S.S	
36	A	C	3	Al_2O_3	
35	ND	–	3	S.S	#4-40 x .750 LG. R.H.C.S.
34	ND	–	4	S.S.	#4-40 HEX NUT
33	ND	–	4	S.S.	#4-40 X .38 LG S.H.C.S.
32	B		4	Cu	
31	B		1	Al_2O_3	
30					
29					
28					
27					
26	B		1	Cu	
25	ND	–	2	Alumel	
24	ND	–	2	Chromel	
23	ND	–	1	Al_2O_3	
22	ND		AS REQ'D	ASTRO CERAM	
21	ND	–	AS REQ'D		HEATER
20	C		1	Ta	
19	ND	–	2	S.S.	#00-96 HEX NUT
18	ND	–	2	S.S.	#00-96 X .125 LG
17	B		4	Cu	
16	ND	–	AS REQ'D		SHEATHED HEATER
15	C		1	Cu	
14	ND	–	1	Alumel	
13	ND	–	1	Chromel	
12	A	A	4	S.S.	#4-40 S.H.C.S. (MODIFIED)
11	C		1	Ni	
10	C		1	Ni	
9	C		1	Ni	
8	D	D	1	Cu	
7	C		1	Nb	
6	C	B	1	Nb	
5	B		2	Al_2O_3	
4	B		1	Nb	
3	C	A	1	Nb	
2	C		1	Mo	
1	A	A	1	Ta	

THERMO ELECTRON
THE ETHYLENE CORPORATION
85 FIRST AVENUE · WALTHAM MASS 02154

DRAWN	CHECKED	ENGINEER
MN		

TITLE: VIII-P-3

SIZE	DRAWING NUMBER	SHEET	REV
H	479-1000	1	L

Figure 2.10

FOLDOUT FRAME 5

The sleeve is brazed at the end opposite the emitter to a flat niobium flange, part 6.

The seal structure of the converter consists of two niobium flanges, parts 6 and 7, brazed to an aluminum oxide insulator, part 5. This latter flange, part 7, is brazed to a molybdenum collector, part 2. The collector is brazed to a copper radiator, part 8, which is coated with chrome oxide to maximize its emissivity.

The interelectrode spacing of this converter is established by the thermal expansion of the emitter and seal structure relative to the collector. With the emitter at 2000°K and the collector at 1000°K, the spacing is about 2.2 mils. At room temperature the emitter and collector surfaces touch.

A cesium reservoir, formed of parts 15, 10, and 11, communicates with the converter through a nickel tubulation, part 9. The reservoir is supported in the direction transverse to the diode axis by means of a spider with the three supports formed of parts 44, 37 and 43. A thin radiation shield, parts 45 and 46, avoids overheating of the reservoir due to radiation from the inner surface of the radiator.

The converter is held to the generator by a niobium flange, parts 4 and 42, and by four stainless screws, part 12.

Work conducted prior to this program had shown good compatibility between the 3 BeO-2 MgO oxide and rhenium containers. Rhenium was consequently chosen as the container material for the TES model. The existence of brittle intermetallics between rhenium and tantalum required that the emitter and emitter support of the converter be made of rhenium or of some other refractory metal that did

not exhibit such intermetallics with rhenium. Because of Thermo Electron's previous experience in joining rhenium to rhenium by welding, the converter's emitter and sleeve were redesigned to be made of rhenium. The difference in thermal expansion between tantalum and rhenium resulted in a difference in interelectrode spacing, as shown by the following calculations.

Figure 2.11 shows the components considered in calculating the spacing of the diode. The emitter and collector surfaces were assumed to be just touching at room temperature. The spacing when the emitter was at 1900°C was calculated as follows:

Expansion of rhenium at 1900°C is 13.9 mils/in.
Expansion of rhenium at 1500°C is 10.96 mils/in.
Expansion of niobium at 700°C is 5.40 mils/in.
Expansion of molybdenum at 650°C is 3.56 mils/in.

The total expansion of the emitter face from the reference plane was:

$$0.220(5.40) + 0.440(10.96) - 0.050(13.9) = 5.32 \text{ mils}$$

The total expansion of the collector face from the reference plane was:

$$0.610(3.56) = 2.17 \text{ mils}$$

The difference in expansions was the spacing, namely, 3.15 mils.

Figure 2.11 also illustrates the means of joining the emitter support sleeve to the upper seal flange. In the Series VIII converter, a tantalum sleeve is beam-welded at its base to a thin niobium flange,

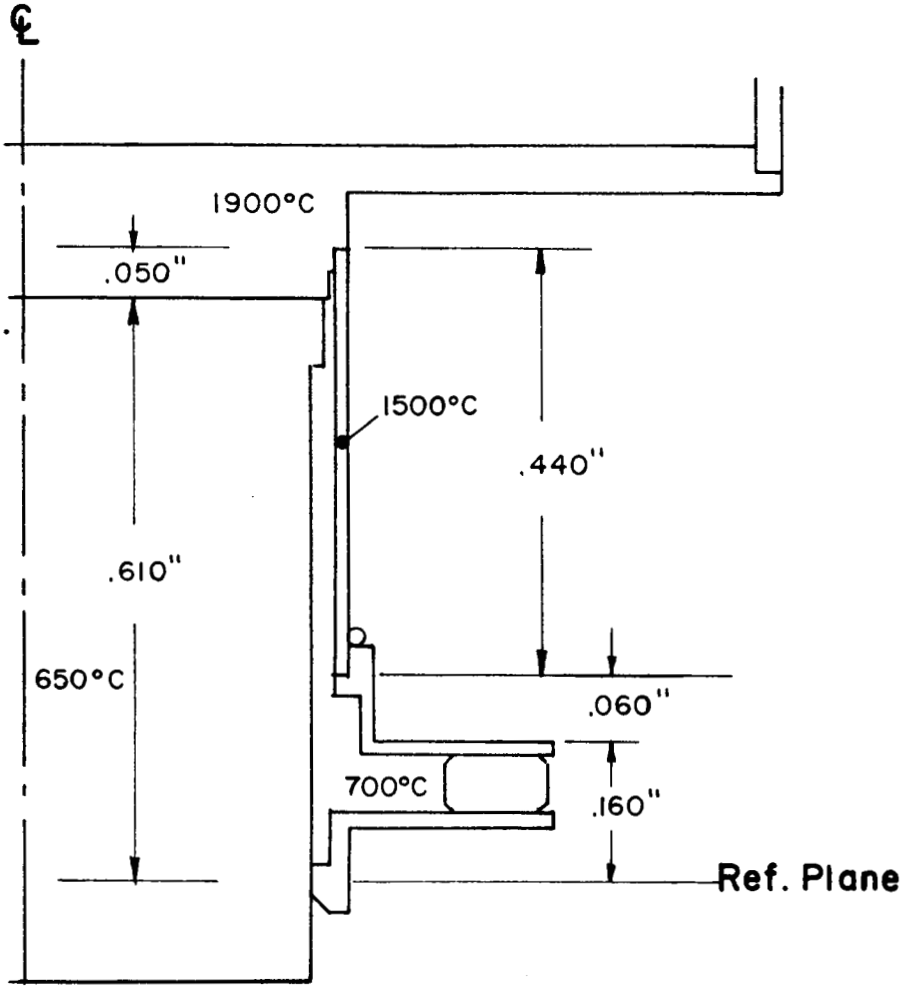

Figure 2.11. Schematic of Emitter-Collector Sub-Assembly.

which is brazed to the insulator ceramic. Because tantalum and niobium do not form brittle intermetallics upon melting, the joint is quite strong. However, since rhenium and niobium do have intermetallic compounds, beam-welding of the joint was undesirable, and brazing (which could be accomplished at much lower temperature) was preferable. To allow for relief of the stress at the rhenium-niobium joint caused by differences in the thermal expansion behavior of both metals, the niobium flange included a section concentric with the collector to permit deflection without placing the strain directly on the metal-to-ceramic joint.

The rhenium sleeve selected for the converter was 8 mils thick, and was ordered from Chase Brass and Copper. This vendor had previously supplied 12-mil tubing which had been incorporated successfully into several thermionic devices, and felt reasonably confident of being able to supply the 8-mil tubing. Because of the unique work-hardening properties of rhenium, which could complicate making accurate thin circular tubes, they were unwilling to attempt any thicknesses less than 8 mils. With an 8-mil sleeve, the heat conduction to the seal would increase over that normally found in the Series VIII converter, but from preliminary calculations the additional amount was not expected to cause overheating of the seal assembly.

Having chosen to construct the oxide container, the emitter, and the emitter support sleeve of rhenium, the most logical way to construct the emitter was to make it part of the bottom of the oxide container. In this way the thermal resistance from the oxide to the emitting surface was minimized. Figure 2.11 shows the way in which the bottom of the container was machined to form an emitter with an emitting area of 2 cm^2. The side of the emitter was grooved to

accommodate the rhenium support sleeve, which in turn was electron-beam welded to the emitter. A hohlraum was provided just above this joint for pyrometric temperature measurements.

2.3.3 Shielding

As can be seen from the calculations in Section 2.2, the operating time of the TES model was expected to be a strong function of the heat losses from the sides and top of the oxide capsule. The model operates in vacuum, and therefore the only mode of loss is radiation.

To minimize radiation losses, a multiple-shield enclosure was designed. It covered both the oxide capsule and an electron-bombardment filament for use in melting the oxide. Figure 2.12 shows the entire TES model design. The capsule is surrounded by two annular rings, parts 41 and 42. These support an electron-bombardment filament, part 43, and are held by two support arms, parts 40 and 44. The radiation shields enclose both the gun and the oxide capsule.

In order to minimize changes in emissivity of the radiation shields adjacent to the capsule and of the capsule surface as evaporation of surface material occurs, the first three shields were designed of rhenium, the same material as the oxide container. Subsequent shield layers were designed of tantalum for ease of fabrication. Past experience had shown that up to 10 layers of carefully spaced shields produced measurable and significant reductions in radiation. Further layers accomplished little and merely complicated the fabrication. Ten shield layers were used throughout in this design. Care was taken to stagger and overlap the end joints in order to minimize end losses.

In order to minimize conduction between adjacent shields, dimples were formed in the material and these acted as point contacts. Such separation was not planned for the three rhenium shields because of the difficulty of forming the metal.

As can be seen from Figure 2.12, the radiation shields were extended beyond the capsule to enclose the emitter support sleeve also.

Holes were provided in the shield assemblies for the two bombardment gun supports. Another hole, also shown in Figure 2.12, was placed in line with the emitter hohlraum to allow pyrometric observation of the emitter temperature.

Figures 2.13 through 2.20 show the shield assembly in more detail.

2.3.4 Heater

The design of the heater for melting the oxide was determined primarily by the necessity of heating the side of the capsule because of the void between the oxide and the lid. Consideration was given to the use of rhenium fins attached to the container lid and extending into the oxide to provide a means of transferring heat from the top, but this approach entailed a very complicated lid structure. Furthermore, the use of fins also dictated the use of powdered oxide to allow the lid to be inserted. Pre-melting the oxide was considered important both for outgassing and for purification.

Radiation heat transfer between the lid and the oxide might also be used to melt the oxide. However, the lid would then have to be raised to a temperature significantly higher than the melting point of the oxide. This method was deemed inadvisable because no compatibility data was available for rhenium and the oxide in this temperature range.

6038

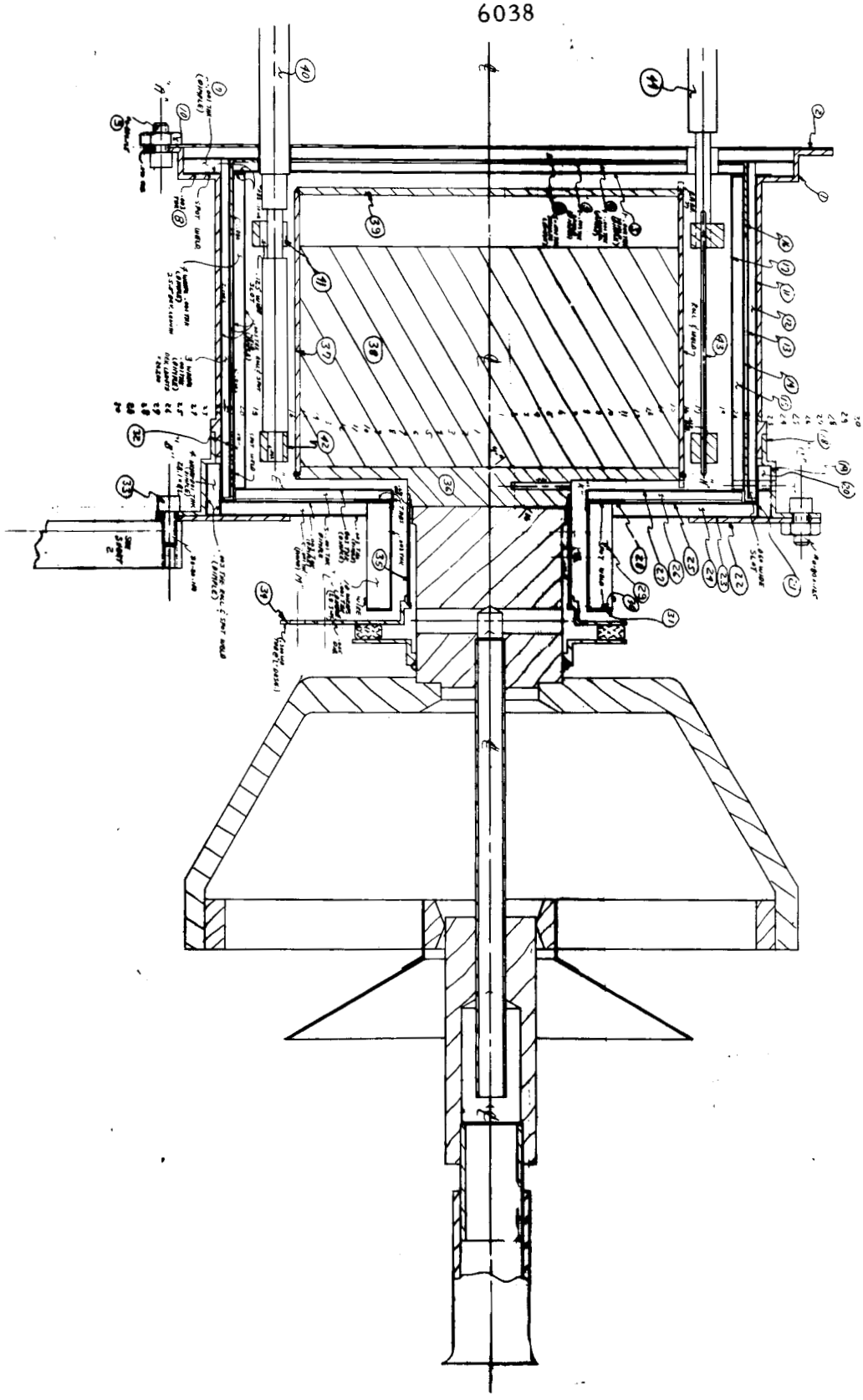

Figure 2.12. Layout of TES Model.

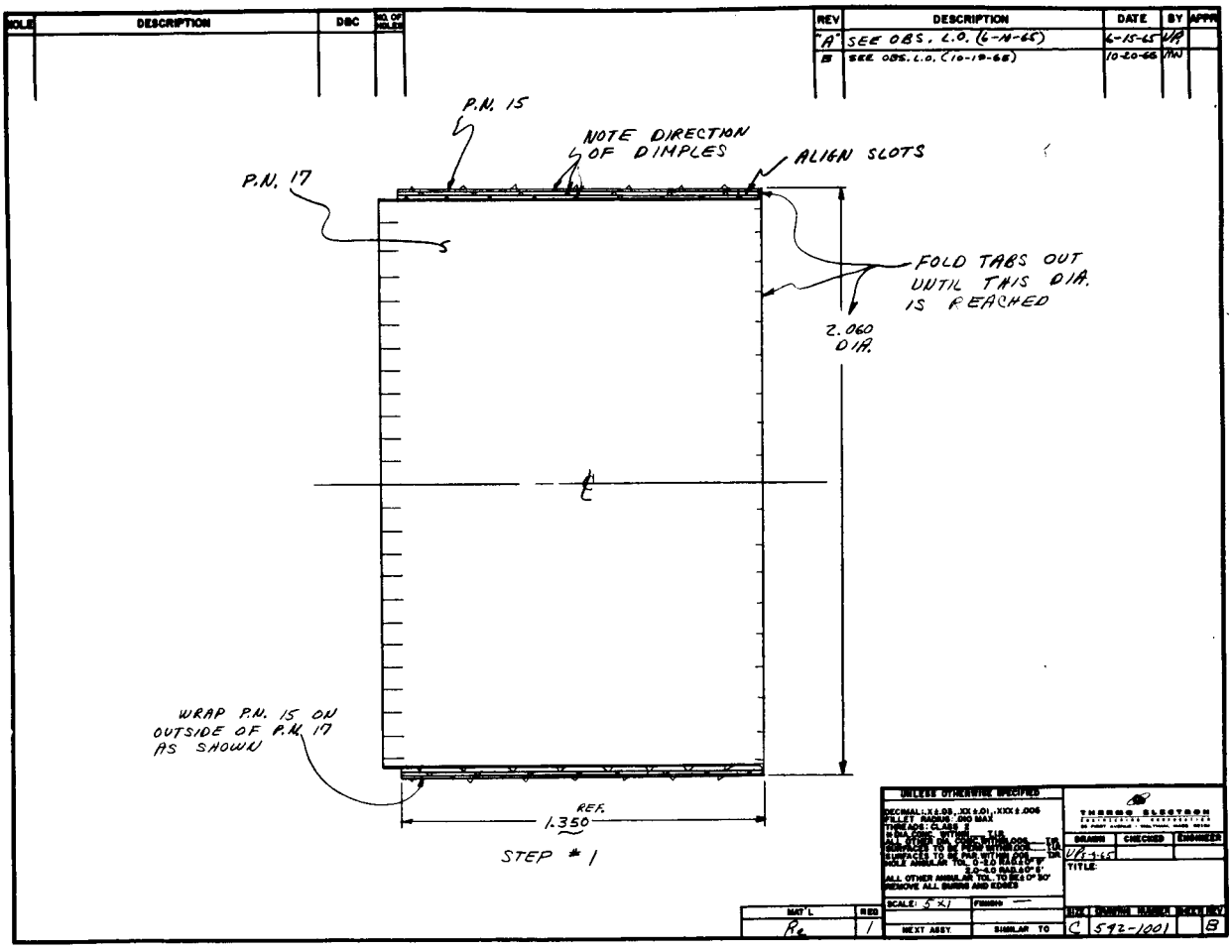

Figure 2.13. Radiation Shield Assembly.

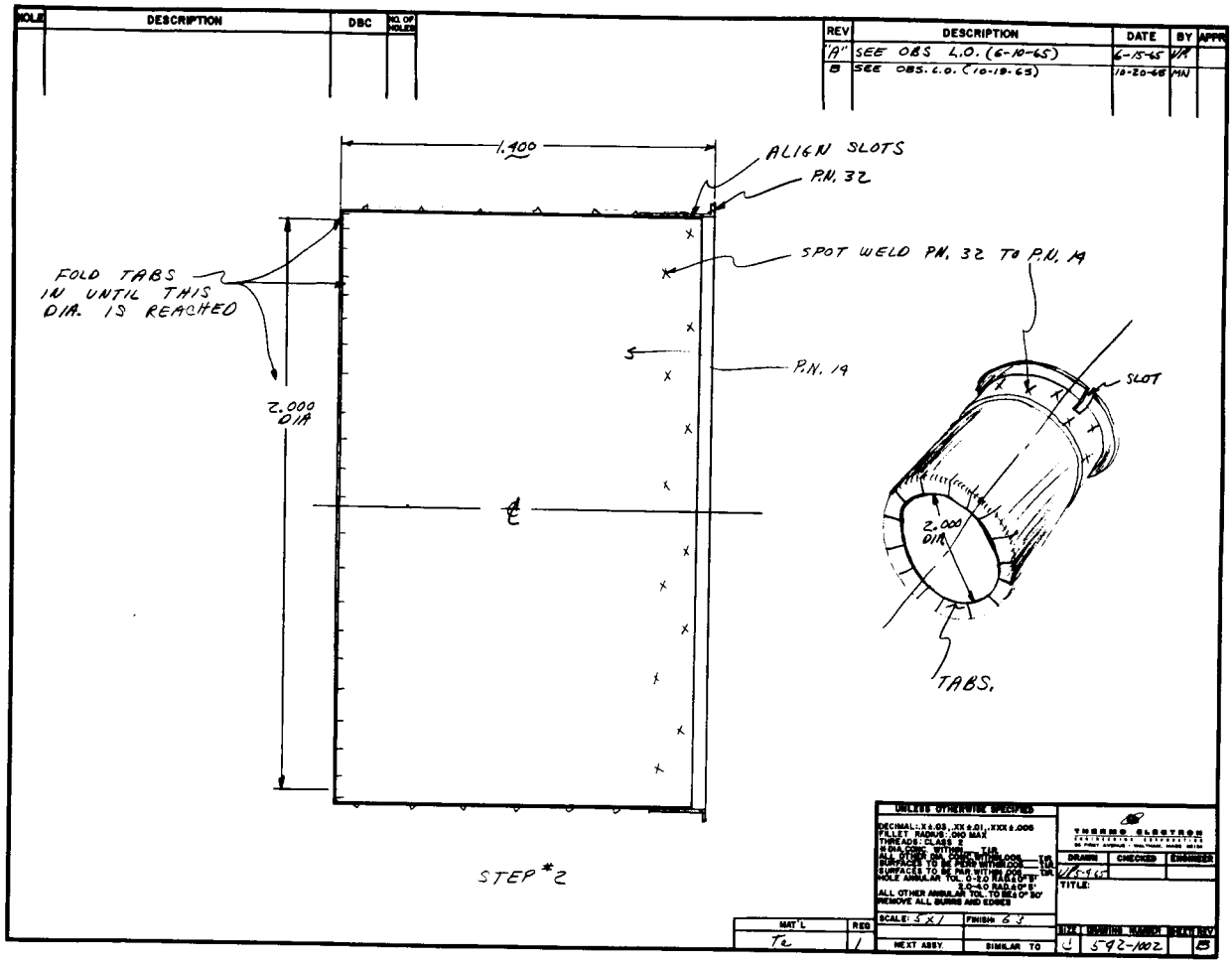

Figure 2.14. Radiation Shield Subassembly.

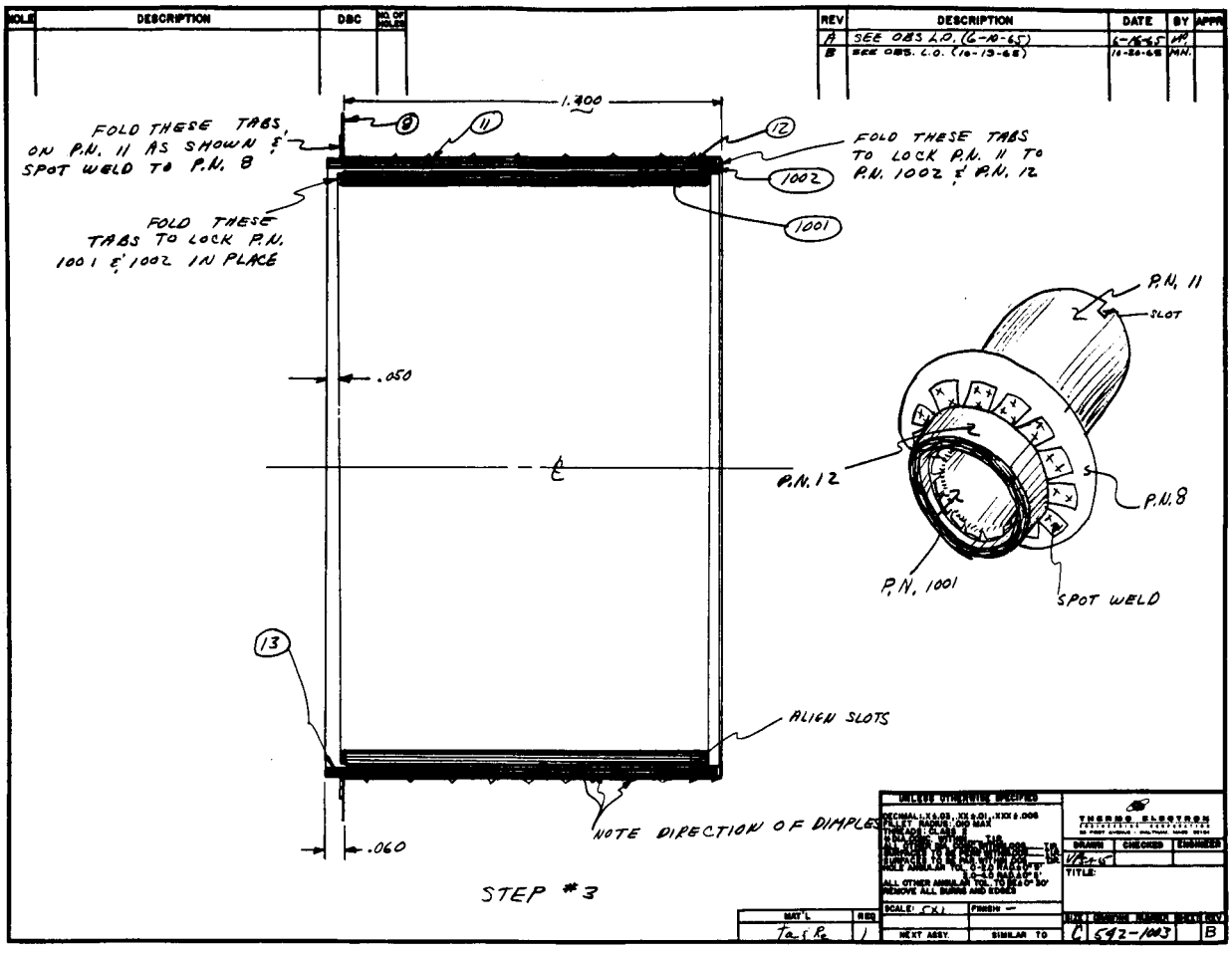

Figure 2.15. Radiation Shield Subassembly.

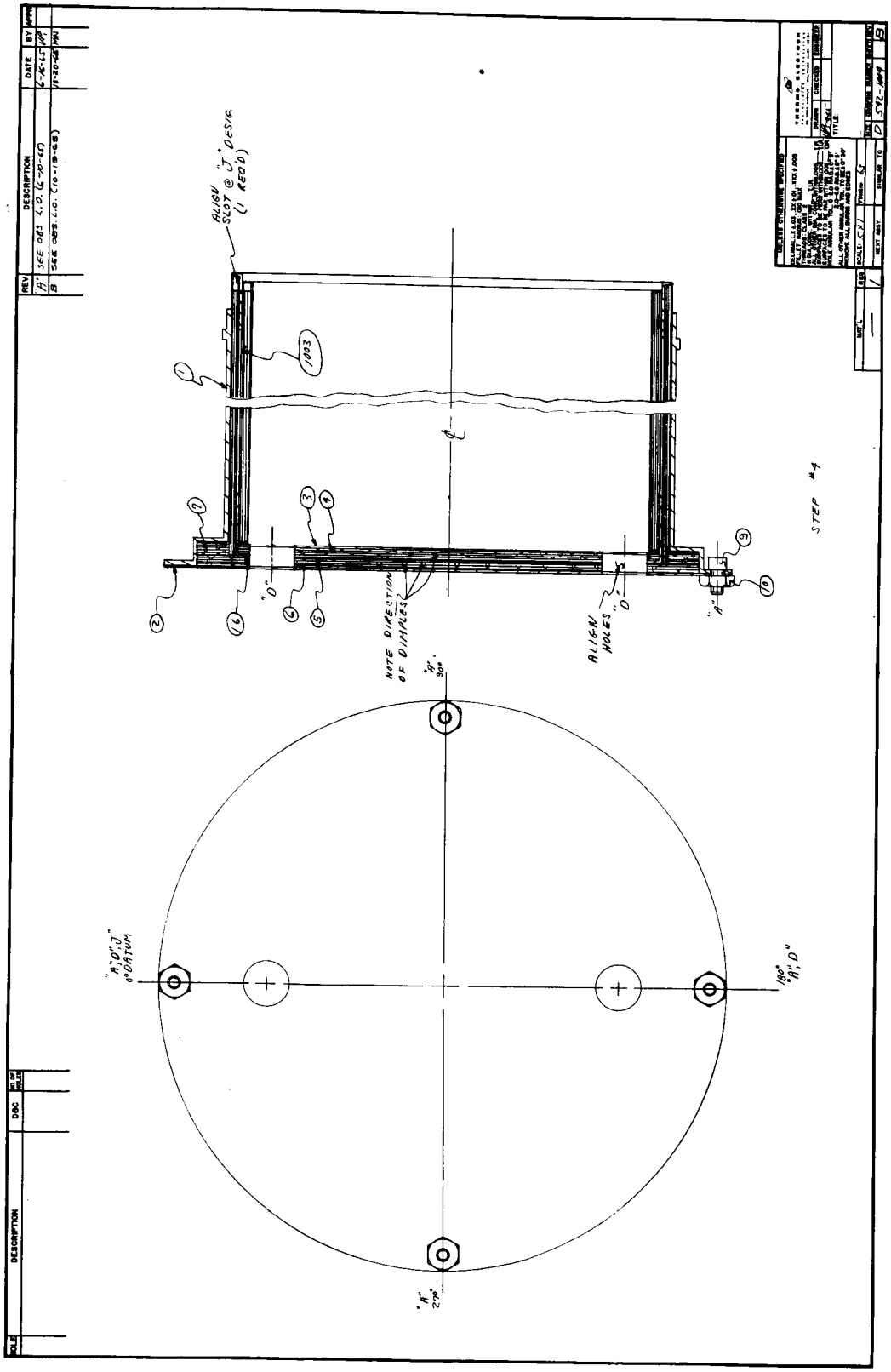

Figure 2.16. Radiation Shield Subassembly.

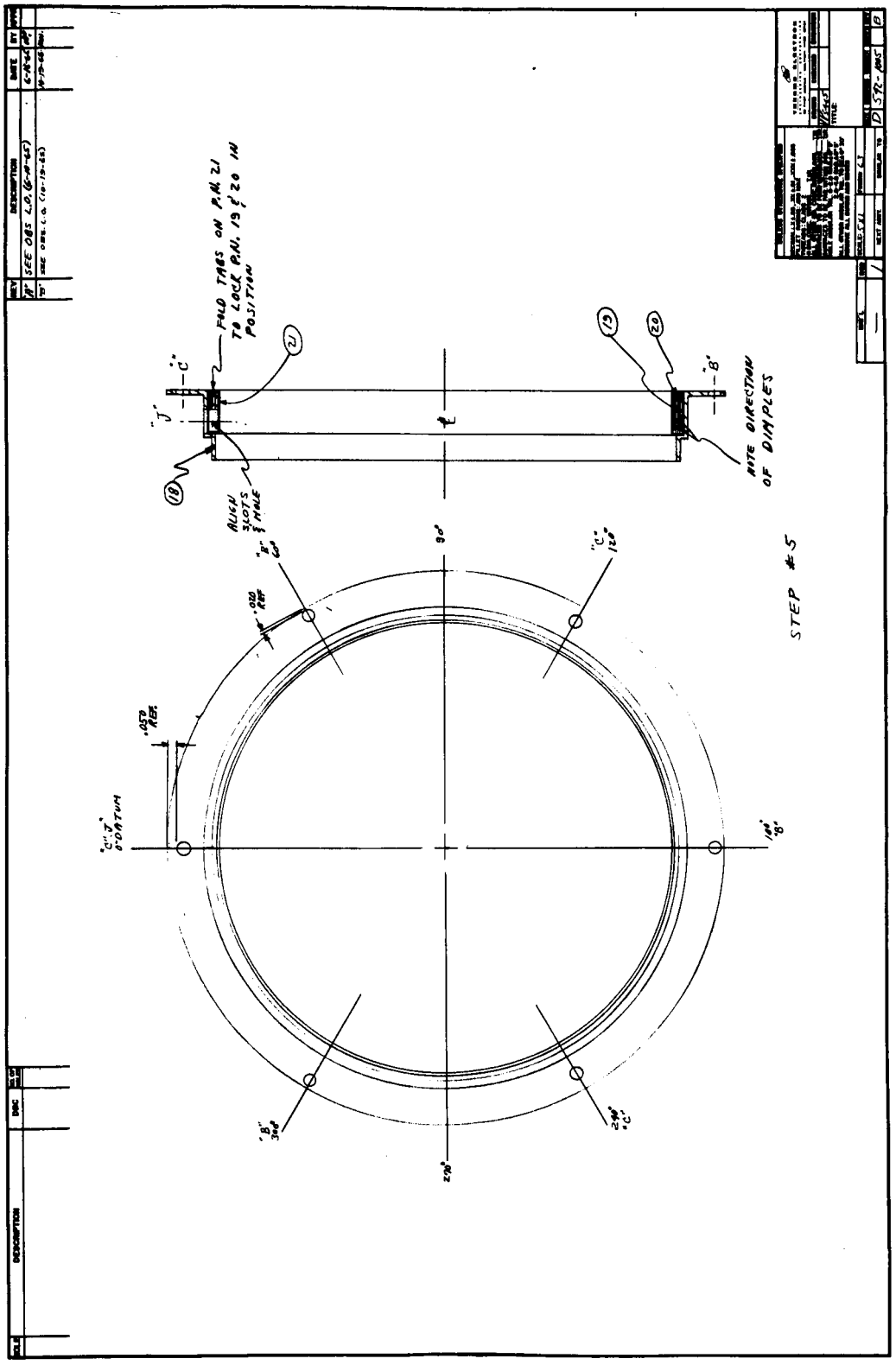

Figure 2.17. Radiation Shield Subassembly.

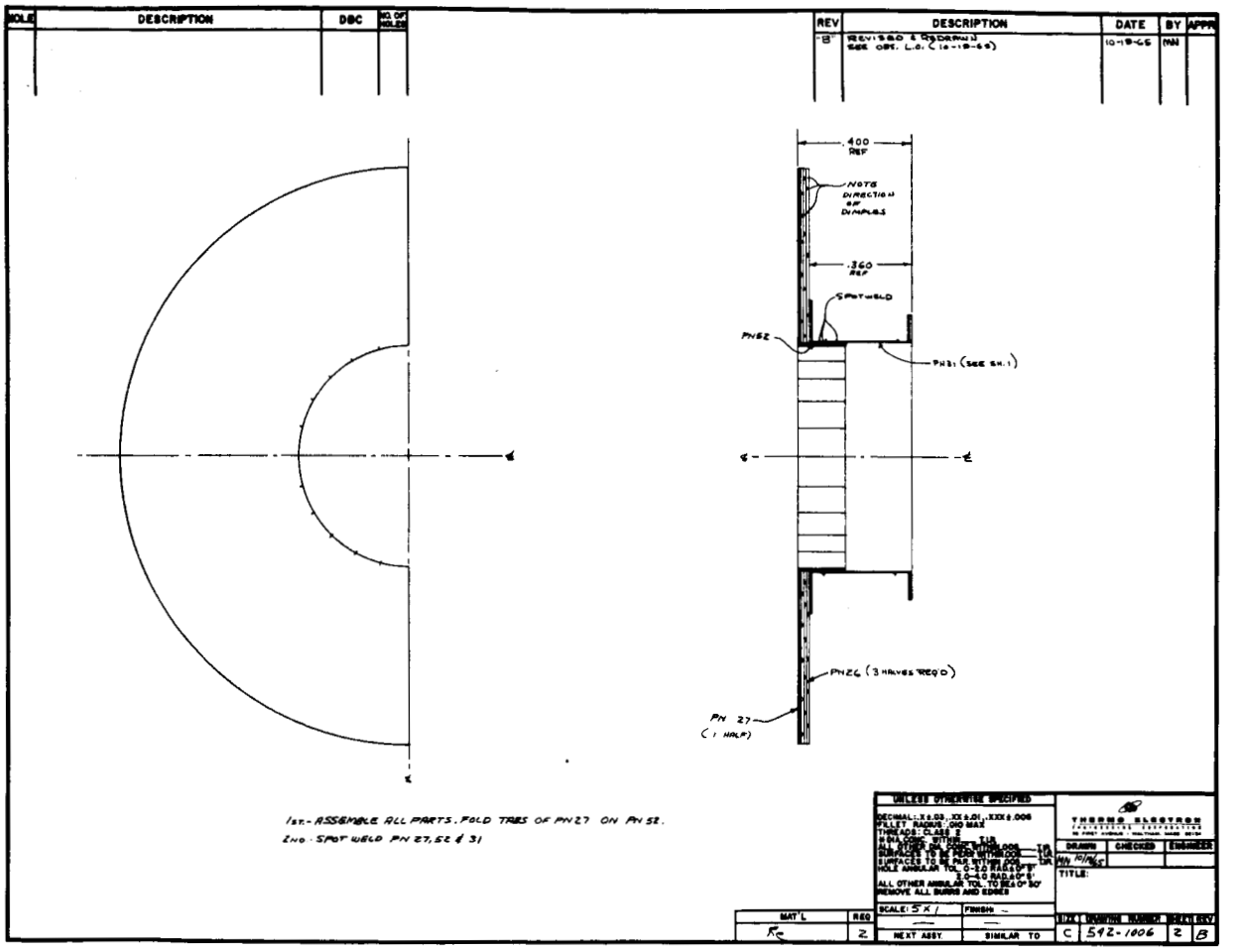

Figure 2.18. Radiation Shield Subassembly.

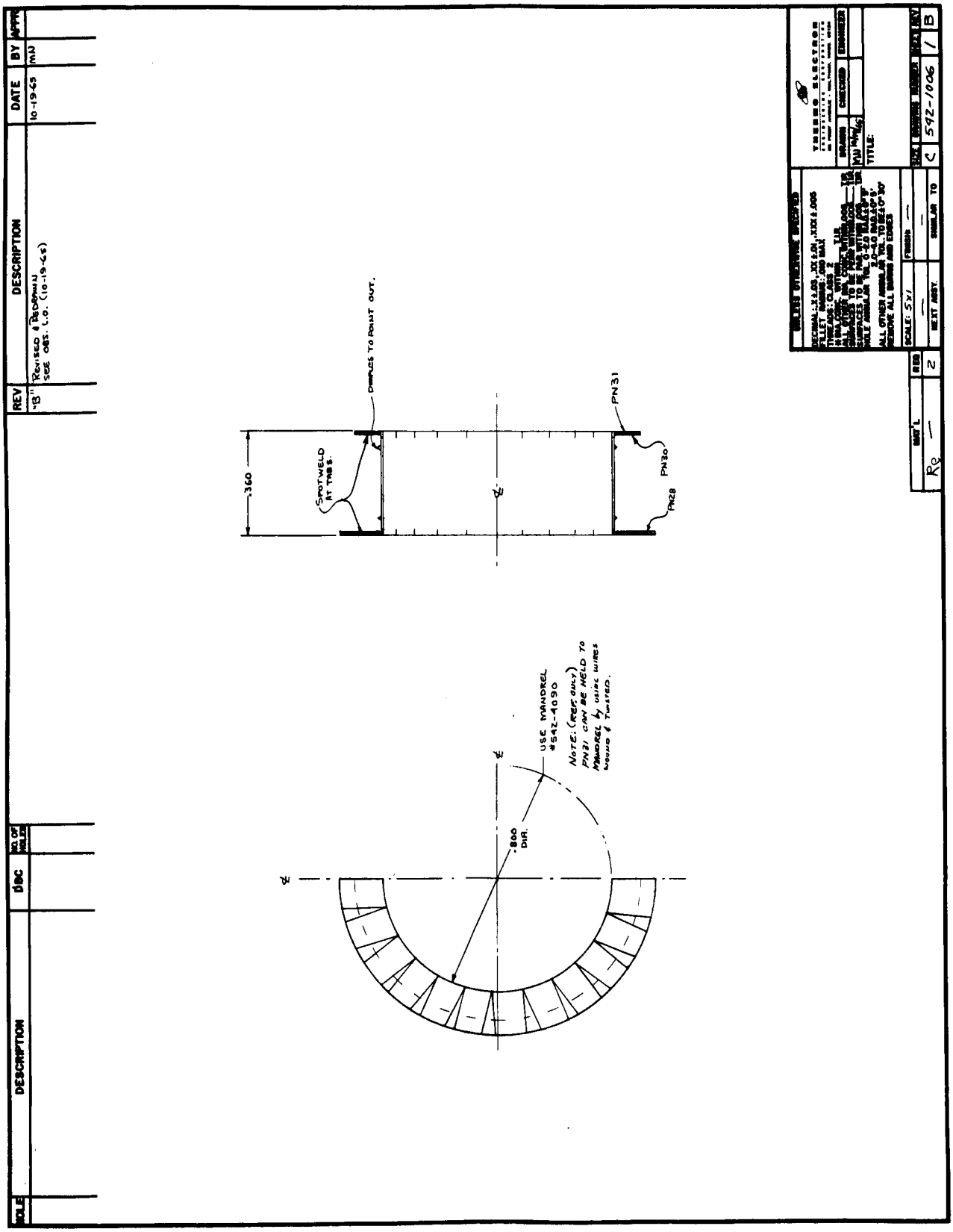

Figure 2.19. Radiation Shield Subassembly.

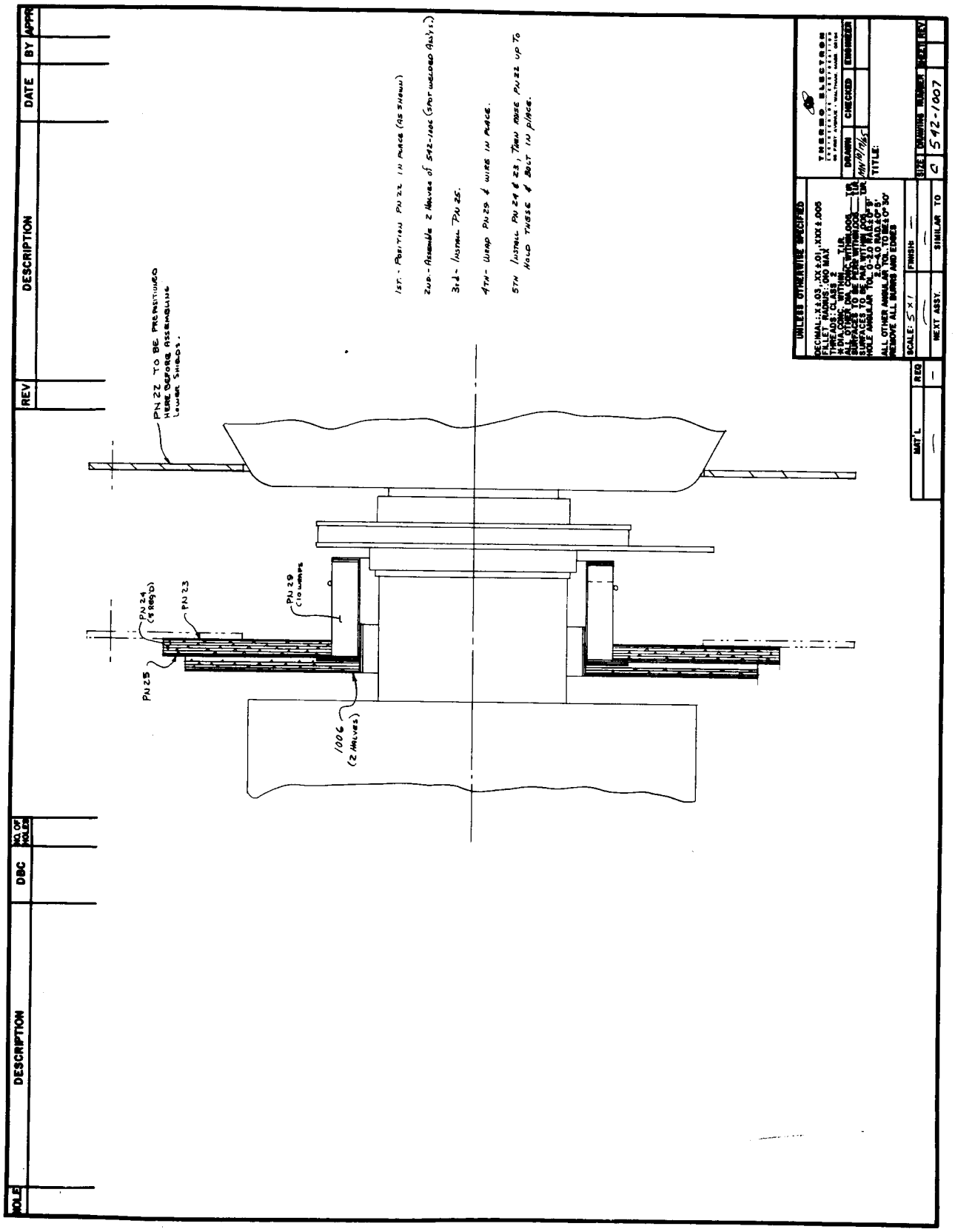

Figure 2.20. Radiation Shield Subassembly.

The two remaining alternatives were direct radiation heating of the side of the capsule or electron bombardment of the side. The latter was chosen since it required a lower filament temperature.

The electron-bombardment gun design was similar to that used many times to heat thermionic diodes except that it was designed for cylindrical geometry. Two support arms of tantalum held two annular rings, also of tantalum. These components were made relatively heavy to minimize joule heating and to conduct heat away to the support structure. The annular rings supported a tungsten wire filament. The design is shown in Figure 2.12. The two vertical supports were then merely attached to an external support structure and to the input current leads. Because the heating efficiency was only of secondary interest, heat loss from conduction from the filament to the external support structure was not important

2.3.5 Test Setup

The design of the test setup is shown in Figure 2.21. Three support legs in the form of threaded rods held a flat plate that supported the converter and the capsule from the converter's radiator. A second plate supported the radiation shield assembly, and a third supported the bombardment gun. A base plate was provided with suitable feedthroughs to accommodate the various leads. The bombardment gun could be moved relative to its support plate to allow accurate positioning with respect to the capsule.

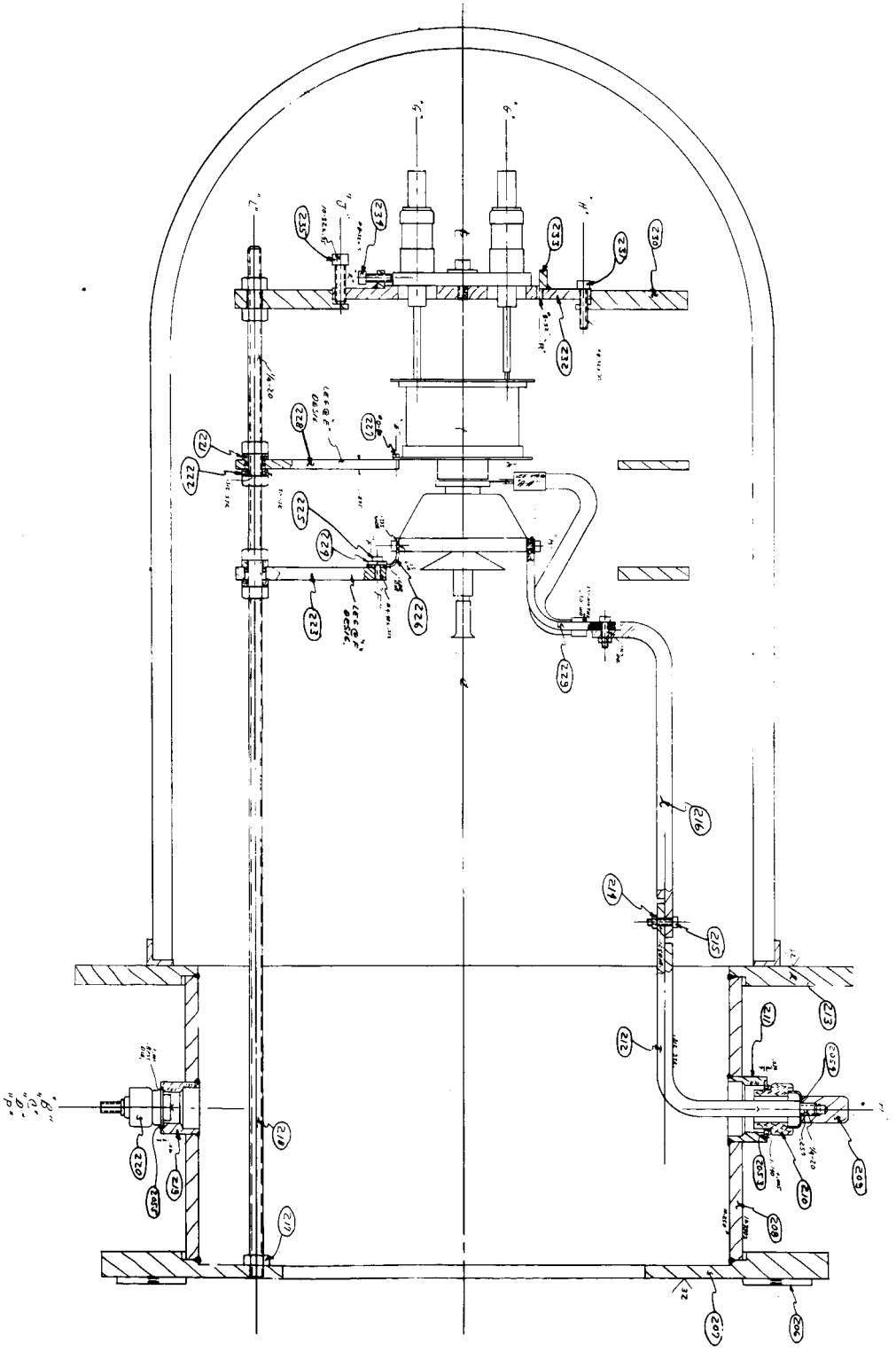

Figure 2.21. Layout of Test Setup.

The manufacturer's certified analysis for this type of rhenium sheet typically showed a total impurity content of 50 ppm. To verify an analysis of impurities of such small quantities requires a series of standards, made by adding measured amounts of impurities to a pure rhenium matrix. This is a long and expensive process, and requires exceptional care. The best laboratory in the country for this type of work was that of Chase Brass and Copper Company, which supplied the rhenium. Their work on the analysis of rhenium for trace impurities had developed the methods and the standards used by other analysts. However, to check against any gross errors, a sample was analyzed quantitatively; this analysis agreed within an order of magnitude with that of Chase Brass.

These examinations confirmed that both satisfactory and unsatisfactory welds were possible with inert-gas welding. However, electron-beam welding appeared to result in a lower inherent probability of contaminating the weld and was chosen for use in the program.

3.1.1.2 Fixture Design and Fabrication for Seam Welding

To ensure uniform melting for seam welding, a motor-driven fixture was designed and fabricated for use in an electron-beam welder. This fixture, shown in Figure 3.4, permitted three-dimensional adjustment, and automatic drive in one direction.

A lead screw, part 3, was driven by a sprocket, part 9, which, in turn, was driven by a sprocket chain coupled to a variable-speed motor. The lead screw actuated a traversing plate, part 8, which carried the head, part 24, that supported the rhenium cylinder. Provisions were included for vertical adjustment with parts 20, 21, 22 and 23. Azimuth adjustments were made by moving the support legs, part 1.

3. FABRICATION

3.1 Capsule Fabrication

3.1.1 Container

Work conducted at GEMSD prior to this program had indicated that failure in rhenium containers enclosing the 3 BeO-2 MgO oxide occurred principally in welded joints. That same work had also indicated that electron-beam welds were preferable to inert-gas welds.

Because samples of rhenium which had been seam-welded in inert gas were available, a brief metallographic examination was made of cross sections of two such welds. The results are described in the next section.

3.1.1.1 Examination of Rhenium Tubing

Photomicrographs were taken of the cross section of a tungsten inert-gas weld made on a rhenium tube by the Chase Brass and Copper Company and are shown in Figures 3.1 and 3.2. These show intergranular cracking, a number of small marks which may be fine pores, and craters formed during electropolishing, which may be due to inclusions. This tube was the earlier of two that were examined. A typical cross section of a recrystallized weld zone of a more recent tube supplied by the same company is shown in Figure 3.3. This weld seemed to be entirely satisfactory.

Two x-rays were made of the weld shown in Figure 3.3. The first revealed one very small pore when examined by an expert under very intense illumination. It also revealed a variation in the thickness of the tube along the sides of the weld zone. This negative was so dense, however, that it was unreproducible.

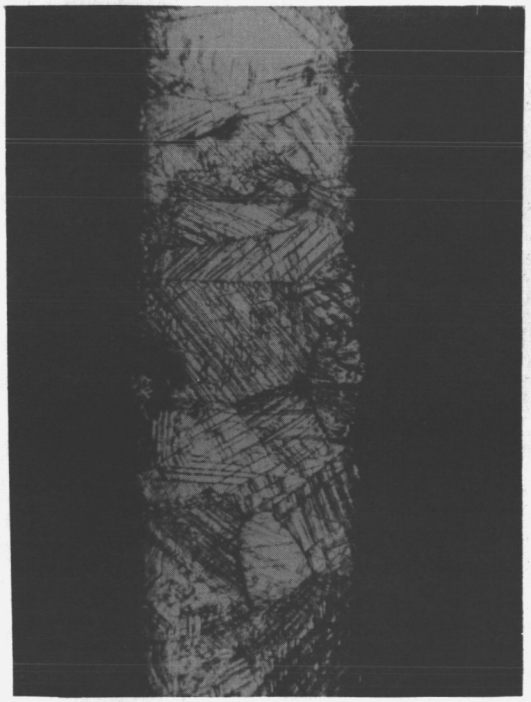

Figure 3.1. Cross Section of Weld Area, Electropolished, at 75X, Showing Crater Defects, Intergranular Cracking, and Columnar Structure.

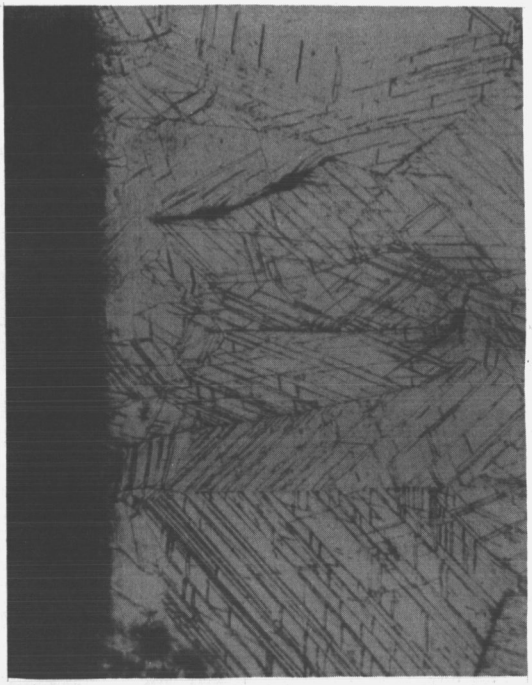

Figure 3.2. Enlargement (150X) of Portion of Weld in Figure 3.1, Revealing Intergranular Cracking, but Showing Crater Defects Less Clearly.

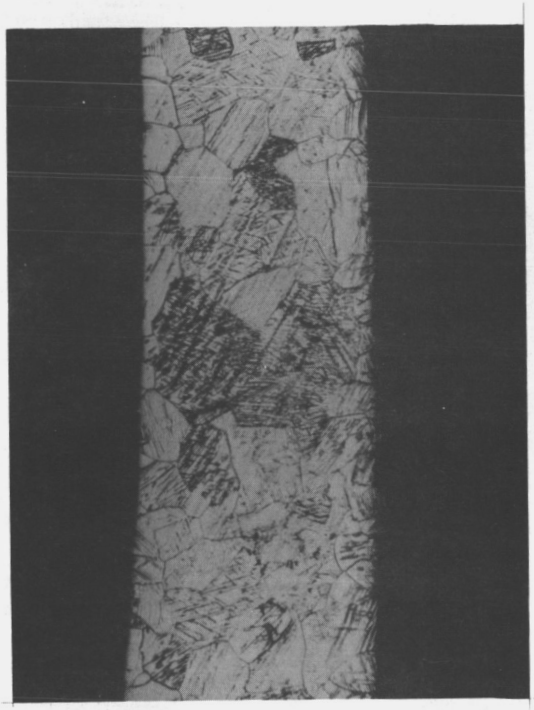

Figure 3.3. Cross Section (75X) of Recrystallized Weld Zone in More Recent Tubing, Showing an Excellent Joint.

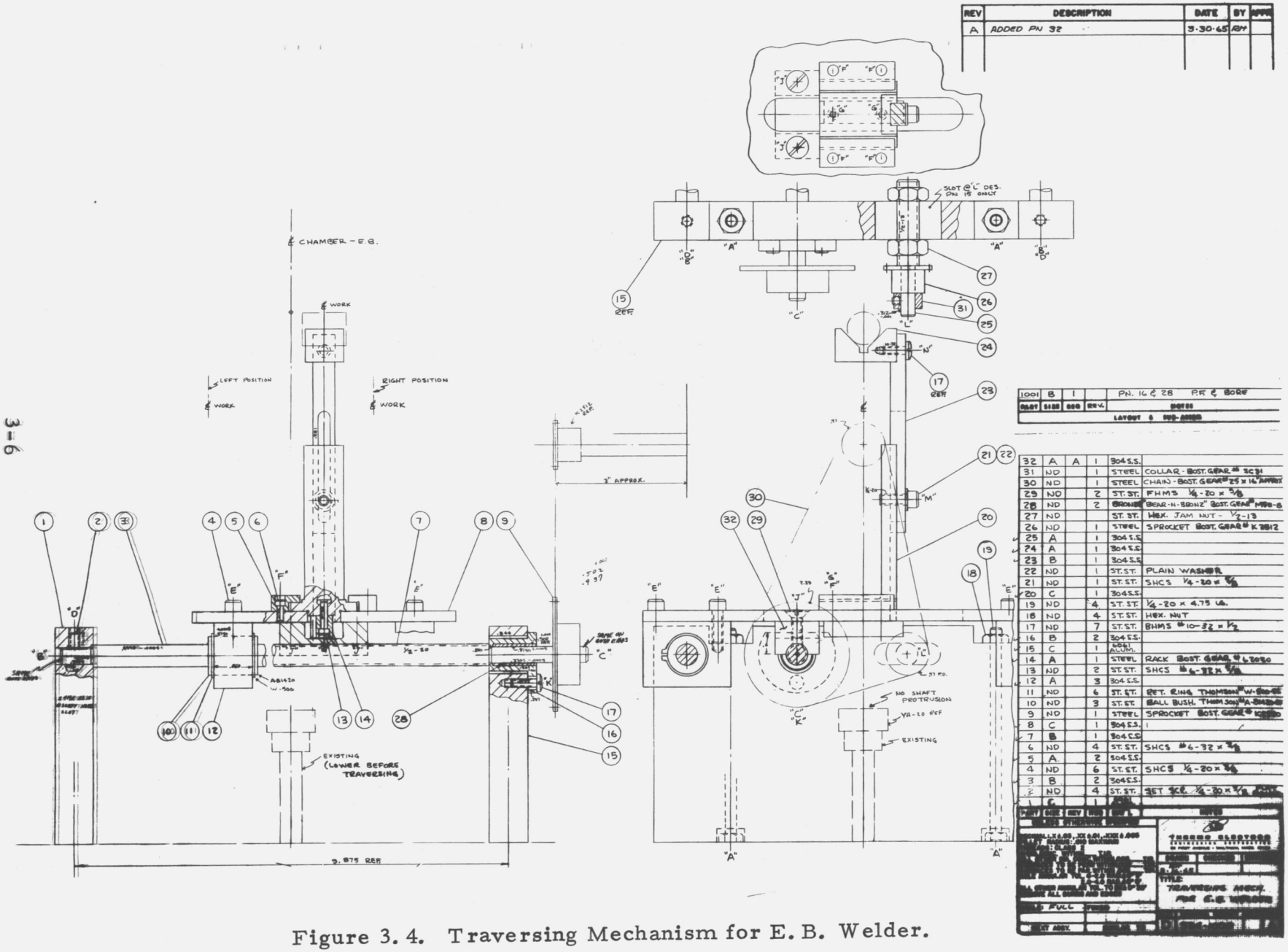

Figure 3.4. Traversing Mechanism for E.B. Welder.

3.1.1.3 Electron-Beam Welding of Rhenium Tubing

Earlier workers in this field had reported failures of welded rhenium containers in the weld area. The welding techniques used produced a large-grained weld zone where grain boundaries extended through the wall of the tube. One explanation which was hypothesized for this mode of failure was that the segregation of trace impurities to grain boundaries in the weld area made these boundaries susceptible to corrosive attack by the contained oxide. The finer-grained material was possibly less susceptible to attack, either because of the extended grain boundaries or because the particular form of segregation found in welds had not occurred.

This hypothesis was plausible enough to justify an attempt to refine the grain size that resulted from the electron-beam welds. This was done by re-rolling the welded tube, which was not perfectly round after welding. The three-roll straightening roller used had the effect of making the tube rounder by deforming the weld zone, so that after re-rolling the maximum difference between two orthogonal diameters on a 1" tube was 0.005 inch. The tube was then subjected to a mild anneal -- 30 minutes at 1500°C -- which acted on the deformed weld zone to produce primary recrystallization and a refinement of the grain structure. This process should not, of course, be confused with the grain growth which occurs at much higher temperatures and acts to coarsen the grain size. The grain refinement was caused by annealing the cold-worked material, and because the weld area suffered the most working, it was most affected by the annealing.

Obviously the circular welds at the ends of the container could not be similarly treated in order to achieve the same grain refinement.

The effects of this treatment are shown in the cross sections of the seam weld, Figure 3.5 before annealing (i.e., as welded), and Figure 3.6 after 30 minutes at 1500°C, both at 75x.

Several rhenium buckets were constructed for use in firing and melting the oxide in preparation for its use in the capsule. These used the above procedure for seam welding. The other welds were also made by electron-beam welding but were not worked to refine the grain. During the preparation of the oxide two buckets developed seam-weld leaks, while none failed at the other joints. The other welds may have experienced less severe stresses. Therefore, the benefit or disadvantages of reworking the welds could not be confirmed.

Figure 3.7 shows a container wall that was seam-welded and reworked. This wall was used in the construction of a complete TES model. Figure 3.8 shows the wall fitted to the emitter, and Figure 3.9 shows the wall fitted to the lid. The assembly procedure consisted of assembling and testing the converter, then welding the wall to the emitter, adding the oxide, and finally welding the lid.

The weld of the wall to the emitter was performed easily. During the weld of the lid a slight sputtering was noticed at one point, but otherwise the welding process appeared similar to many others made earlier on other parts.

Following the lid weld the entire TES model was soaked in helium and then leak-checked. A very slight indication was observed with the leak detector, but it was considered so small as to be background noise.

As will be discussed later, the container of the TES model leaked during test, and a second container was constructed.

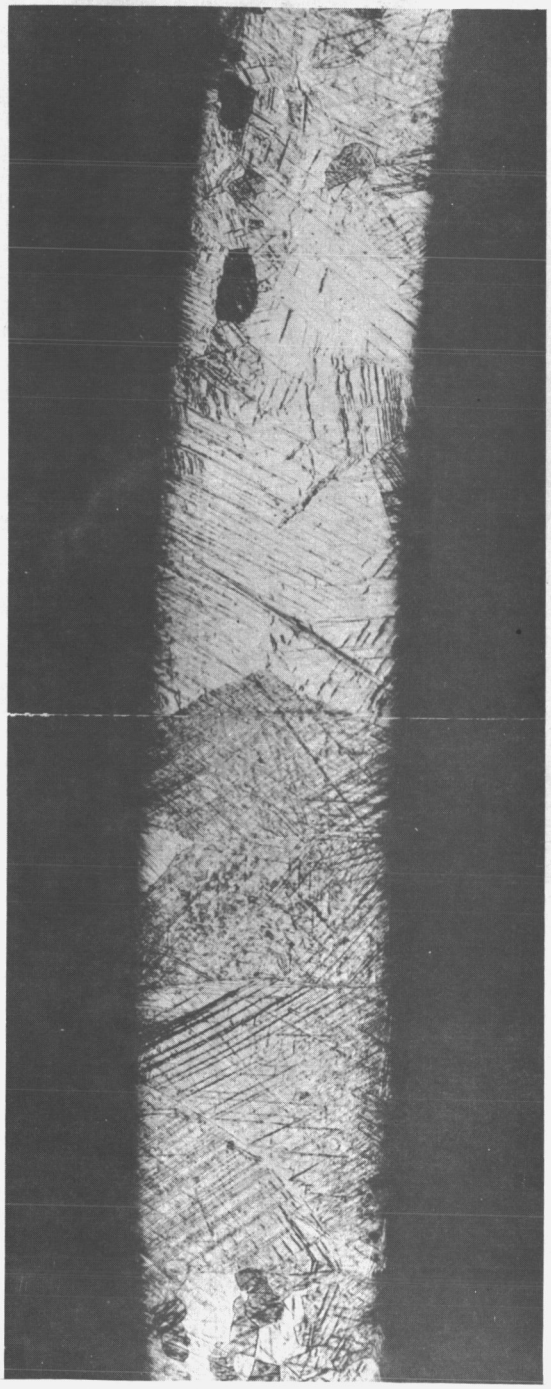

Figure 3.5. Cross Section of Seam Weld in 0.02" Re Sheet Tube, as Welded Structure, Electropolished and Etched, 75X.

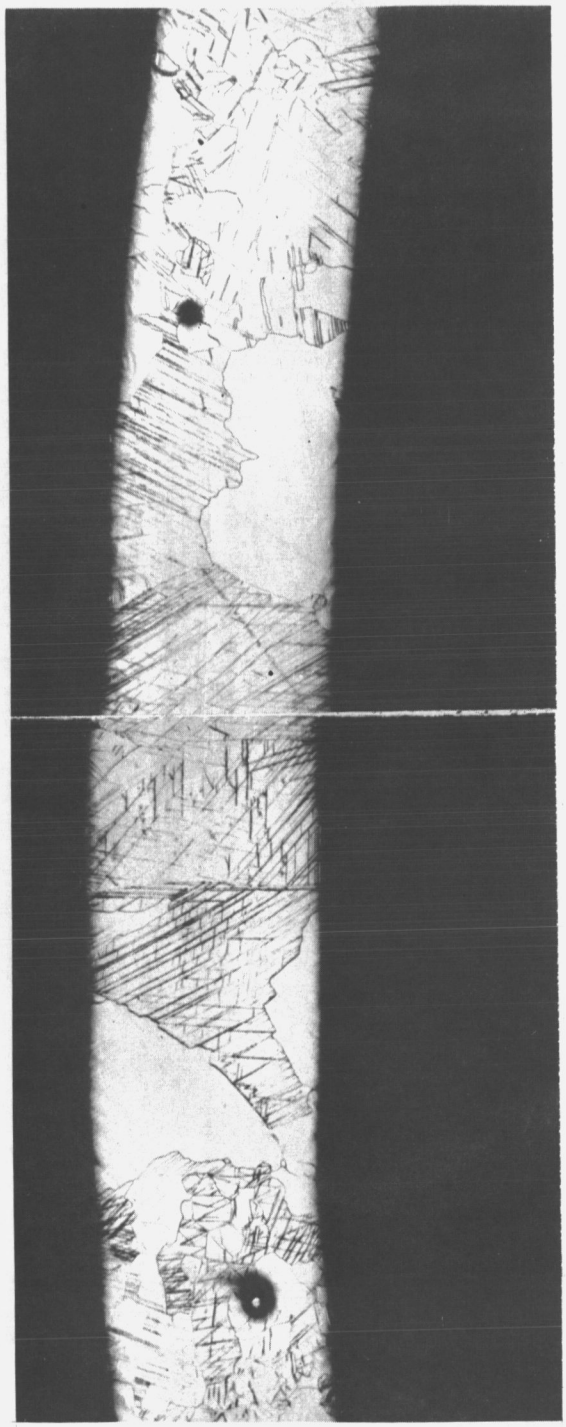

Figure 3.6. Refined Grain Structure of Weld Shown in Figure 10, after Re-Rolling and Annealing 30 Min. at 1500°C, Electropolished and Etched, 75X.

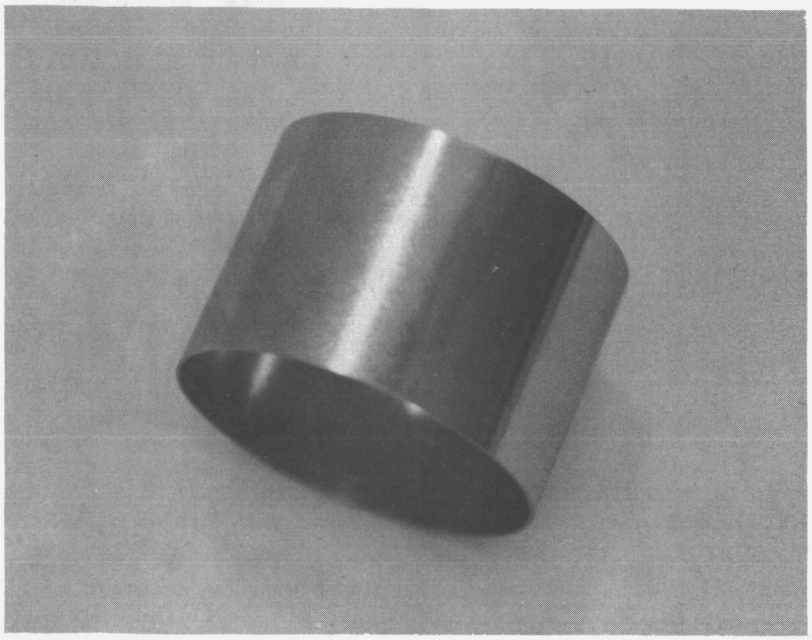

Figure 3.7. Container Wall.

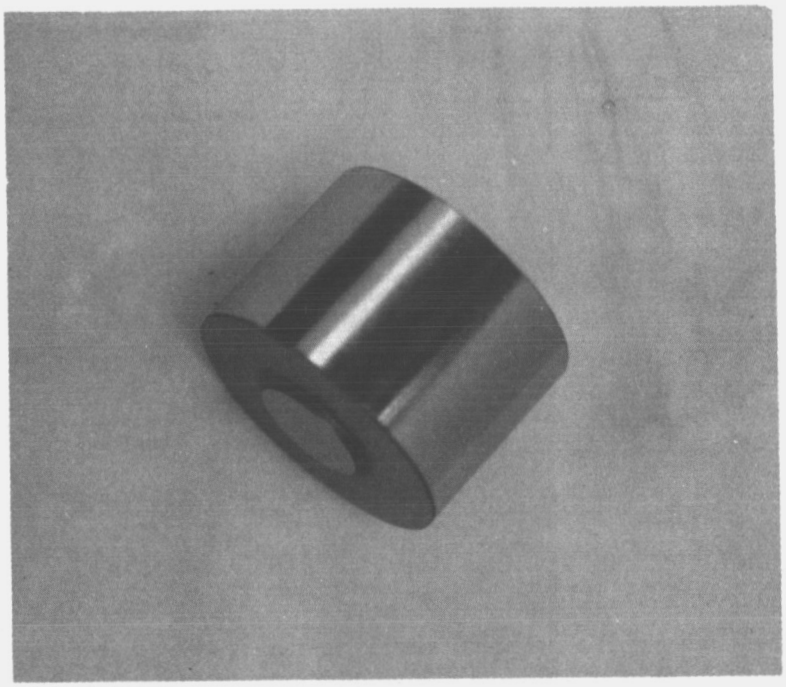

Figure 3.8. Container Wall Fitted to Emitter.

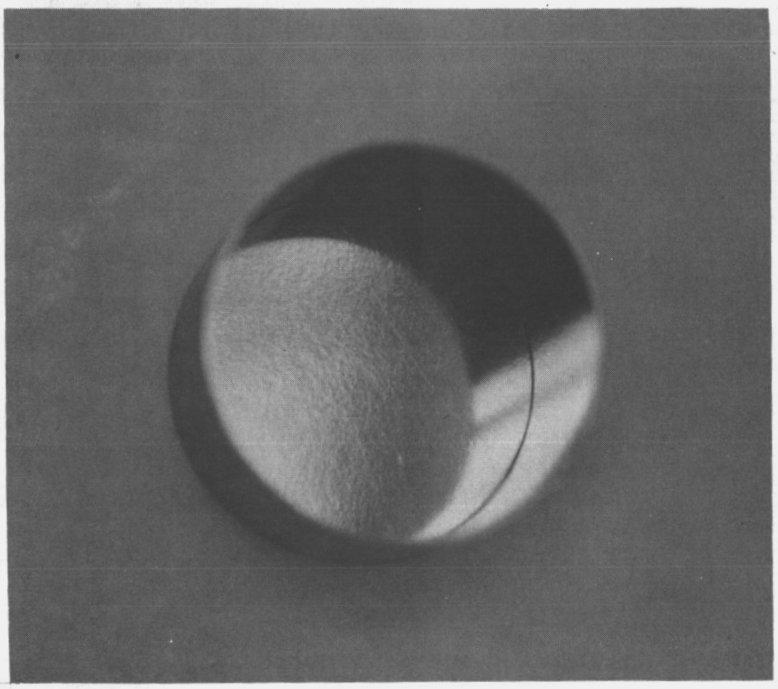

Figure 3.9. Container Wall Fitted to Top Lid.

In this second case, the complete container was fabricated and tested before being coupled to the thermionic converter. This container was welded in the same manner as that just described. However, to prevent contamination of the lid weld by the oxide during welding, a thin rhenium shield was spot-welded to the lid. This shield covered the top of the oxide and fit snugly against the inner wall of the container. The shield was 3 mils thick along the top and 1 mil thick where it abutted upon the wall of the container. The sides of the shield extended 1/4 inch down the side of the container.

During welding of the lid, some buckling occurred. Therefore, the lid was held down with a tungsten weight and tack-welded in four places. Then the complete weld was made. No sputtering was noticed, but more rhenium material had to be added in one region.

3.1.2 Oxide Preparation

As explained in the introduction to this report, the intent of this program was to demonstrate the feasibility of coupling a thermionic converter to a container of thermal energy storage material. Other efforts were concurrently under way[4] to measure the characteristics of the thermal energy storage materials, their compatibility with container materials, and the best means of purifying, preparing and containing the material. In line with the objective of demonstrating a TES model, the 3 BeO - 2 MgO mixture was chosen for use primarily because its characteristics were best known. Various pertinent characteristics of the binary mixture and its components are listed in Table 3.1. Beryllia and Magnesia powders were purchased, their purity was compared with the manufacturer's analysis, and in some cases additional purification was attempted. The powders were mixed

TABLE 3.1

CHARACTERISTICS OF 3 BeO-2MgO AND ITS COMPONENTS[4]

Melting Point of:	
BeO	2550°C
MgO	2800°C
3BeO-2 MgO	1870°C
Specific Heat of 3 BeO-2 MgO	0.25 cal/gm°C
Heat of fusion of 3 BeO-2 MgO	370 cal/gm
Thermal Expansion of 3 BeO - 2 MgO	
(Room temperature to 1900°C)	31.8%
(During fusion)	23.8%
Thermal Conductivity of 3 BeO - 2 MgO	
at 500°C	0.3 w/cm°C
at 1000°C	0.18
at 1500°C	0.14
at 1650°C	0.12

in an alcohol slurry, and the resulting mixture was heated and melted. The resulting solid binary slugs were analyzed to confirm the ratio of BeO to MgO. Finally, the slugs were air-fired for additional purification and then were machined to the tolerances required for use in the TES model's container. The following sections describe these steps in more detail.

3.1.2.1 Analysis of BeO and MgO Powders

BeO powder was purchased from the Minerals Concentrates Company with impurities of about 100 ppm. A typical analysis is shown in Table 3.2. This was the best available commercial source. A comparison between Minerals Concentrates Company and Brush Beryllium Corporation is also shown in Table 3.2.

TABLE 3.2

	Minox AAA (ppm)	Brush (ppm)
Al	40	100
Ca or CaO	8	30-40
Si or SiO_2	18	100
Fe	20	75-100
Mg		30-40
Total	<100	<400

No attempt was made at further purification of the BeO powder.

MgO powder was purchased from the Morton Chemical Company and from Fisher Scientific. According to the manufacturers' analyses, the Fisher material had the higher purity. Semi-quantitative

analyses were conducted on both samples to substantiate the manufacturers' analyses. The results are listed in Table 3.3.

On the basis of these results the following ten elements were estimated quantitatively: Ag, Ba, Ca, Cu, Fe, Na, Pb, Si, Sr, and Ti. These ten elements were chosen either because they were present in a relatively high concentration in the samples, or because it was felt they might be present as volatile compounds which could interfere with successful melting.

Vendors of single-crystal BeO and MgO were found, but use of such single crystals was ruled out for use on this program because starting with solids required the additional operation of crushing before mixing.

The results of the quantitative analysis of the MgO samples are shown in Table 3.4, which includes the results of both the manufacturers' and Thermo Electron's qualitative analyses.

The quantitative estimates all fell in or below the lower half of the qualitative estimate bracket for the same element, except that the qualitative estimates for Sr were an order of magnitude high. The manufacturers' analyses were all substantiated except in two cases: Morton Chemical's analysis showed 40 ppm of Ti compared with our value of 90 ppm, and Fisher's analysis showed 5000 ppm (= 0.5%) of Na compared with our value of 110 ppm.

The manufacturers generally seemed to overstate the impurity contents of their products. The Morton material appeared considerably less pure than the Fisher M-51. However, the Fisher material was found to give substantial deposits on a glass bell jar when

TABLE 3.3

MANUFACTURERS' AND THERMO ELECTRON'S
SPECTROSCOPIC ANALYSES OF AS-RECEIVED SAMPLES OF MgO

	Fisher M-51		Morton	
Element	Manufacturer's Analysis	Thermo Electron's Analysis	Manufacturer's Analysis	Thermo Electron's Analysis
Ba	10	1-10	<1	--
Ag		1-10	<2	1-10
B		--	30	10-100
Ca	500	300-3000	1800	1000-10000
Co		--		<1
Cr		3-30		10-100
Al			140	
Cu		3-30	2	10-100
Fe	40	30-300	300	100-1000
Mo		--		3-30
Mu	1	<1		1-10
Na	5000	30-300	<2	<3
Cl	50		21	
Ni		1-10		1-10
Pb	20	--		1-10
Si		100-1000	1000	300-3000
Sn		1-10		2-20
Sr	50	10-100		3-30
S	70		130	
Ti			40	100-1000
Zr				3-30
K	50			

ppm throughout

TABLE 3.4

MAGNESIUM OXIDE ANALYSES

	FISHER M-51			MORTON		
		Our Analyses			Our Analyses	
	Vendor	Qualit.	Quant.	Vendor	Qualit.	Quant.
Al				140		
Ag		1-10	0.8	<2	1-10	0.8
B				30	10-100	
Ba	10	1-10	1	<1		<1
Ca	500	300-3000	280	1800	1K-10K	1100
Cl	50			21		
Co					<1	
Ca		3-30	3	2	10-100	3
Fe	40	30-300	15	300	100-1000	220
K	50					
Cr		3-30			10-100	
Mo					3-30	
Mn	1	<1			1-10	
Na	5000	30-300	110	<2		<5
Ni		1-10			1-10	
Pb	20		<1		1-10	3
S	10			130		
Si		100-1000	180	1000	300-3000	650
Sn		1-10			2-20	
Sr	50	10-100	1.5		3-30	<0.5
Ti			<2	40	100-1000	90
Zr					3-30	
Σ	Na + 750		590	3500		2100

fired under conditions for which the Morton material gave much less deposit. This presumably reflected a difference in the volatilities of the impurities. Because the spectrographic analyses detected only the presence of metals, but not the molecule in which they were combined, it may be that an element which was present in one material in some involatile form, was present in the other material as a volatile compound, or that the impurities present in one were involatile, while the different elements in the other were volatile.

A sample of the Fisher material was fired in a Ta bucket (because no other was available at the time). The predicted reaction between MgO and Ta occurred, so that the principal impurity in the fired material was Ta. The Ca level did not change from that of the raw stock, but the Sr and Fe levels dropped to 1/3, Si to 1/10, and Na to 1/000 of the levels found (by the same analyst) in the stock material. This firing was accompanied by considerable deposition on the bell jar. The deposit was found to give an alkaline reaction with water, suggesting that it contained sodium or sodium oxide. Sodium was a minor impurity in Morton MgO, compared with Ca.

Both MgO powders were then fired in a rhenium container, and the results are shown in Table 3.5. Considerable purification of the Morton MgO with respect to Si and Ti was achieved, while the Fisher MgO lost Na, but gained Fe and some Ca, and remained cleaner overall. The earlier hypothesis that Fisher MgO lost Na on firing was therefore substantiated.

In summary, some purification of MgO was achieved. The Fisher material lost a substantial amount of Na, but appeared to

TABLE 3.5

IMPURITIES IN MgO BEFORE
AND AFTER FIRING TO 2000°C IN VACUUM

	Morton		Fisher	
	Before	After	Before	After
Ca	1100	1200	280	350*
Si	650	150*	180	150
Fe	220	250	15	30*
Ti	90	40*	<2	<5
Re	--	30	<10	<10
Cu	3	5	3	4
Na	<5	3.5	110	2*
Sr	<0.5	<0.5	1.5	1.0

* Indicates significant changes.

These are quantitative spectrographic analyses, all made by TEECO's analyst.

gain some Fe and Ca, perhaps during handling. Morton material appeared to gain small amounts of Fe and Ca too, but lost Si and Ti, while remaining less pure overall.

3.1.2.2 Preparation of the 3 BeO - 2 MgO Mixture

The conventional way of mixing ceramic powders is to batter them with hard abrasive balls in a rotating ball mill. This, however, was apt to introduce contaminants as the container was milled away. Consequently a blender was used for mixing while the particles were suspended in a liquid. The chosen liquid was ethyl alcohol, which did not cause hydrolysis of the MgO, was reasonably volatile, and could later be removed.

Suitable proportions of liquid and solid were used, and the extremely rapid and vigorous action of the blender seemed to mix the powders adequately.

The next step was the removal of the alcohol from the slurry. The first attempts relied on evacuating the space containing the bucket, either with a water aspirator, or with a rotary vacuum pump, to 15 in. Hg vacuum. These methods accelerated evaporation from the surface of the slurry, so that the top layer thickened to form a skin. However, as the pressure was further reduced, boiling occurred explosively in the slurry below the skin, projecting a large burst of wet oxide over the inside of the bell jar. Alternative approaches were sought, and the most satisfactory appeared to be heating the bucket and slurry on a hot plate, while stirring, until a thick paste was formed. The final removal of alcohol could then be achieved with a vacuum pump, without drastic boiling. This experimentation was

conducted with MgO, without BeO, because it was felt that the results would be equally applicable to the mixture, and this in fact proved to be the case.

Weighed amounts of BeO and MgO powder were then combined to produce 4 g of mixture in the proportion 3 BeO-2 MgO. The powders were blended for 30 seconds with 10 ml of ethyl alcohol, and the resulting slurry was poured into a rhenium bucket. This was placed on a hot plate to warm the contents to about 65°C, and the slurry was stirred until most of the alcohol had evaporated and a thick paste was left. Figure 3.10 shows the rhenium bucket with slurry in the BeO hood mounted on a hot plate. The bucket was then transferred to a vacuum system and pumped down. The pressure dropped slowly as the residual alcohol evaporated, and a base pressure of 2 to 2 x 10^{-6} was achieved without the sputtering and bubbling which had accompanied earlier attempts to evacuate the volume surrounding the wet slurry.

The bucket was then heated by electron-bombardment of the bottom. Substantial temperature gradients existed above the length of the bucket away from the heated area. In the last stages of drying the oxide mixture developed gross cracks, and as it sintered and shrank the cracks widened, until several portions of the mixture were adhering to the wall of the container but not to each other.

Because of evaporation of contaminants onto the bell jar, and temperature gradients in the bucket, it was impossible to make accurate measurements of the temperature at which melting started. However, melting of almost the whole of the mixture was achieved, although one segment persisted in adhering to the side of the bucket so far from the bottom that it never reached the melting temperature.

The melted material wet the rhenium, particularly the sides of the bucket, and left the center of the bottom bare. Bubbles were seen to be released from the oxides during their molten period, and the heat input was increased so that most of the mixture was well above the melting point. Because the oxides used in this experiment had not undergone purification, there was considerable evaporation of impurities, and probably of oxide too, onto the Vycor. The test was terminated after 15 minutes at temperature. After cooling, the oxide was easily removed from the bucket.

The first melt (Melt #1, Morton MgO) was examined for impurities and to determine the BeO/MgO ratio. Spectroscopic analysis revealed that the melt had picked up Re to the extent of 0.5 to 5.0%, and had lost some iron. The only explanation that could be offered for the high level of Re was to ascribe its occurrence to the high temperature, 2600°, to which this melt had been exposed. All other impurities detected were present in amounts similar to those found in the oxides before melting.

The weight ratio of the two oxides was found to be 1:1. The target ratio was 0.931:1. A cross section of this melt, examined under the microscope, was found to contain some very large bubbles, but very few fine pores. No discernable microstructure was seen. The melt was a light gray color, which was ascribed to the fact that this melt was made with as-received unpurified oxides early in the program.

A second melt (Melt #2, Morton MgO) was made, aimed primarily at achieving a larger quantity of molten material. Sufficient unpurified oxides were blended with alcohol to more than fill the

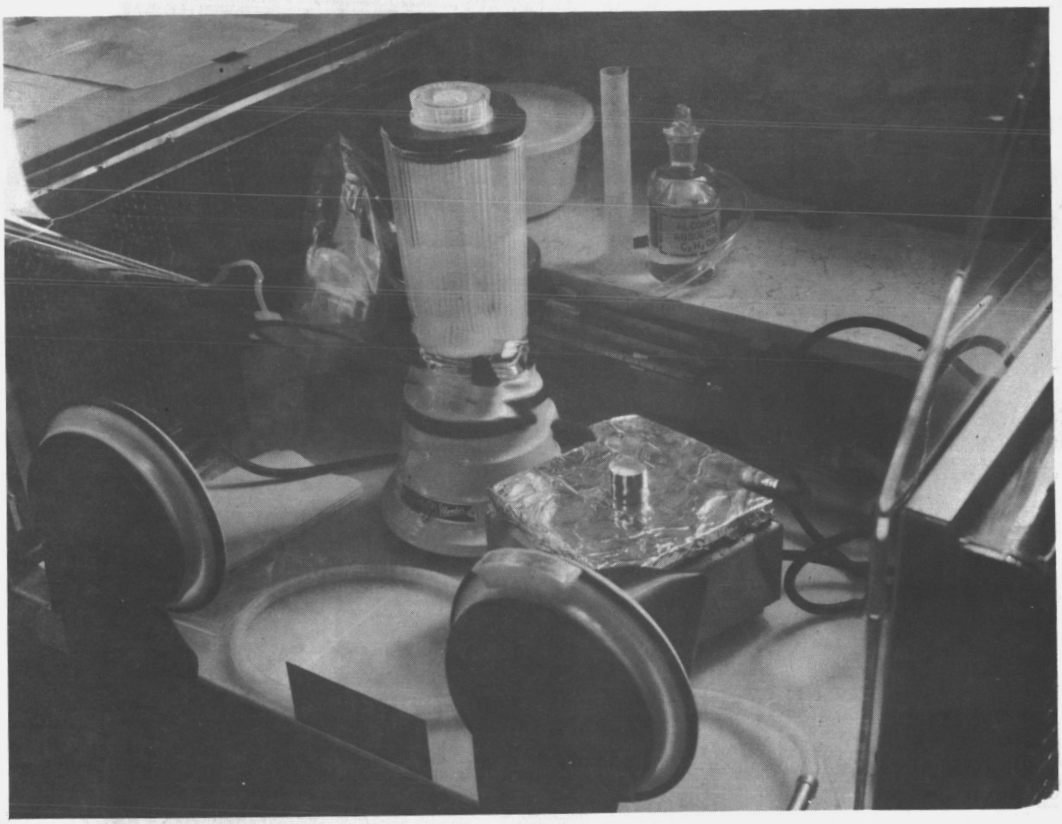

Figure 3.10. BeO Handling Facility.

melting bucket, and it was filled about 70% with oxide slurry. This was warmed to drive off most of the alcohol, and then evacuated and heated to the melting point. After a minute or so at the melting point, the heat was removed and, after a cooling period, more of the same batch of oxide was added, dried out, pumped down, and remelted. This procedure was repeated twice more.

The resulting slug occupied about 1/3 of the container, slipped readily out of the container when cold, and solidified with a shallow rounded crater at the top, implying that it contracted on freezing. No quantitative measurement of the volume could be made because of the irregular pores in the material. It had the gray color characteristic of the first melt (both were made with unpurified oxides). It was examined for BeO/MgO ratio and spectroscopically for trace impurities. The principal trace was iron, followed next by silicon, and these and the other traces were present in amounts comparable with those present in the starting oxides, but purification with respect to Ca was considerable, and some Ti was lost. No rhenium was detected, despite the discoloration of the material, and a detectability limit of 1 ppm. This melt was never at the high temperature reached by the first melt. The BeO/MgO weight ratio was found to be 0.947, which agrees with the target ratio of 0.931 within the limits of experimental error. MgO evaporation was not a significant problem.

Since air firing was a standard method of cleaning ceramics, it was applied to part of the second slug. Firing was carried out for 1 hour at 1200°C in air, with the sample supported on pure Al_2O_3 ceramics. Some cleaning of the specimen was found, and it

was therefore fired for another five hours under the same conditions. This left the specimen clean, that is, of yellowish-white appearance throughout, except for some metallic gray flecks.

A third melt, using Fisher MgO in place of Morton, was very clean and free from gray contamination on removal from the container. This is shown in Figure 3.11. Apparently the purer Fisher oxide produced a cleaner product when used without special purification. During melting, considerable deposition occurred on the bell-jar, implying that purification occurred during melting.

Externally and internally, no change in the appearance of the rhenium containers was noticed.

Although the vacuum firing of as-received MgO powders from Fisher Scientific and Morton Chemical earlier in the program resulted in an overall decrease in impurity levels, purification was complicated and slow because of the tendency of the dry, uncompacted oxide to "explode" and spatter during the early stages of evacuation and heating. In order to investigate speeding the fabrication of oxide, a melt was made (Melt #3) using the purer of the two oxides, Fisher MgO, and BeO from Mineral Concentrates Co. without prior cleaning. The technique of blending the two powders with ethyl alcohol was used. The result was an oxide with a very clean appearance. To confirm the fact that this melt was as pure as would be possible starting with purified oxides, the melt was chemically analyzed. The results are shown in Table 3.6.

Since the results showed that substantial purification was accomplished (comparable to starting with purified oxides) during melting

in vacuum, the same procedure was adopted to make 100 grams of eutectic for the TES model. A portion of the 100 grams is shown in Figure 3.12.

As shown in Table 3.6, 100 to 1000 ppm of Re were detected. The rhenium was only detected after an explicit request to the analyst to look for it. It was reported as not detected on the first examination of Melt #3. Similar experience was encountered with Melt#2. The technique for the detection of Re seemed unreliable and erratic.

A piece of 0.02" Re sheet was added to Melt #2. A typical cross section of this specimen after melting and metallographic preparation is shown in Figure 3.13. This shows a cross section of the sheet (at 150x) close to the sheared edge. The straight edges of the section corresponded to the rolled surfaces of the sheet, while the sheared edge became rounded during specimen preparation. The black areas were the result of an interaction between Re and the melt. These black areas were only found near sheared edges of the sheet. There was no sign of interaction close to the surfaces of the sheet, as would be expected with a typical corrosion reaction.

In order to explain the interaction, a similar piece of Re sheet was added to Melt #3, from which a control sample had been taken. This specimen was examined after it had been immersed in oxide mixture during several melting cycles. Figure 3.14 shows the flat surface of the sheet after this test. Slight grain-boundary attack had occurred. The long circular arcs intersecting several grains seem to be traces of bubbles in the oxide present at some time on the metal surface, and may have been associated with segregation of insoluble

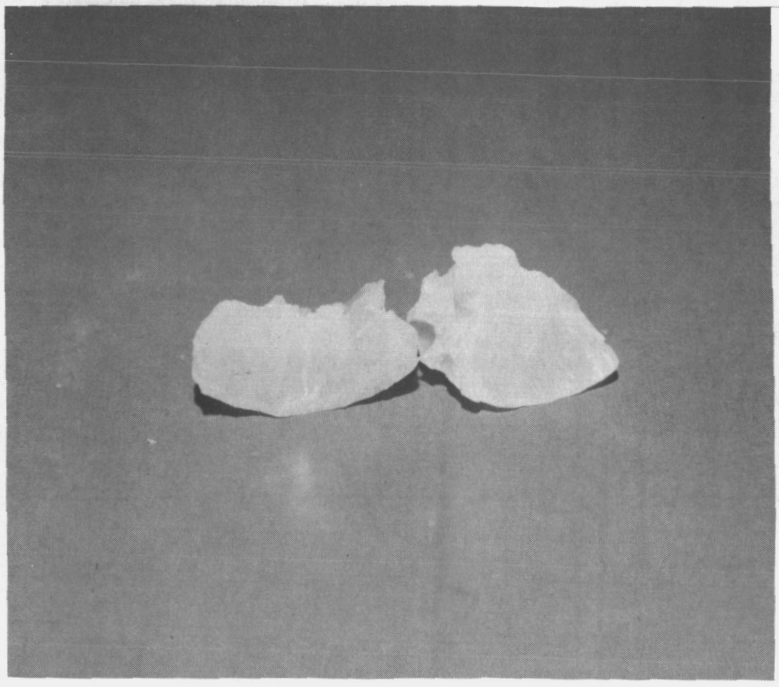

Figure 3.11. 3BeO-2MgO Eutectic from Melt #3.

TABLE 3.6

ANALYSIS OF MELT #3

Element	3 BeO-2MgO Melt #3	Purified MgO Powder from Fisher
Re	100-1000*	ND**
Si	100-1000	150
Ca	<1	350
Al	ND	ND
Ti	ND	ND
Fe	30-300	30
Ni	1-10	1-10
Cr	1-10	1-10
Ca	1-10	4

* Numerals are ppm

** ND means not detected

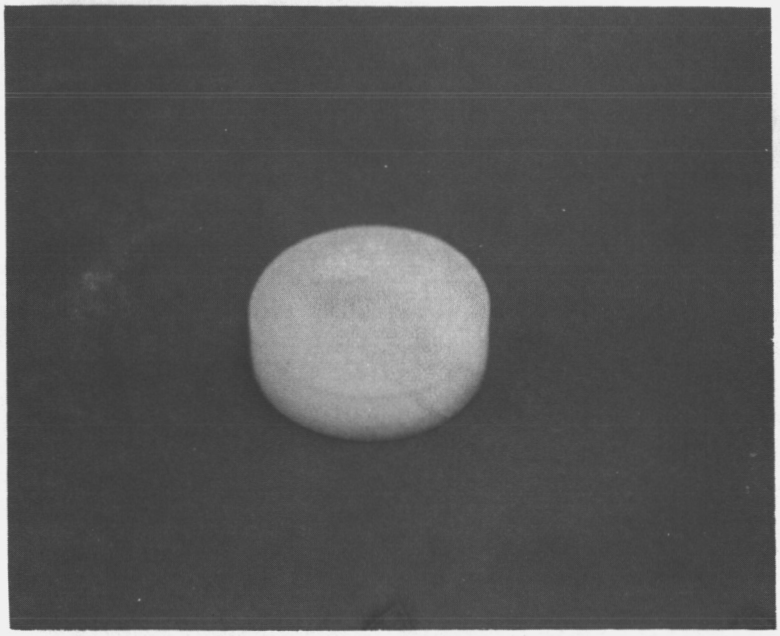

Figure 3.12. 3BeO-MgO Oxide.

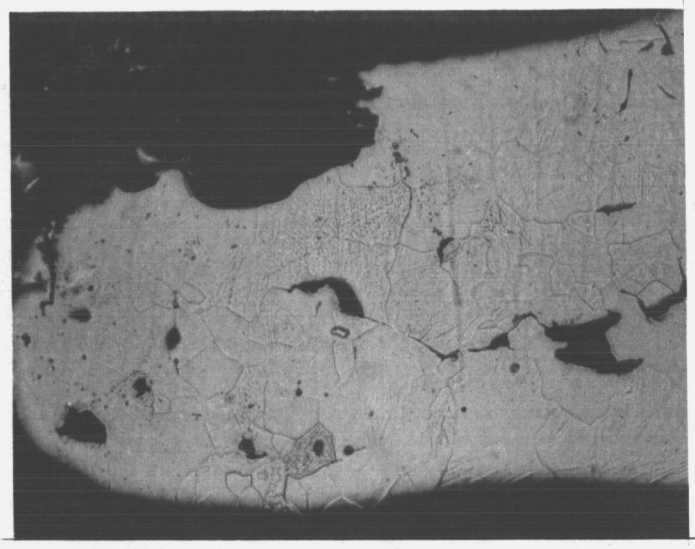

Figure 3.13. Cross Section of Rhenium Sheet (150X).

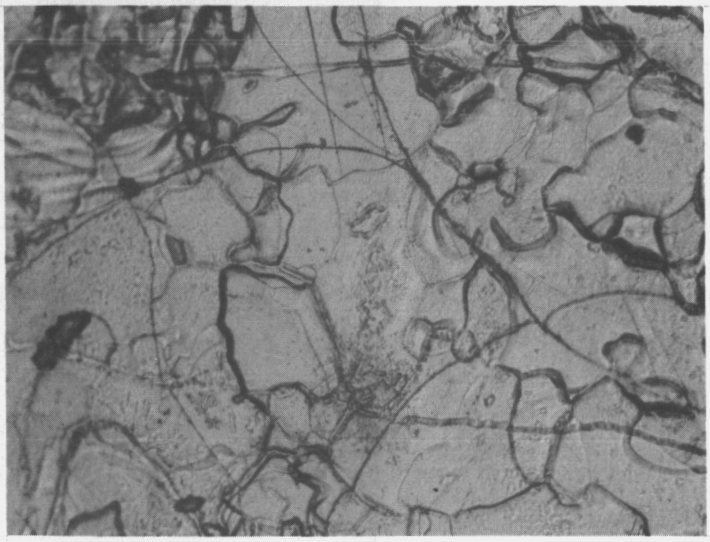

Figure 3.14. Surface of Rhenium Sheet.

ingredients of the melt at the bubble - metal oxide interface. Figures 3.15 and 3.16 (at 310x) show an area of the sheet. In the former figure, a large (out-of-focus) lump of oxide was adherent to the surface, and in the latter this was removed. There was no difference in appearance between the surface where the oxide particle had adhered and the surrounding area. The crescent-shaped and circular marks on these figures were probably caused by the segregation of impurities mentioned above. Figure 3.17 (150 x) shows a typical control cross section of as-received Re; comparing this with Figures 3.15 and 3.16, the surface can be seen to be clearly changed by immersion in the molten oxide. However, this test with carefully prepared surfaces revealed none of the effect seen in Figure 3.13, and the best evidence of the ability of Re to withstand the molten oxide was the continued integrity of the buckets used repeatedly for preparing the large batch of oxide.

Previously the weight ratios of BeO/MgO for Melts #1 and #2 were found to be 1:1 and 0.947:1. The target ratio for 3BeO/2MgO was 0.931:1, and the actual ratio of Melt #3 was measured to be 1.22:1. Because of the previous experience with Melts #1 and #2, this result was quite unexpected. However, a sample taken from the 100 grams prepared for the TES model was found to have a weight ratio of 1.05 ± 3%. With a weight ratio of 1.05:1 rather than 0.931:1, it was estimated that an additional 20 to 50°K would be required to melt the oxide completely. Subsequently, an estimated BeO:MgO phase diagram was published by BMI[4] and is shown as Figure 3.18.

To establish a degree of confidence in the proposed container design, a one-inch-diameter rhenium container, 20 mils thick and 0.870" high, was fabricated. The container was filled with 20 grams

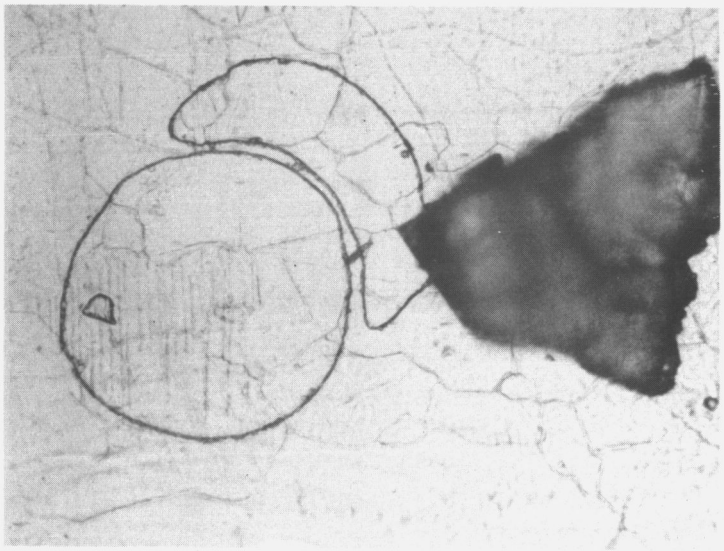

Figure 3.15. Surface of Rhenium Sheet with Oxide Particle Attached (310X).

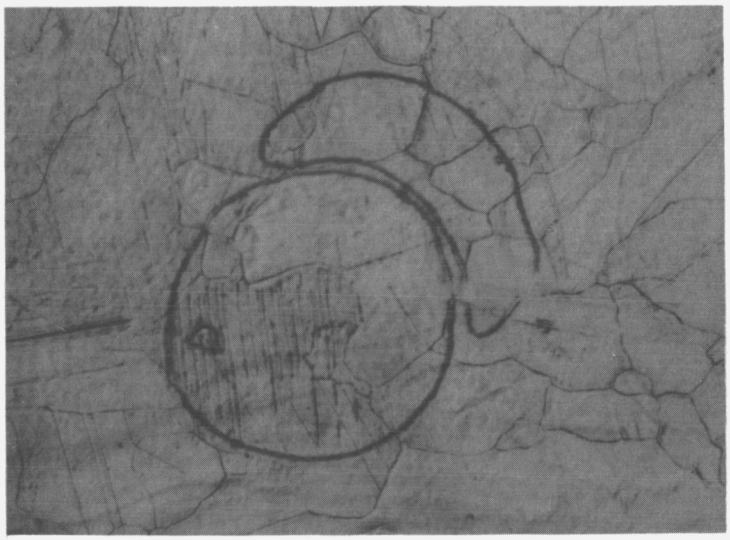

Figure 3.16. Surface of Rhenium Sheet with Oxide Particle Detached (310X).

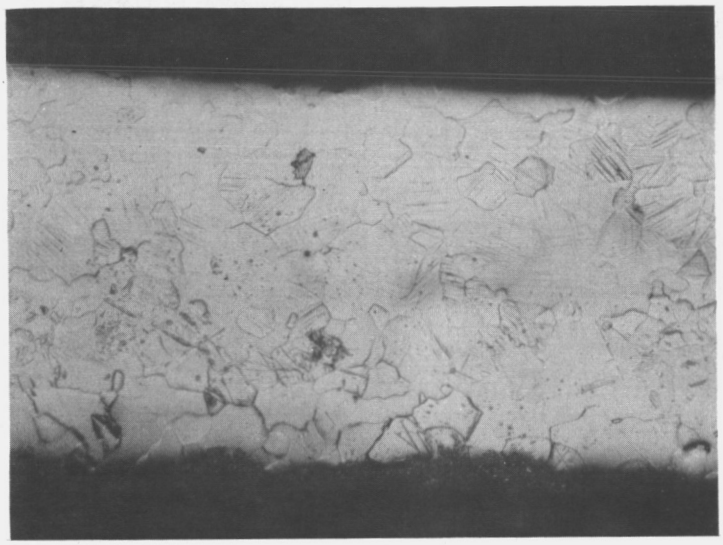

Figure 3.17. Cross Section of Rhenium Sheet Control (150×).

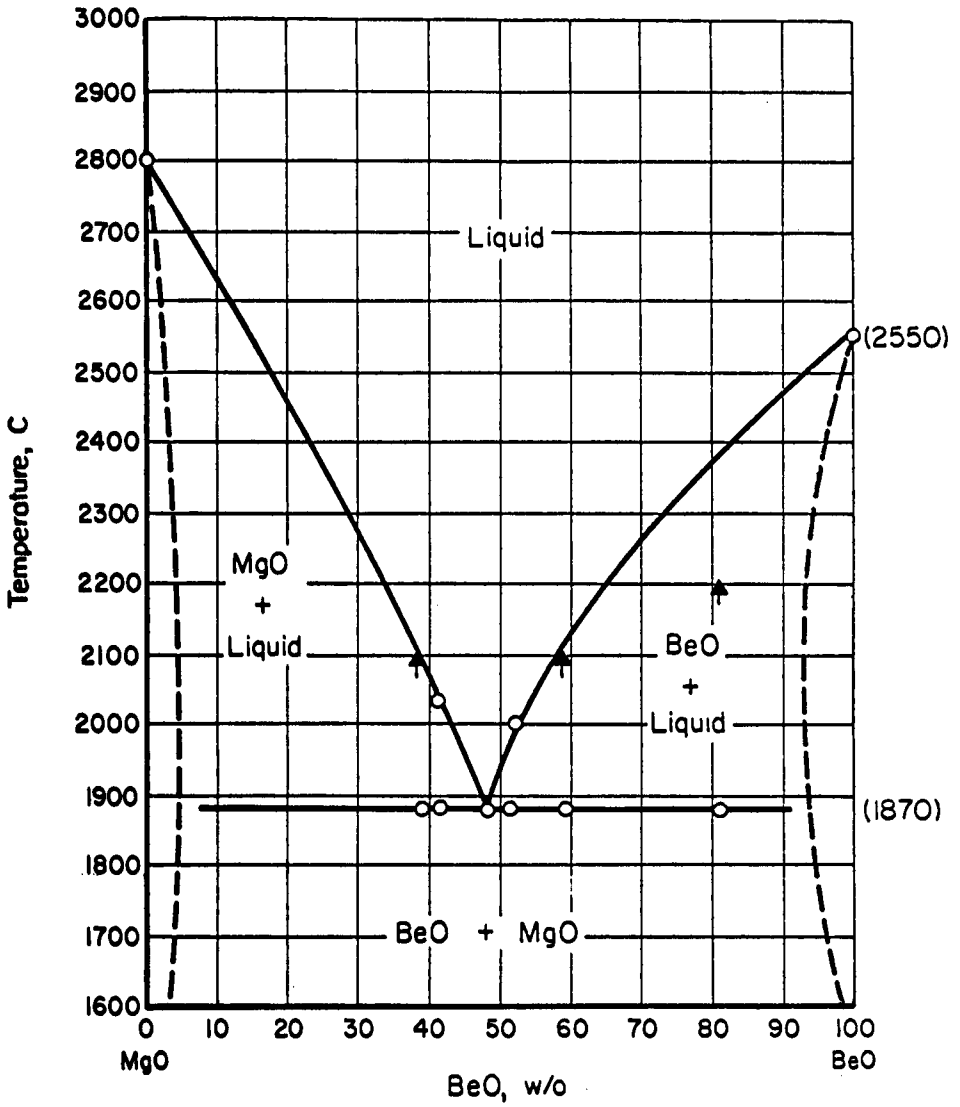

Figure 3.18. Proposed BeO-MgO Phase Diagram.

of oxide, was welded shut and was tested by heating it above and below the melting point of the oxide. The testing is described in Section 4.1. In summary, the capsule adequately withstood heating and cycling. The container remained leak-tight, and there was no observable change in its appearance. Based on this test, the TES model was loaded with oxide and welded.

Since the TES model's container leaked at the lid weld on the first melting of the oxide, a second batch of oxide was prepared. The techniques previously developed on the program were adopted. Since a large pre-melt container was on hand, it was used to hold the mixed powder, which was subsequently melted. Difficulty was encountered in removing the oxide slugs from the container. At first the cause of the problem appeared to be oxide which had adhered to the upper portions of the cylindrical container, interfering with removal of the oxide slug. This container later developed a crack in the vicinity of the cylindrical seam, which allowed oxide to escape from the container during melting.

The rhenium container was then cut and examined. From the photomicrographs it was obvious that no gross corrosion of the rhenium exposed to 3BeO-2MgO was occurring. However, in the body of the rhenium material, which was 0.020" thick, there were cavities at the grain boundaries. These voids were examined with an electron-beam microanalyzer to see if they contained any impurities. Spectral patterns of the elements present in the voids and the clean matrix material revealed no foreign elements. Since Mg was suspected as possibly being present in the voids, a detailed search for Mg showed that it was present in most of the voids. The microanalyzer was not capable of detecting beryllium.

While the first large pre-melt container was being analyzed, a second pre-melt container, approximately the same size as the first, was made. From the previous oxide fabrication there were two slugs, approximately 35 grams each but irregular in shape on the top surface with large distributed voids. These two slugs were ground by an outside vendor to a diameter such that, at the melting point of 3BeO-2MgO, the clearance between the solid oxide and the container would be 10 mils.

The two slugs were placed in the new pre-melt container and melted. In the process the oxide crept up the sides of the container, touching the thermal shield which was supported across the top of the rhenium bucket. The run was stopped, and after cooling the run was repeated without the shield. The rf induction coil was positioned to heat the bottom of the container hotter than the top, so that during melting the entire oxide mass would sink into the bucket. But as the oxide in the lower section of the container melted, it moved away from the side walls and resolidified into a central core, forcing the mass to an even greater height. The slug was then reversed and replaced in the container. During the next attempt at melting, a crack appeared in the container in the vicinity of the seam weld.

From the results of this second container failure, the microprobe analysis of the first, and the observations of a large slug of oxide during melting, it appears that the cause of the cracks in the container might be stress generated by localized melting and trapping of molten oxide. Trapped liquid along the side walls could expand against the solid oxide with no clearance remaining between the oxide and the container. Furthermore, rhenium is anisotropic, and therefore its

expansion coefficient is different in two perpendicular directions in the crystal lattice. Ordinary rhenium sheet has a strong preferred orientation because of the rolling and annealing processes used in manufacture. In the vicinity of the heat-affected zone of the weld the grains are random. The seam-welded rhenium cylinders are cold-rolled to a limited extent. However, with the available equipment the amount of cold work which could be put into the rhenium cylinder was limited. The stress of the expanding oxide could have caused the crack in the seam-weld area. The lower container weld was not stressed so severely as the side weld, and no cracks were observed in it.

In view of these results, the following plan was established for the preparation of the oxide:

1. Mix the powders as before.
2. Pack and melt the powder in 1" rhenium container.
3. Repeat this procedure until 100 grams of 3BeO-2MgO have been accumulated.
4. Re-melt the smaller slugs in a new pre-melt container, not to form one piece but to make three or four pieces which can be machined to the proper diameter and thickness.
5. Stack the machined oxide slugs in the model container to fill the container volume with 70% oxide.

By working with more than one slug, the problem of temperature gradients in the large pre-melt container and oxide can be substantially reduced. With a final machining operation of the slugs the characteristic concave surface can also be removed.

After a successful final weld of the top of the rhenium container, the planned heating arrangement would be modified so that melting of the slug would begin on the free (upper) surface.

One hundred grams of 3BeO-2MgO were prepared in the one-inch-diameter rhenium container. No problems were encountered, and the oxide was very clean in appearance, indicating purification upon melting. From these smaller slugs, four large slugs, approximately 25 grams each, were made in the new 1.5-inch pre-melt container.

The oxide charge for the next container consisted of these four discs. The discs were ground (by Nuclear Metals, Concord, Mass.) to remove the high edges and improve flatness. The diameter of one of the discs was reduced by grinding to 1.46" to allow room for a rhenium shield at the top of the container. The dimensions of the discs are shown in Table 3.7.

The volume of this oxide charge, when molten, was 28.1 cm^3. The container volume at 1900°C, allowing for rhenium expansion, was 34.5 cm^3. Therefore, the container was 81.5% full.

The expansion of the solid oxide charge from room temperature to melting point was 20.7 mils/inch. The expansion of the rhenium container was 13 mils/inch. Thus the clearance required for the slugs was 11.5 mils. The clearance provided was 13 mils; clearance at the top of the container during closure weld was 0.1 inch.

3.2 Converter Fabrication

The Series VIII SET converter that was coupled to the TES container was fabricated essentially the same way as all earlier converters of this type. The rhenium emitter support sleeve that replaced the tantalum sleeve used on conventional Series VIII converters was attached to the niobium seal flange by melting the niobium onto the

TABLE 3.7

DIMENSIONS OF THE FOUR 3 BeO-2 MgO DISCS
USED IN THE SECOND TES CONTAINER

Disc	Weight (g)	Volume (Cm^3)	Density	Density 3.25	Thickness at Center (in.)	Thickness at edge (in.)	Diameter (in.)
#1	20.4	7.76	2.63	81%	0.259	0.277	1.504
#2	18.4	7.18	2.56	79%	0.240	0.256	1.504
#3	17.3	6.75	2.56	79%	0.223	0.244	1.504
#4	13.4	6.73	1.99	61%	0.235	0.257	1.46
Total	69.5	28.42	2.45	75%		1.034	

rhenium. The emitter piece, which also functioned as the bottom of the TES container, was electron-beam welded to the emitter support sleeve. The converter underwent the assembly, outgassing, and cesiating processes without incident.

Since rhenium sleeves had not been used previously on SET converters, a component test was made using an available rhenium sleeve and a niobium flange. The joint was made in the electron-beam welder, and is shown in Figure 3.19.

The joint was cycled rapidly to 900°C twenty times, and leak-checked after the tenth and the twentieth cycles. The joint was leak-tight both times. Then the joint was rapidly cycled to 1500°C approximately thirty times. This higher temperature was selected as a possible operating condition for another application. The joint was still sound and leak-tight and was considered satisfactory for use.

The 8-mil rhenium sleeve purchased from Chase Brass and Copper was then cut to the proper length for the converter and is shown in Figure 3.20. Figure 3.21 shows the sleeve fitted to the emitter (which is also integral with the bottom of the container) before cleaning, outgassing, and welding. Figure 3.22 shows the sleeve after welding to both the emitter and the seal flange.

The assembly procedure for the Series VIII converter can best be described with the aid of Figure 3.23, which shows the design. For use in the TES model certain parts of the basic Series VIII design were deleted, as can be seen by comparison with Figure 2.12. The converter's mounting flange, parts 4, 42, and 12, were not needed and interfered with effective radiation shielding of the emitter sleeve. The support ceramic, part 31 was normally used to support

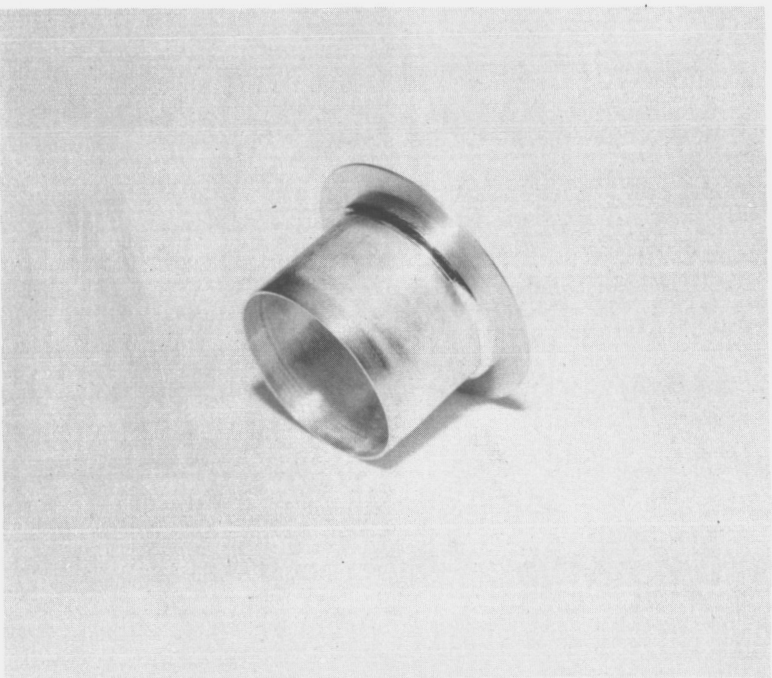

Figure 3.19. Niobium Flange Beam-Welded to a Rhenium Sleeve.

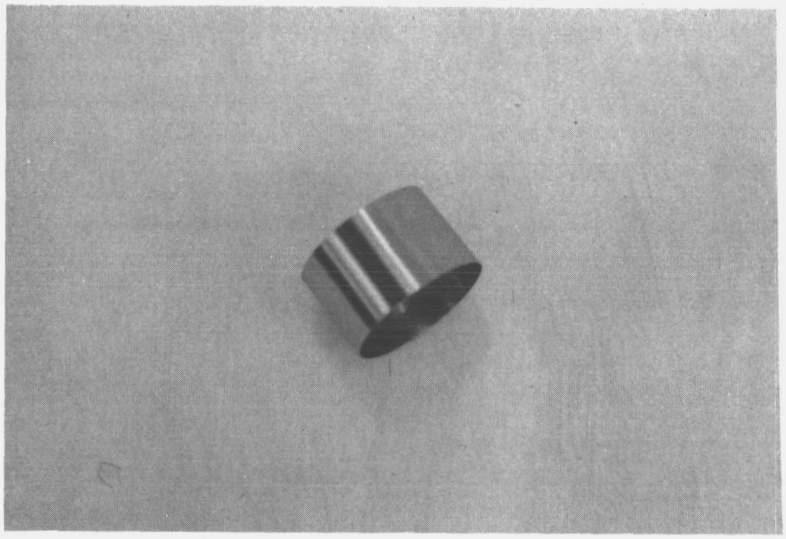

Figure 3.20. Converter Sleeve.

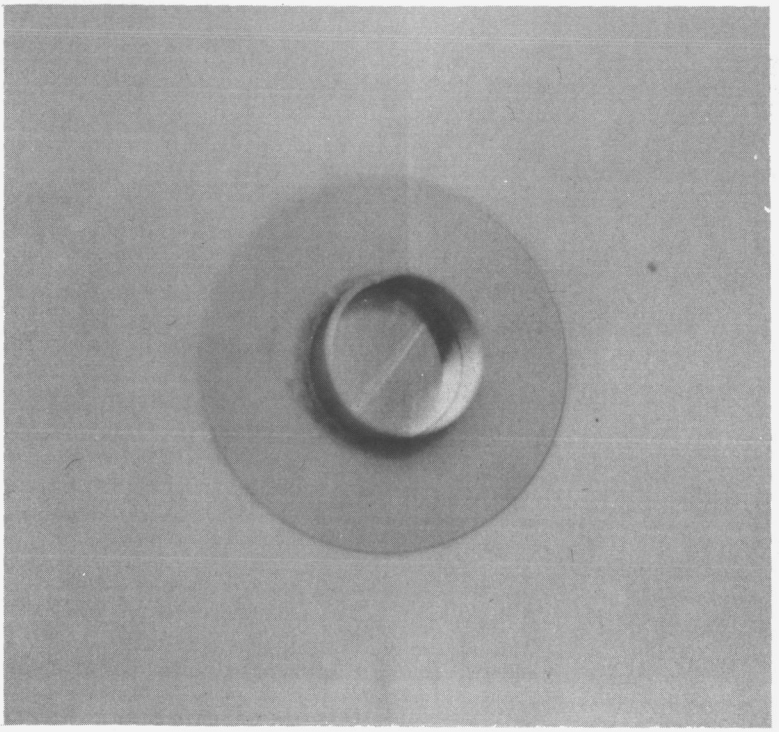

Figure 3.21. Converter Sleeve Fitted to the Emitter.

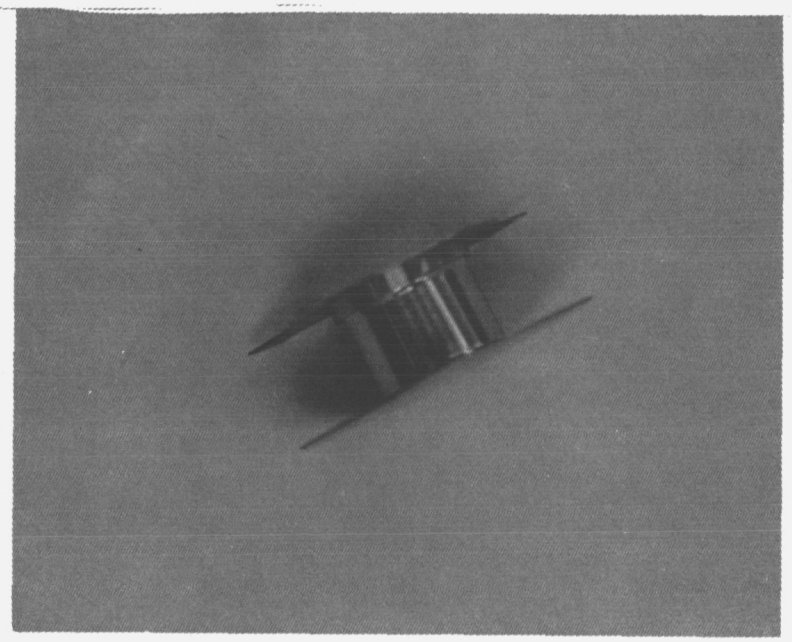

Figure 3.22. Converter Sleeve Welded to Emitter and Flange.

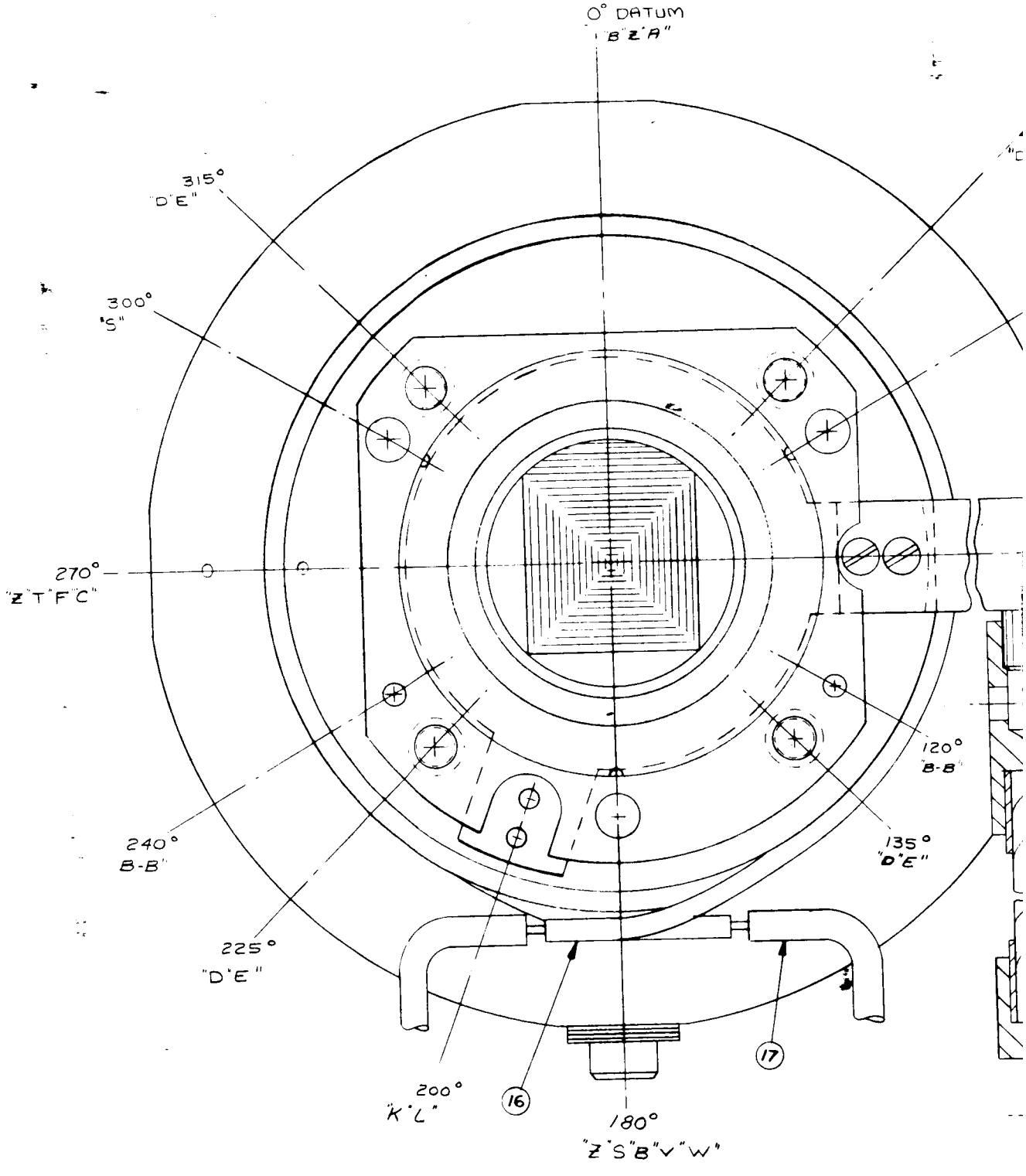

FOLDOUT FRAME 1

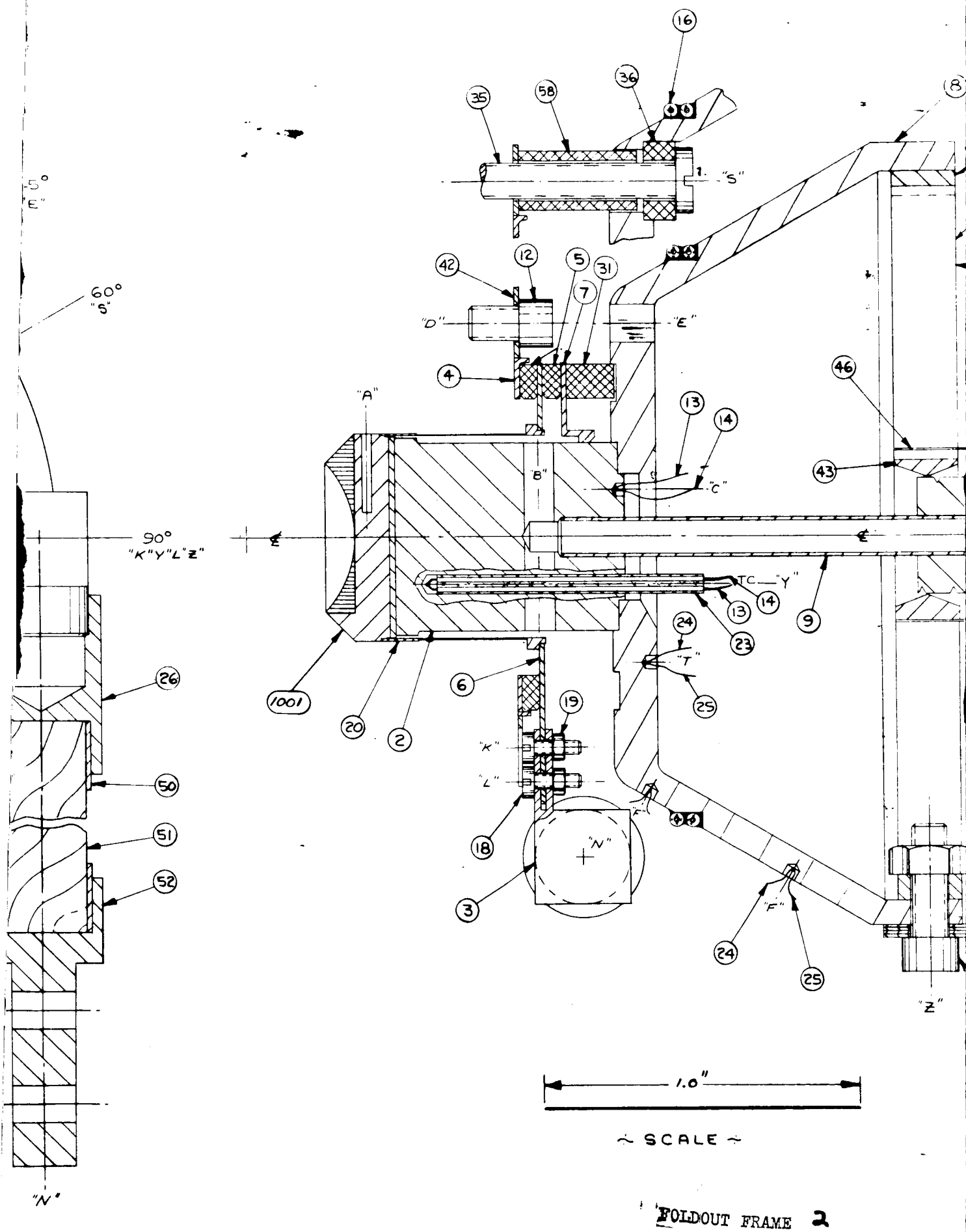

1.0"

~ SCALE ~

FOLDOUT FRAME 2

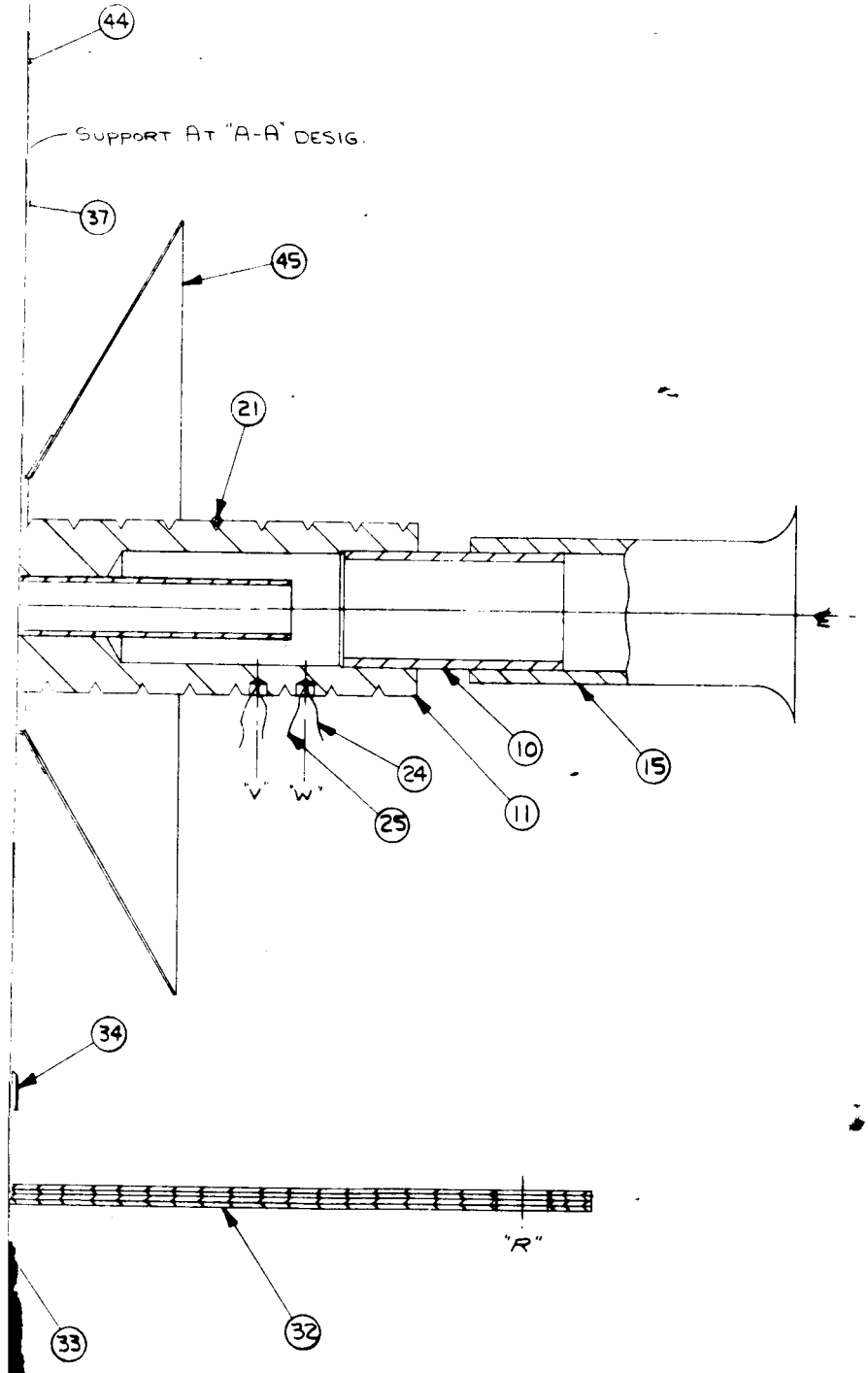
44
SUPPORT AT "A-A" DESIG.
37
45
21
"V"
"W"
24
25
10
11
15
34
"R"
33
32

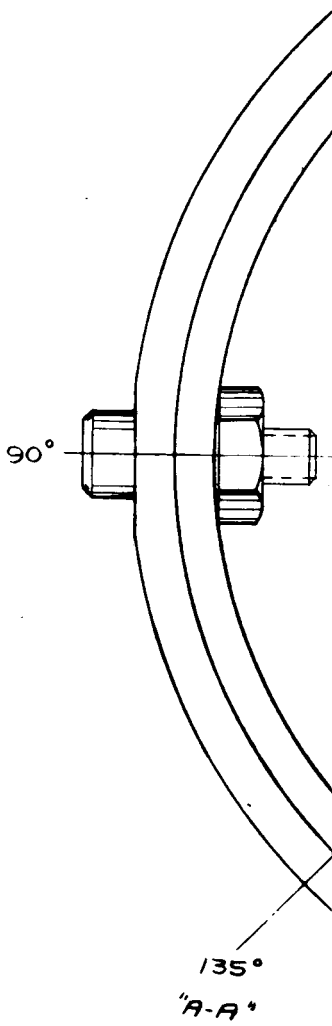
90°
135°
"A-A"

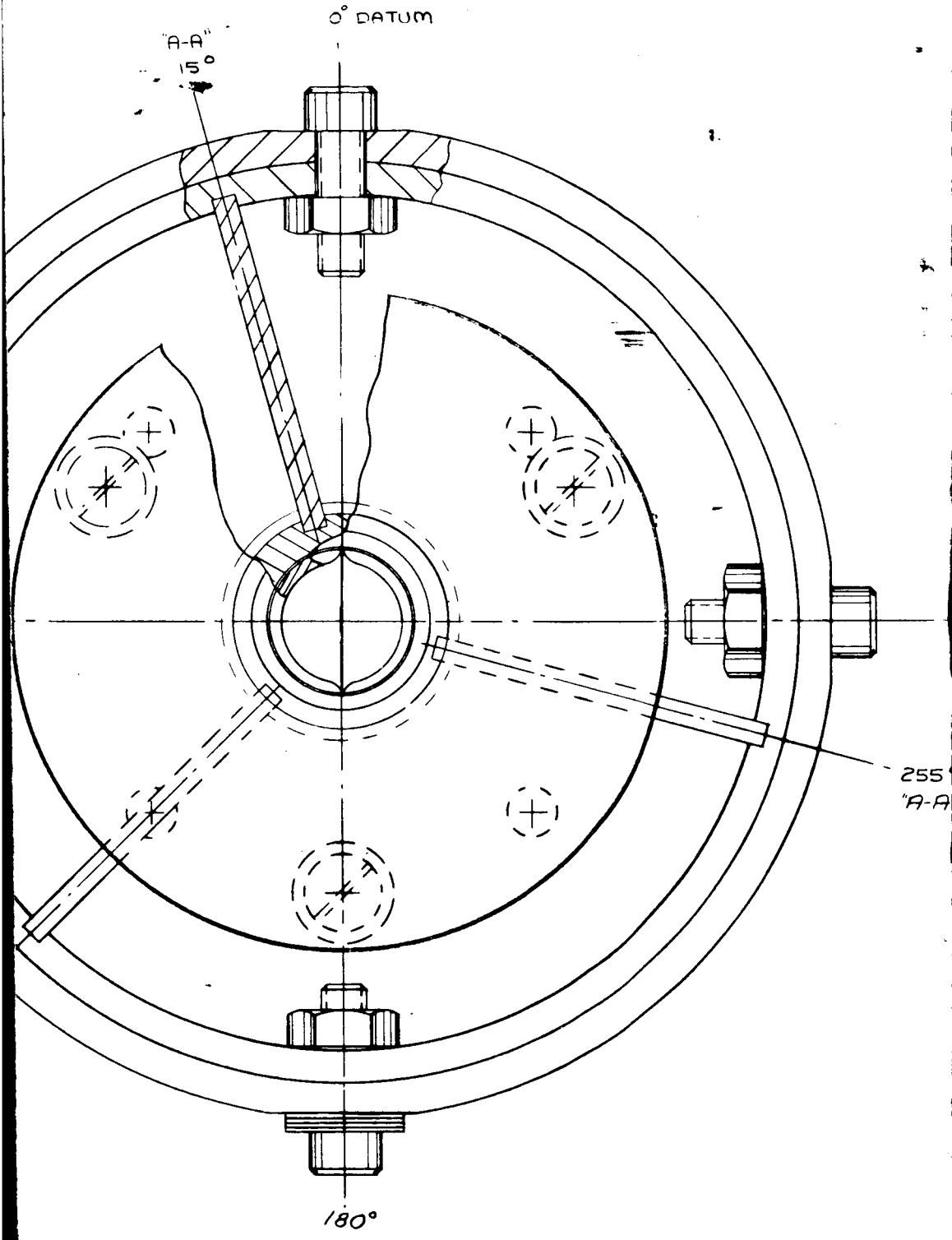

FOLDOUT FRAME 4

5

1001	D	A	1	Re EMITTER	PN 1,47,48,49 PRESS. BOND.
58	A		3	Al_2O_3	
57					
56					
55					
54					
53					
52	B		1	Cu	
51	B		1	Cu	
50	B		2	Ni	
49	A		1	Ta	
48	A		1	Ta	
47	A		1	Re	
46	C		1	Ni	
45	B		1	Ni	
44	D		1	S.S.	
43	B		1	S.S.	
42	C	D	1	Nb	
41	OBS.				
40	OBS.				
39	OBS.				
38	OBS.				
37	B		3	S.S	
36	A	C	3	Al_2O_3	
35	ND	-	3	S.S	#4-40 x .750 LG. R.H.C.S.
34	ND	-	4	S.S.	#4-40 HEX NUT
33	ND	-	4	S.S.	#4-40 X .38 LG S.H.C.S.
32	B		4	Cu	
31	B		1	Al_2O_3	
30					
29					
28					
27					
26	B		1	Cu	
25	ND	-	2	Alumel	
24	ND	-	2	Chromel	
23	ND	-	1	Al_2O_3	
22	ND		AS REQ'D	ASTRO CERAM	
21	ND	-	AS REQ'D		HEATER
20	C		1	Ta	
19	ND	-	2	S.S.	#00-96 HEX NUT
18	ND	-	2	S.S	#00-96 X .125 LG
17	B		4	Cu	
16	ND	-	AS REQ'D		SHEATHED HEATER
15	C		1	Cu	
14	ND	-	1	Alumel	
13	ND	-	1	Chromel	
12	A	A	4	S.S.	#4-40 S.H.C.S. (MODIFIED)
11	C/C		1	Ni	
10	C		1	Ni	
9	C		1	Ni	
8	D/D	/D	1	Cu	
7	C		1	Nb	
6	C	B	1	Nb	
5	B		2	Al_2O_3	
4	B		1	Nb	
3	C	A	1	Nb	
2	C		1	Mo	
1	A	A	1	Ta	

PART	SIZE	REV	REQ	MAT'L	NOTES

THERMO ELECTRON
THERMO ELECTRON CORPORATION
85 FIRST AVENUE · WALTHAM, MASS. 02154

DRAWN	CHECKED	ENGINEER
MN		

TITLE: VIII-P-3

SIZE	DRAWING NUMBER	SHEET	REV.
H	479-1000	1	L

270°

Figure 3.23

FOLDOUT FRAME 5

the radiator and was also unnecessary. The radiator support screws, parts 35, 36, and 38, were also deleted.

The emitter, part 1, is welded to the sleeve, part 20, using the electron-beam welder. This assembly is welded to emitter flange, part 6. As mentioned in Section 2.3.2, the emitter and sleeve of the TES model are made of rhenium. Next this assembly is brazed to the seal structure, which is composed of parts 4, 5, and 7; at the same time the collector, part 2, is brazed to the collector flange, part 7, and the cesium reservoir tubulation assembly, consisting of parts 9, 10, 11 and 15, which have been previously joined. The last braze joins the seal structure to the mounting flange, part 42, and simultaneously the radiator, part 8, to the collector base. No brazing or welding difficulties were encountered during assembly.

For outgassing, the converter was mounted on a 100-liter/sec Vac-Ion vacuum system. An 8-liter/sec pump was used for internal outgassing of the converter.

3.3 Fabrication of the Thermal Shielding

The design of the thermal shielding was described in Section 2.3.3. Using that design, a complete shielding assembly was constructed, deviating from the design only in that the first three shields were made of tantalum rather than rhenium. The major components of the shield assembly are shown in Figure 3.24 and the completed assembly in Figure 3.25.

A dummy TES container, supported through the opening in the assembly, was heated with the electron-bombardment heater. Measurements were made of the heat flux leaving the cylindrical part of the

PAGE 50 BLANK

shielding and the container temperature. The heat flux was measured with a thermocouple, and the container temperature was measured pyrometrically in a hohlraum machined into the container.

With the dummy container at a temperature of 2200°K, this loss represented 4.2% of the heat flux which would leave a surface at the same temperature, but with a thermal emissivity equal to 0.26 (the emissivity of the tantalum dummy container). From these results, it appeared that the values of heat loss were not excessive, and that the shielding design would permit a satisfactory demonstration of the feasibility model.

These test results justified the assembly of the final version of the shielding, which was made around the converter and TES container after these had been joined. This assembly, which included the use of rhenium sheet in the inner three shields, required very careful and delicate handling and manipulation of the thin shields but was completed without difficulty.

3.4 Fabrication of the Electron-Bombardment Heater

The heater design was discussed in Section 2.3.4. The unit is shown in Figure 3.26. It was built and tested with filament wires of 0.010"-, 0.015"-, and 0.020"-diameter tungsten and 0.015"-diameter rhenium in four separate tests. The 0.010" tungsten wire was not rigid enough, while the 0.020" wires required high values of starting filament current — in excess of 100 amperes. The 0.015" tungsten wire provided adequate rigidity without excessive filament currents. The assembly with 0.015" wires could be mounted, dismounted, and handled after operation. The expected life of this gun was of the order of 500 hours. Under similar operating conditions the rhenium filaments evaporated

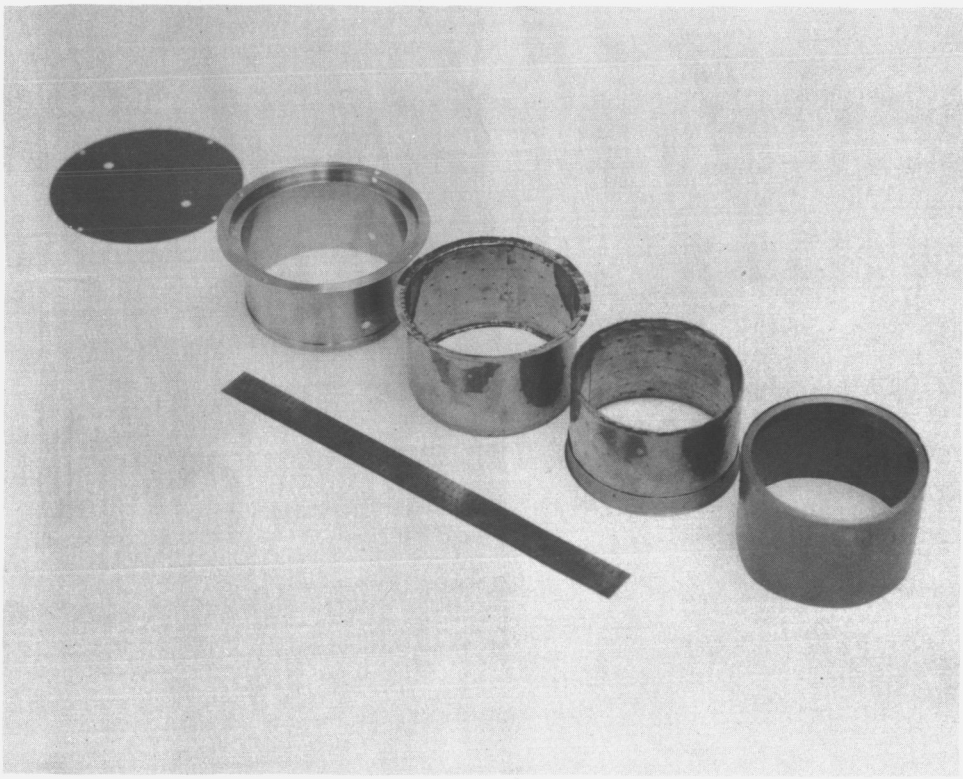

Figure 3.24. Exploded View of Major Thermal Shield Subassemblies.

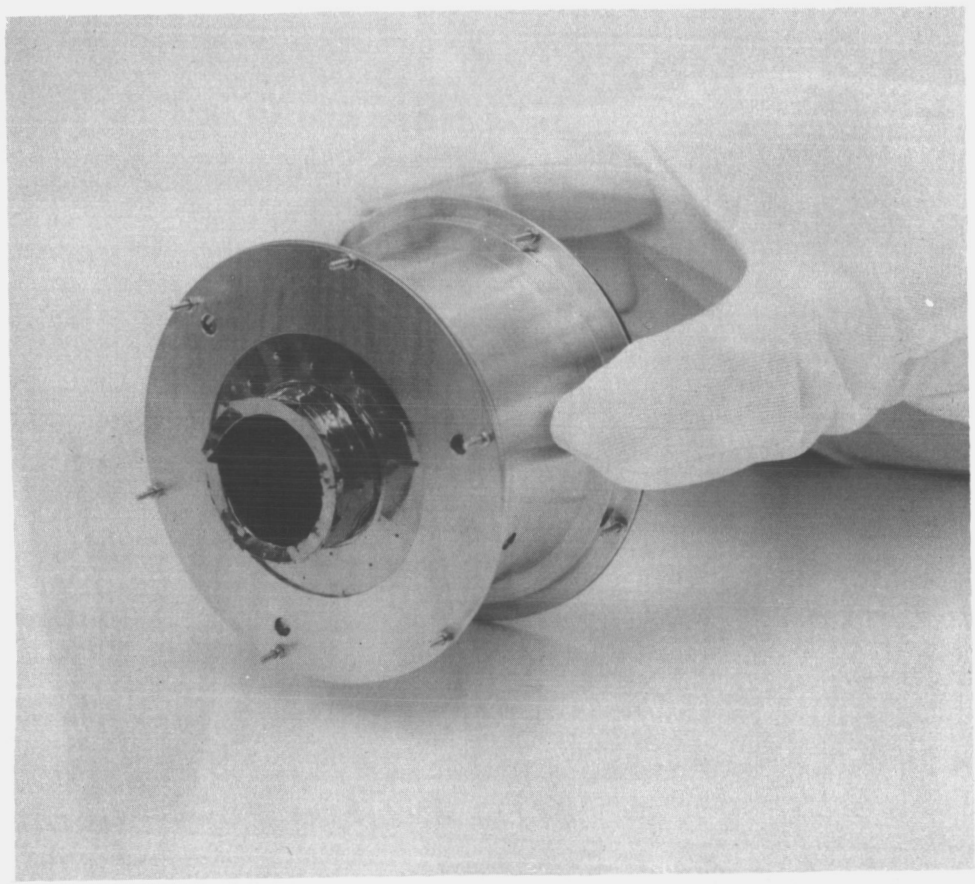

Figure 3.25. Thermal Shield Assembly.

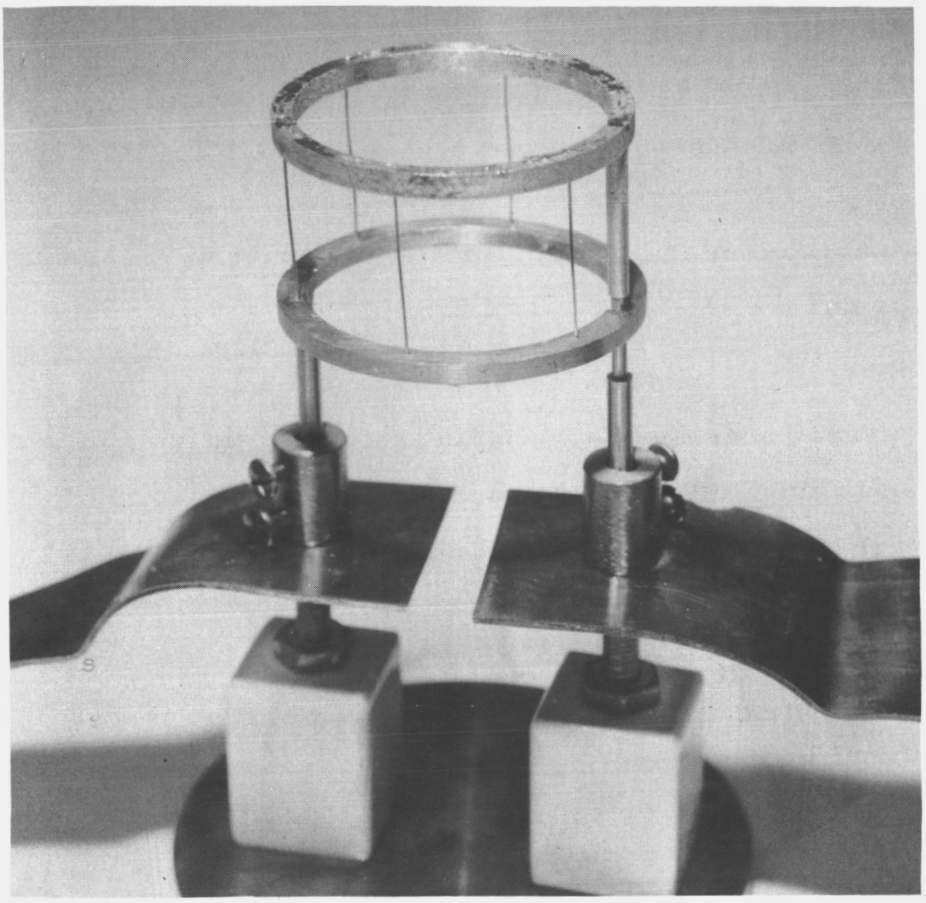

Figure 3.26. Electron-Bombardment Heater for TES Container.

more rapidly and were less rigid. Based on these results, the heater in the TES model used 0.015" tungsten wire filaments.

3.5 Conclusions and Recommendations

The experience gained in the fabrication of the TES model showed that the original design was basically successful. As will be described later, tests of the model and subsequently of a container with oxide showed that containment of the oxide required considerable further research. However, this was a separate problem. Construction and assembly of the four major components (the converter, the container, the heater and the shielding) was accomplished satisfactorily.

Tests of the heater with the TES model showed that greater clearance was necessary between the heater and the shielding to avoid very tedious adjustment of the heater's position. Also, insufficient viewing area was provided for viewing the emitter holhraum through the shielding, so that slight movements of the shields tended to obscure the holhraum and required continuing adjustments. Changes to avoid these problems can and should be made on any future model.

4. TESTING

4.1 Capsule Tests

When the methods of preparing purified pre-melted slugs of 3 BeO-2 MgO had been judged satisfactory, and after a number of electron-beam welds had been made on various rhenium pre-melt containers, a small capsule test was performed to establish a degree of confidence in the proposed design.

A 1-inch diameter rhenium container, 20 mils thick and 0.870 inch high, was fabricated. This container was filled with 20 grams of oxide and was welded shut. The capsule is shown in Figures 4.1 and 4.2, and it was estimated to be 66% full. The container accumulated 8 hours at temperatures above the melting point. It also was subjected to 16 thermal cycles. Each cycle consisted of heating it fairly rapidly with RF to a temperature above the melting point, holding it there for a few minutes, and then completely shutting off the power to the capsule. The capsule then cooled to room temperature. The container showed no signs of oxide leakage, nor was there any unusual change in the appearance of the rhenium.

The melting point was determined by bringing the container to approximately 2300° K and observing the radiation from the surface with a recording pyrometer during cooling. A plot of temperature vs time revealed the isothermal plateau. The melting point was established by measuring the temperature with a pyrometer during the plateau.

Following the successful test of this capsule, a full-sized container was attached to a converter, filled with oxide, and welded

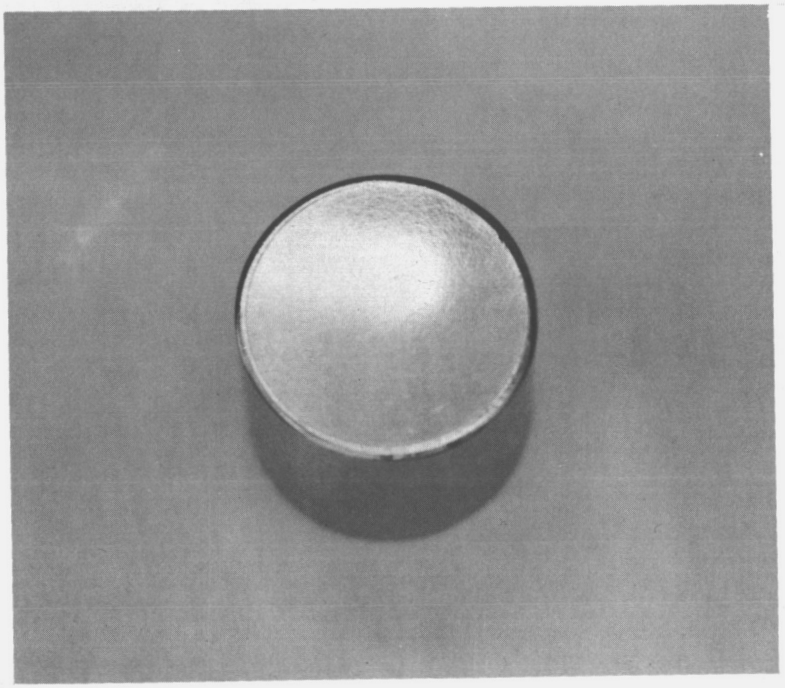

Figure 4.1. Top Weld of Test Container with Oxide after Cycling.

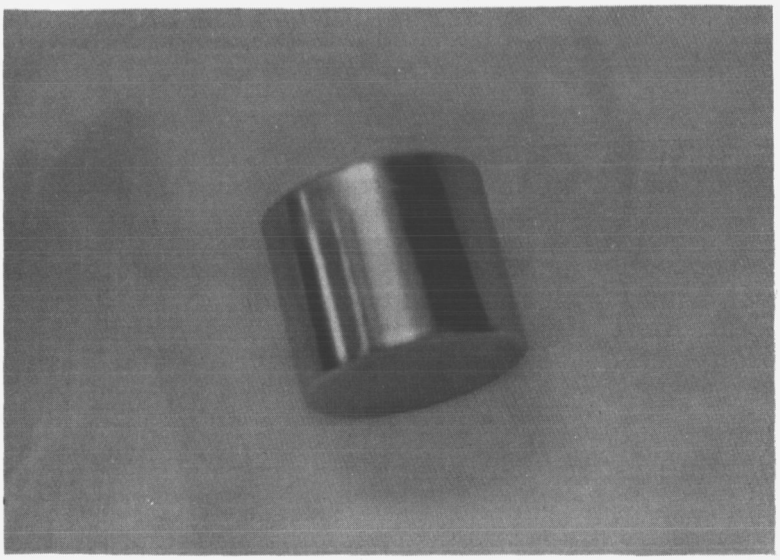

Figure 4. 2. Side View of Test Container with Oxide after Cycling.

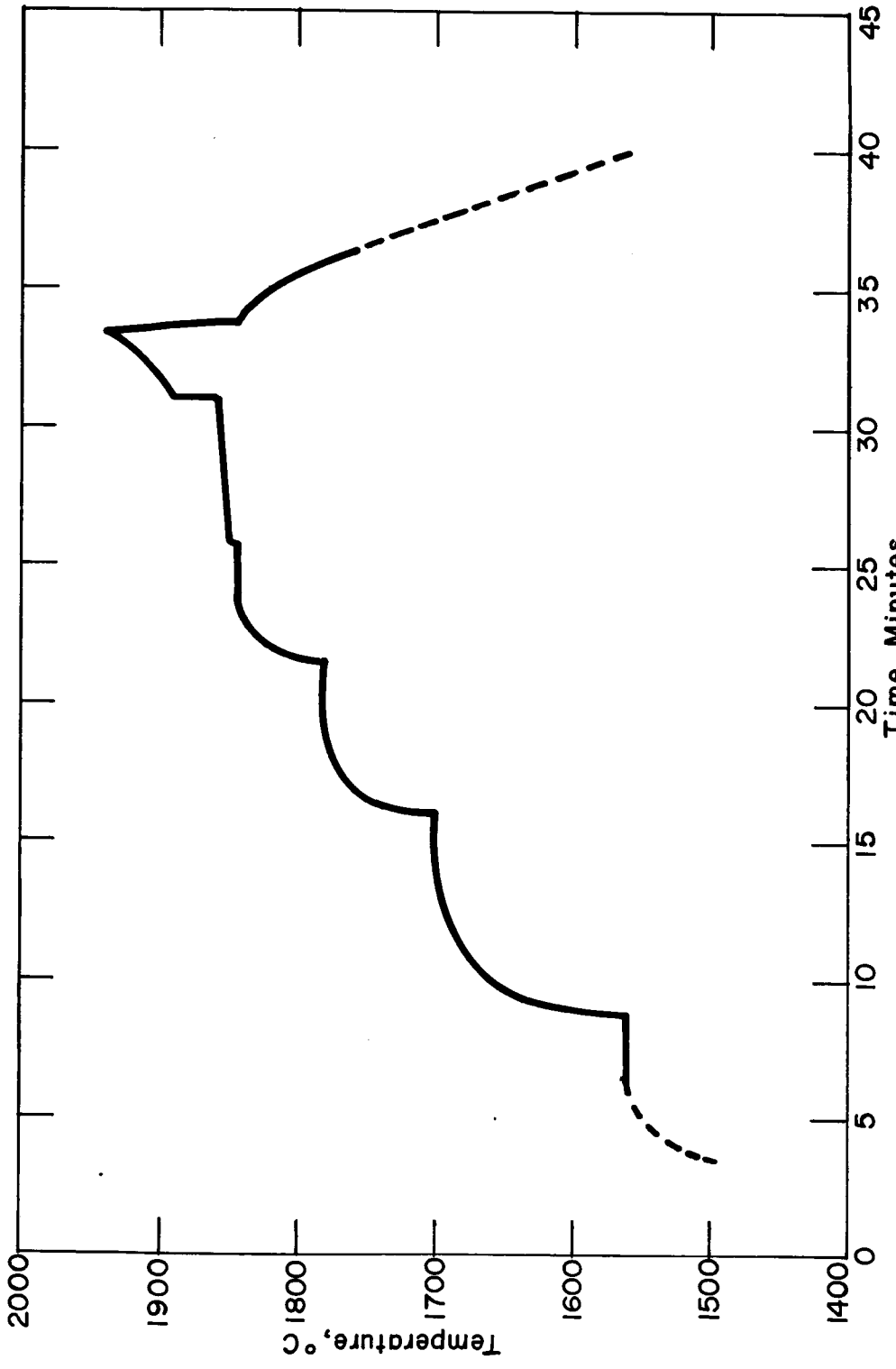

Figure 4.3. Temperature-Time Record of a Heating Cycle on the Second TES Container.

At an estimated container temperature of 1940° C one of the container support wires overheated and yielded. Power was shut off.

The cooling curve shows rapid initial cooling (liquid), then a short plateau, followed by approximately 2 minutes of slower cooling during which the oxide is solidifying.

The container, shown in Figure 4.4, was then examined visually and x-rayed. The top and bottom showed a slight bulging outward. A helium-soak leak check showed no leak. X-rays showed that over half of the oxide had melted.

The container support was then strengthened by increasing the diameter of the wires and using tungsten rather than tantalum. The 0.030" Ta wires were changed to 0.040" W, and the container was again brought to oxide melting temperature.

As during the first run, power was increased in steps. At a temperature of 1910° C molten oxide started to flow out of the container, as shown in Figure 4.5. The circumferential weld at the emitter end of the container appeared to have failed. Both top and bottom ends of the container had bulged outward about three times the amount noticed after the first run. Finally, the colder areas of the bell jar were covered with a metallic deposit, an analysis of which is shown in Table 4.1.

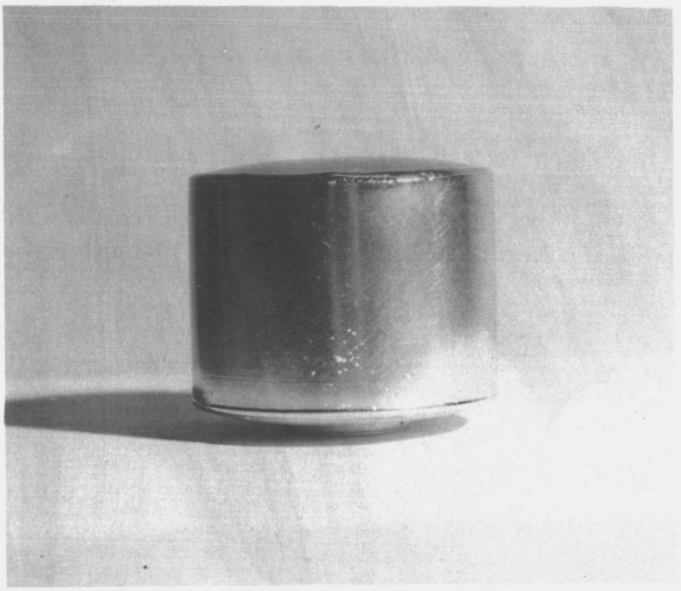

Figure 4.4. Container after First Heating Showing Bulging at Top and Bottom.

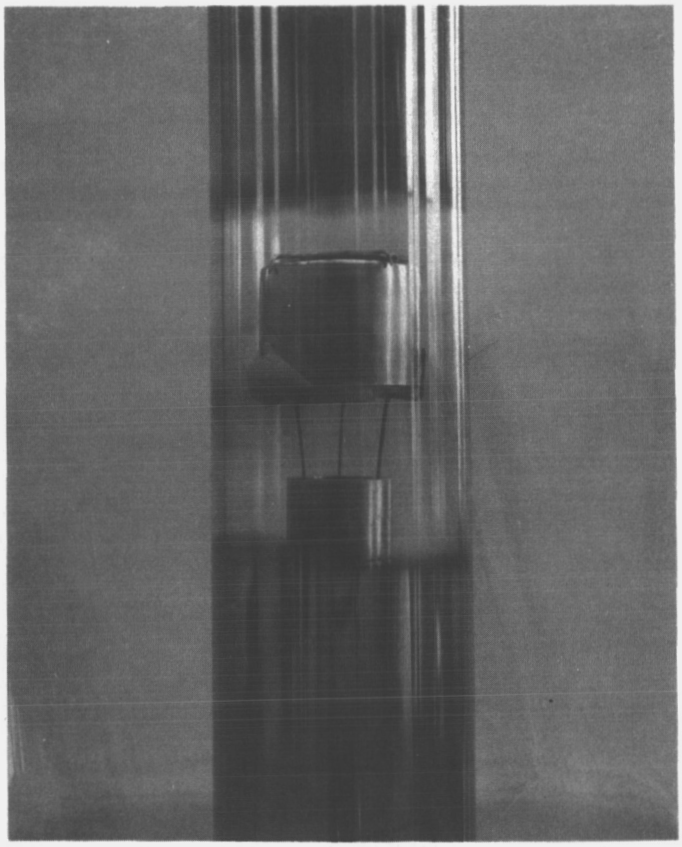

Figure 4. 5. Container after Oxide has heated Out of Bottom Weld.

TABLE 4.1

ANALYSIS OF THE DEPOSIT FOUND
ON THE INNER SURFACE OF THE BELL JAR
FOLLOWING RUPTURE OF A TES CONTAINER

Mg	>10%
Si, Fe	0.3 - 3%
Al	0.1 - 1%
Be, Cu	0.01 - 0.1%
Cr, Ti, Na, Pb, Sn	0.003 - 0.03%
Ag, B, Ni	0.001 - 0.01%

4.2 Converter Testing

Following construction of the Series VIII type converter and before the addition of the side walls of the container, the converter was electrically heated and tested. Figure 4.6 shows the test in progress. The electron-bombardment heater is at the top. The bottom of the TES container, which also constitutes the converter's emitter, can be seen just below.

Figure 4.7 shows the converter performance at hohlraum temperatures of 1900, 2000 and 2150°K. Also shown on this figure are the optimum cesium temperatures at various current-voltage conditions. This data confirms the assumption made earlier that operation at constant current requires little change in cesium pressure. At constant voltage, wide changes are required.

The earlier calculated performance of the TES model was based on an expected converter performance. The actual and expected data are shown in Figures 4.7 and 2.5, respectively.

4.3 TES Feasibility Model Testing

Following the testing of the converter, the side walls of the container were added, as were the oxide and the container lid. The electron-bombardment heater and the thermal shields were added next. The complete model is shown ready for test in Figure 4.8.

At the outset of testing a number of adjustments of the shields and bombardment gun were necessary because of shorting as the parts became heated. The shields provided around the emitter sleeve were removed at this time to prevent their touching the emitter. Also, it

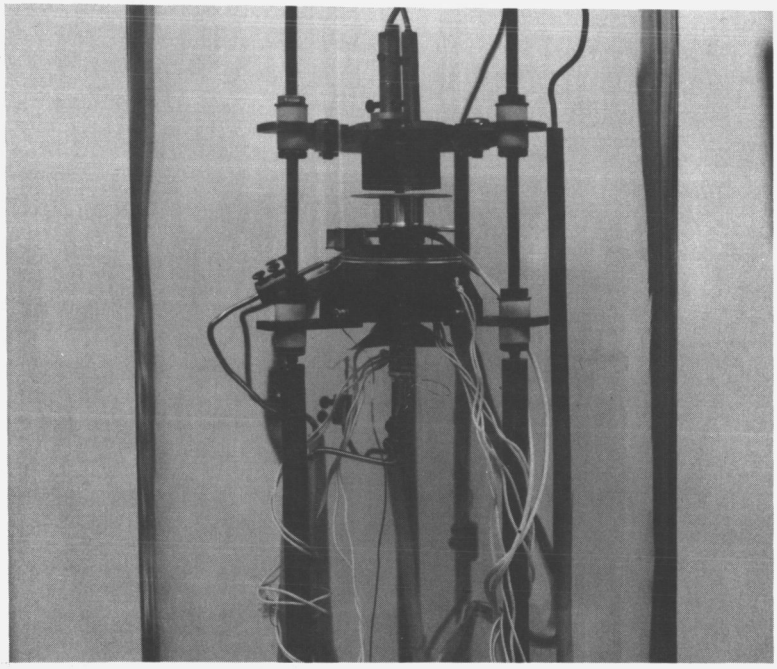

Figure 4.6. TES Converter Under Test.

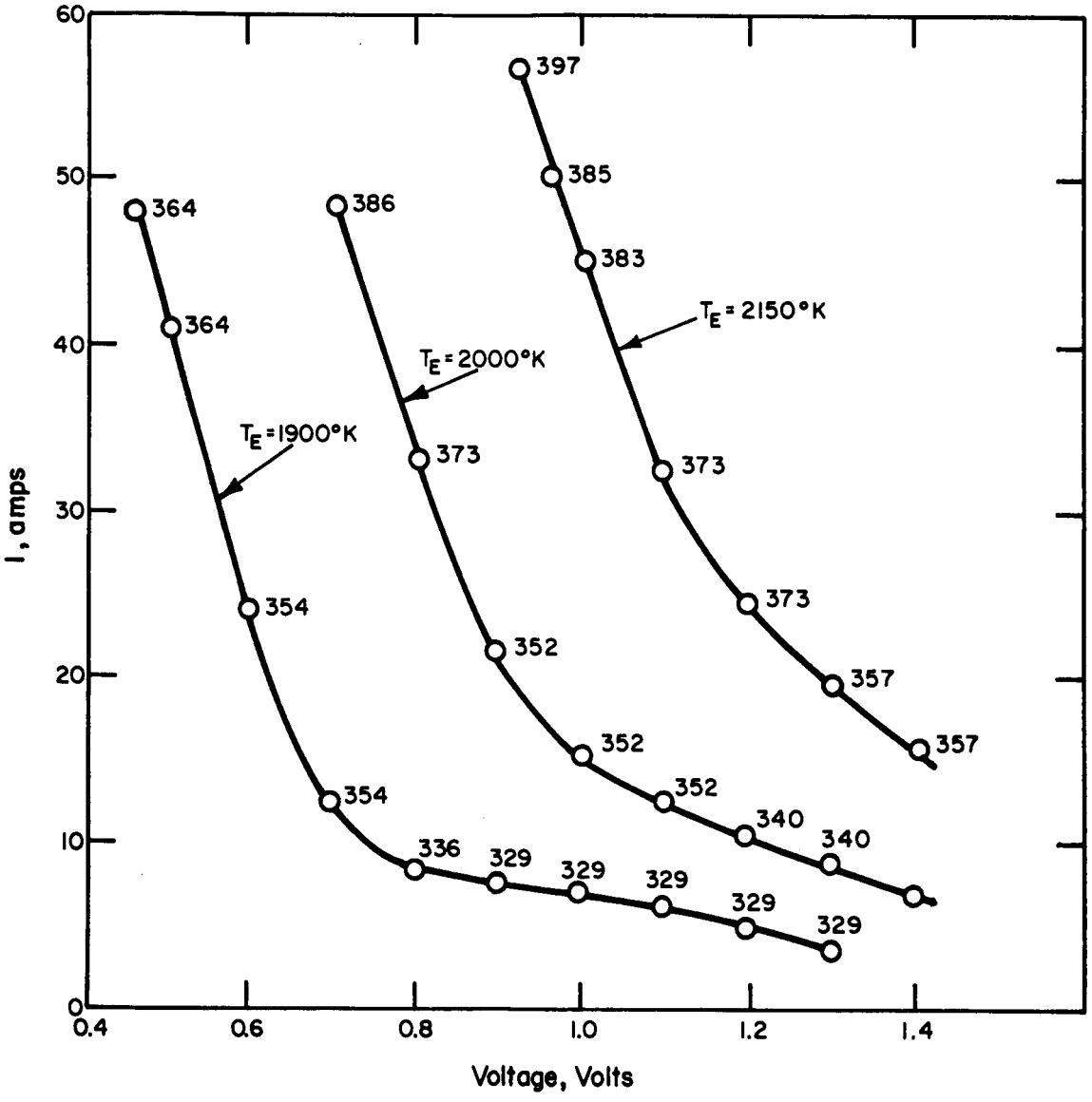

Figure 4.7. Converter Performance.

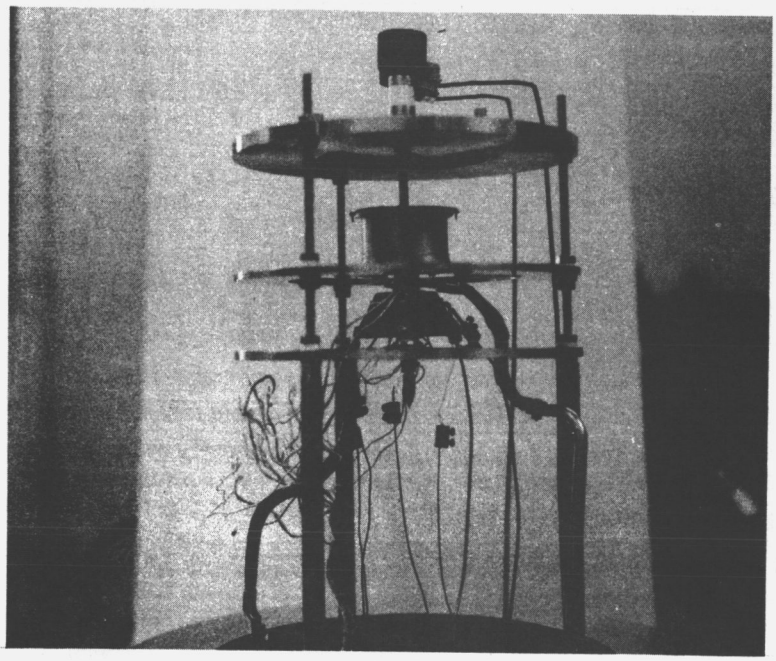

Figure 4.8. TES Feasibility Model Testing.

was observed at this time that the electron-bombardment gun was "running away" when the container approached the melting point. Several adjustments of the shielding and gun finally resulted in a position suitable for heating the device to the melting point of the oxide. The problem associated with the instability of the gun was solved in two ways. First, the bottom tantalum support ring of the gun, which originally had been covered with rhenium to increase its work function and thereby reduce its emission, had the rhenium removed, causing heavier bombardment of the bottom of the container. Secondly, a bank of light bulbs was placed in series with the high voltage of the electron-bombardment power supply. The resistance of light bulbs increases with the current going through them; therefore, when the gun current rose the light bulb resistance also increased, reducing the applied voltage and thereby stabilizing the device.

After the required changes were made to the shielding and the gun, the model was heated to the oxide melting temperature. At that time a large amount of vapor was observed striking and collecting on the bell jar. Power to the device was immediately shut off. Figure 4.9 shows the output voltage of the device as a function of time during the cool-down cycle. The model had been instrumented on a recorder so that this data could be taken following power termination. As can be seen from the test results, the performance of the device did approximate the calculated performance.

On cool-down and subsequent opening of the system and removal of the shields around the container, it was observed that oxide had seeped out of the container and that some had collected on the top surface, as can be seen in Figure 4.10. A later careful microscopic

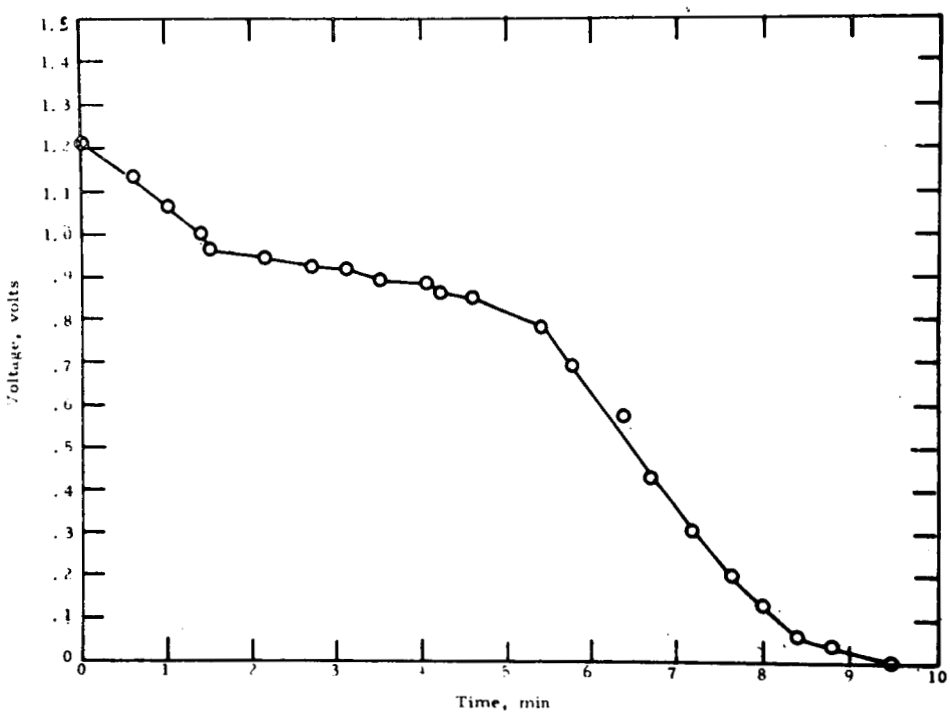

Figure 4.9. TES Model Performance with Thermally Stored Input.

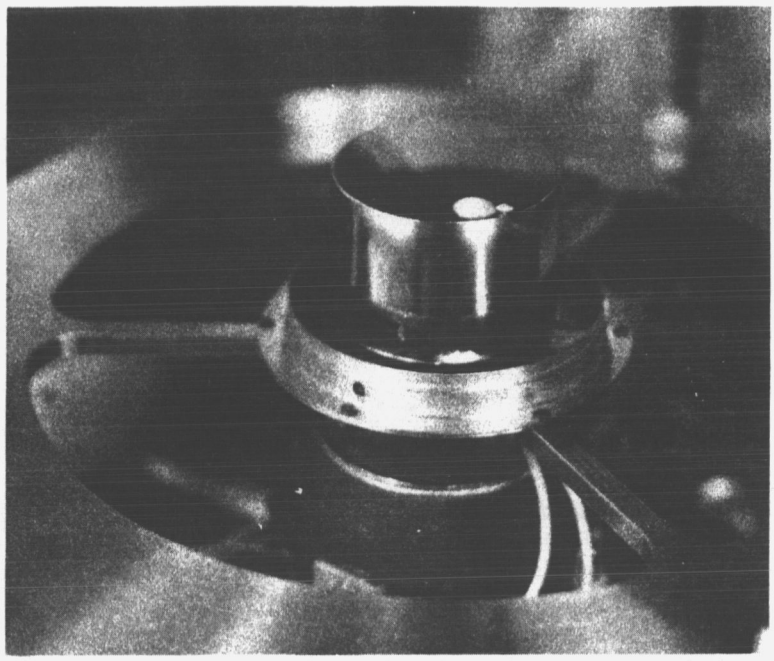

Figure 4.10. TES Container Showing Oxide Leakage.

examination of the upper weld region showed a small hole close to the smaller of the two oxide circles, which appeared to have oxide at the bottom of it and was deep enough so that it probably extended through the container. Figure 4.11 is an x-ray view of the oxide following the above test. It shows that melting of the bulk of the oxide had probably been achieved.

Following observation of the container leak, an attempt was made to re-weld the container, but this was unsuccessful. During the re-welding, while the upper weld was hot, it was observed that oxide was sputtering out of other regions of the weld, indicating that the weld was probably contaminated. A subsequent attempt to allow a successful weld by heavily heating the upper region of the container to drive the oxide away from the weld was also successful.

4.4 Conclusions and Recommendations

These test results showed that a container of thermal-energy-storage material can be integrated with a thermionic converter using available fabrication technology. Furthermore, the exposed surface of the container can be adequately shielded with multi-layer radiation shields to concentrate the bulk of the heat into the thermionic emitter. Finally, the method of calculating the output of the model during cool-down was proved valid.

However, before a long-lived model can be constructed the problem of containing the oxide must be solved. Now that definitive property data describing the 3 BeO - 2 MgO oxide is available, containment tests can be performed to establish the phenomena taking place

within the sealed capsule. Further experimentation is also necessary to establish a reliable means of preventing contamination of the final weld by the oxide. When this information is available a second TES model with the dark-cycle operating capability of an actual mission can be built.

These tests also showed that greater clearance was necessary between the heater and the shielding to avoid very tedious adjustment of the heater's position. Also, insufficient viewing area was provided for viewing the emitter hohlraum through the shielding, so that slight movements of the shields tended to obscure the hohlraum and made continuing adjustments necessary. Changes to avoid these problems can and should be made on any future model.

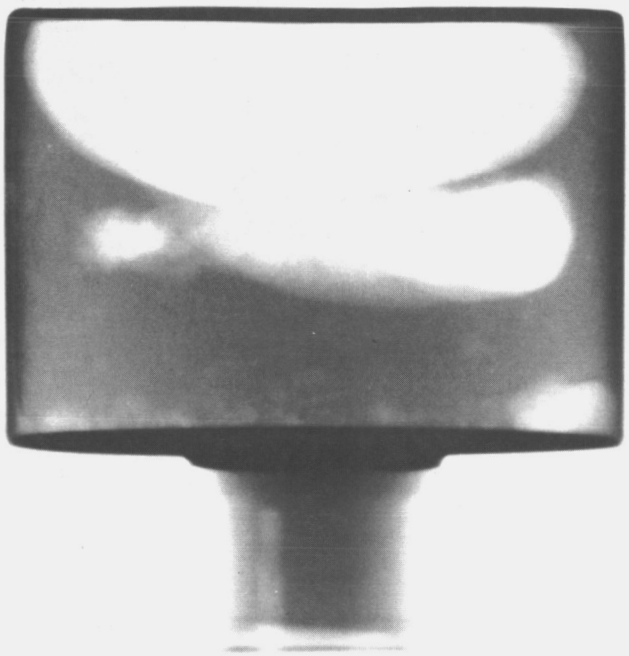

Figure 4.11. X-Ray View of the Oxide.

REFERENCES

1. Batutis, E. F., "Final Technical Report--Thermal Energy Storage, Research and Development Program, December, 1960, to May, 1961," MSVD, General Electric Company, for NASA-Lewis Contract NAS 5-826.

2. Batutis, E. F., "Final Technical Report--A Study of Select Ceramic Oxide Compositions as High Temperature Thermal Energy Storage Materials, February, 1962,to February, 1963," MSD, General Electric Company, for NASA-Lewis Contract NAS 5-826 Mod. 1.

3. Batutis, E. F., and Kuper, R. D., "Final Technical Report--A Study to Develop Necessary Design Data for Integration of Thermal Energy Storage and Thermionic Converter Devices, March, 1963, to January, 1964," MSD, General Electric Company, for NASA-Lewis Contract NAS 3-2784.

4. Moak, D. P., et al, "Thermal-Energy Storage Supporting Research," Final Technical Report, Sept. 30, 1966, Battelle Memorial Institute, Columbus, Ohio, JPL Contract 950978.